The Role of Gauge Fields in Cold and Dense Quark Matter

Dissertation
zur Erlangung des Doktorgrades
der Naturwissenschaften

vorgelegt beim Fachbereich Physik
der Johann Wolfgang Goethe-Universität
in Frankfurt am Main

von
Jorge Noronha
aus Pernambuco, Brasilien

Frankfurt am Main, 2007
(D 30)

vom Fachbereich Physik der Johann Wolfgang Goethe–Universität
als Dissertation angenommen.

Dekan: Prof. Dr. W. Aßmus

Gutachter: Prof. Dr. D.-H. Rischke, HD Dr. J. Schaffner-Bielich

Datum der Disputation: 3.12.2007

Abstract

In this thesis we investigate the role played by gauge fields in providing new observable signatures that can attest to the presence of color superconductivity in neutron stars. We show that thermal gluon fluctuations in color-flavor locked superconductors can substantially increase their critical temperature and also change the order of the transition, which becomes a strong first-order phase transition. Moreover, we explore the effects of strong magnetic fields on the properties of color-flavor locked superconducting matter. We find that both the energy gaps as well as the magnetization are oscillating functions of the magnetic field. Also, it is shown that the magnetization can be so strong that homogeneous quark matter becomes metastable for a range of parameters. This points towards the existence of magnetic domains or other types of magnetic inhomogeneities in the hypothesized quark cores of magnetars. Obviously, our results only apply if the strong magnetic fields observed on the surface of magnetars can be transmitted to their inner core. This can occur if the superconducting protons expected to exist in the outer core form a type-II superconductor. However, it has been argued that the observed long periodic oscillations in isolated pulsars can only be explained if the outer core is a type-I superconductor rather than type-II. We show that this is not the only solution for the precession puzzle by demonstrating that the long-term variation in the spin of PSR 1828-11 can be explained in terms of Tkachenko oscillations within superfluid shells.

Zusammenfassung

Die Farbsupraleitung war in den letzten Jahren Gegenstand intensiver Untersuchungen, obwohl es bisher keine experimentellen Belege gibt, die die Existenz dieses Phänomens bestätigen würden. Der wohl wichtigste Grund für dieses Interesse liegt darin, dass sich zeigen lässt, dass die Existenz der Farbsupraleitung direkt aus der asymptotischen Freiheit der Quantenchromodynamik (QCD) folgt. Da die QCD als die korrekte Theorie der starken Wechselwirkung angesehen wird, geht es nur noch darum, Bedingungen zu finden, unter denen dieser neue Zustand der Materie beobachtet werden kann.

In Anbetracht der speziellen Bedingungen, die für das Auftreten der Farbsupraleitung erforderlich sind, stellt sich heraus, dass Quarkmaterie ohne Confinement am wahrscheinlichsten im inneren Kern von Neutronensternen anzutreffen sein wird, wo Dichten von bis zum Zehnfachen der nuklearen Sättigungsdichte und Temperaturen $T < 1$ MeV vorherrschen. In der vorliegenden Arbeit haben wir untersucht, welche Rolle Eichfelder spielen, um neue Observable zu für das Auftreten von Farbsupraleitung im Zentrum kompakter Sterne zu finden. Wir diskutieren nun, wie diese neuen observablen Effekte erhalten wurden.

Der Ordnungsparameter der "Color-flavor locked" (CFL) Phase bricht gleichzeitig die Farb- und Flavor-Symmetrie. Daher bedingt die Ausbildung des farbsupraleitenden Zustands ein kompliziertes Wechselspiel zwischen den Gluonen und den Cooper-Paaren, denn beide tragen nichtabelsche Farbladungen. In der CFL-Phase besitzen die Gluonen eine nichtverschwindende Farb-Meissner-Masse, die eine wichtige Rolle spielt, wenn thermische Fluktuationen berücksichtigt werden. Wir haben systematisch den Effekt von Eichfeldfluktuationen auf die Ginzburg-Landau (GL) freie Energiedichte eines homogenen CFL-Farbsupraleiters in Zweischleifennäherung berechnet. In elektronischen Supraleitern induziert ein fluktuierendes elektromagnetisches Feld einen schwachen Erste-Ordnung-Phasenübergang. Analog dazu ändert das Hinzufügen von thermischen Fluktuationen zur GL freien Energiedichte bei einem CFL-Supraleiter die Ordnung des Phasenübergangs.

Wir haben die Temperatur des fluktuationsinduzierten Erste-Ordnung-Phasenübergangs sowohl analytisch wie numerisch ermittelt und auch die latente Wärme und die Maximaltemperatur der überhitzten Superphase berechnet. Auch wurde gezeigt, dass der London-Limes für farbmagnetische Wechselwirkung in CFL Farbsupraleitern nicht existiert. Dies ist eine Konsequenz der Schwäche der elektromagnetischen Wechselwirkung im Vergleich zur starken Wechselwirkung, also $\alpha_e \ll \alpha_s$. Werden deshalb die thermischen Gluonen-Fluktuationen berücksichtigt, dann ist die Näherung lokaler Kopplung zwischen dem Ordnungsparameter der Farbsupraleitung und den Gluonen in der CFL-Phase nicht gültig.

Die kritische Temperatur der Supraleitung, die man für den Erste-Ordnung Phasenübergang

erhält, ist bedeutend größer als der entsprechende Wert ohne Berücksichtigung der Gluonenfluktuationen. Weiterhin ändert sich die Energielücke im Anregungsspektrum der Quasiteilchen sprunghaft von Null (bei hoher Temperatur) auf einen endlich Wert bei der neuen kritischen Temperatur. Die Frage ist noch offen, wie sich dieses Verhalten auf das Abkühlen eines Proto-Neutronensterns mit CFL-Kern auswirkt.

An der Oberfläche kompakter Sterne existieren starke Magnetfelder: zum Beispiel gilt für gewöhnliche Neutronensterne $B \lesssim 10^{12}$ G während für Magnetare Feldstärken bis $B \simeq 10^{16}$ G erreicht werden können. Oft kann man annehmen, dass die Leitfähigkeit der Materie im Inneren von Neutronensternen praktisch unendlich groß ist, da die Zeitskalen für Dissipation groß gegenüber den anderen relevanten Zeitskalen sind. In diesem Fall sagen die magnetohydrodynamischen Gleichungen vorher, dass der magnetische Fluss durch jede geschlossene Oberfläche, die sich mit der Flüssigkeit bewegt, konstant ist. Unter der Annahme, dass die Feldlinen den Innenbereich des Sterns durchdringen, folgt aus der Erhaltung des Magnetflusses, dass die magnetische Feldstärke im inneren Kern eines Magnetars Werte von über $B \simeq 10^{18}$ G erreicht. Dieser große Wert entspricht bereits der physikalischen Obergrenze für das Magnetfeld eines gravitativ gebundenen Sterns.

Der superdichte, kalte Kern von gewöhnlichen Neutronensternen besteht sehr wahrscheinlich aus irgendeiner Art farbsupraleitender Quarkmaterie. Es gibt keinen Grund, dieselbe Idee nicht auch auf Magnetsterne anzuwenden. Die durch ein Feld von ungefähr 10^{18} G definierte Energieskala ist etwa von der Größenordnung 100 MeV. Dies ist vergleichbar mit der farbsupraleitenden Lücke, die im Energiespektrum der Quasiteilchen und in der Masse des s–Quarks auftaucht. Da Quarks geladene Teilchen sind, ist anzunehmen, dass solch ein starkes magnetisches Feld die Kopplung der Quarks beeinflusst.

CFL–Supraleiter sind keine elektromagnetischen Supraleiter, weil die anfängliche lokale Symmetrie, die dem Elektromagnetismus entspricht, im Medium nicht wirklich gebrochen, aber rotiert ist. In dieser Arbeit haben wir die Effekte eines moderat starken magnetischen Feldes auf die Dynamik der Bildung von Cooper–Paaren in kalter und dichter, masseloser Quarkmaterie, bestehend aus Quarks mit drei unterschiedlichen Flavors, untersucht. Wir haben die entsprechende Gap–Gleichung numerisch gelöst und die Magnetisierung für ein Vielzahl magnetischer Felder ($eB/\mu^2 \lesssim 1$), wobei μ das quarkchemische Potential ist, berechnet. Wir fanden, dass mit anwachsendem magnetischen Feld das System einen kontinuierlichen Cross–Over von der gewöhnlichen CFL–Phase zur magnetischen CFL–Phase(mCFL) vollzieht. Bemerkenswert ist, dass für $eB/\mu^2 \lesssim 0.1$, was (sofern $\mu = 500$ MeV) einem $B \lesssim 4.2 \times 10^{18}$ G entspricht, kein großer Unterschied zwischen der Lücke im Energiespektrum der mCFL– und der CFL–Phase besteht.

Unsere magnetischen Lösungen für die Lücken im Energiespektrum spiegeln die magnetischen Oszillationen wieder, die eine direkte Konsequenz der Landau Quantisierung der Energieniveaus im magnetischen Feld sind. Die Tatsache, dass die Lücke in der mCFL–Phase als Funktion des magnetischen Feldes oszilliert, kann auch analytisch durch die Lifshitz-Kosevich Analyse der Gap–Gleichung gezeigt werden. Ähnliche magnetische Oszillationen wurden für den Typ–II des elektrischen Supraleiters vorhergesagt und später auch beobachtet. Die Folgen dieser Oszillationen auf die Transporteigenschaften des mCFL–Supraleiters sind bislang unverstanden.

Wir untersuchten, wie sich die unterschiedlichen Längenskalen, welche die mCFL–Phase definieren, als Funktion von eB/μ^2 verhalten. Die Kohärenzlängen sind umgekehrt proportional zu den Lücken im Energiespektrum. Wenn die magnetische Länge so großist wie der Abstand

zwischen den Quarks, was für $\mu = 500$ MeV bei $B \simeq 7 \times 10^{18}$ G auftritt, muss eine sorgfältigere Analyse der Annahmen über die elektromagnetischen Eigenschaften des Farbsupraleiters gemacht werden. Für stärkere Felder wird die magnetische Länge kleiner als der Abstand zwischen den Quarks und in diesem Grenzfall besteht der wichtigste durch das Feld hervorgerufene Effekt in der magnetischen Katalyse der chiralen Symmetriebrechung.

Die freie Energiedichte in der mCFL–Phase und die entsprechende Gap–Gleichung sind im Prinzip ultraviolett divergent und müssen folglich regularisiert werden. In effektiven Quark–Modellen wie dem Nambu-Jona-Lasinio (NJL) Modell, das hier benutzt wurde, wird gewöhnlich der Phasenraum durch die Einführung eines scharf definierten Cut–Offs im Impulsraum beschränkt. Da allerdings das System in einem magnetischen Feld besondere Eigenschaften aufweist, ist ein solches Vorgehen nicht sehr nützlich. Die Einführung eines scharfen Cut–Offs für ein Energiespektrum mit diskreten Landauniveaus führt zu unphysikalischen Diskontinuitäten in vielen thermodynamischen Größen.

Unter Verwendung der Methode der Eigenzeit Regularisierung wurden die Gapgleichungen für die mCFL Phase analytisch untersucht. Es konnten analytische Lösungen für die Grenzfälle eines sehr starken und eines verschwindenden Magnetfeldes gefunden werden. Es konnte ausserdem gezeigt werden, dass Quarkmaterie in der mCFL Phase de Haas-van Alphen Oszillationen unterliegt. Die Amplitude dieser Oszillationen kann dabei für einen großen Teil des Parameterraumes die Größe der magnetischen Feldstärke erreichen. Da die Magnetisierung dichter hadronischer Materie vernachlässigbar ist, könnte die endliche Magnetisierung von Quarkmaterie im farbsupraleitenden Zustand neue Möglichkeiten bieten um rein hadronische Magnetare von Magnetaren mit Farbsupraleitung zu unterscheiden. Die Oszillationen könnten als Indiz dafür gewertet werden, dass homogene Quarkmaterie in einem für Magnetare relevanten Bereich des Parameterraumes, instabil wird.

Die Art der gefundenen Instabilitäten deutet auf eine konkave freie Energiedichte in dem besagten Parameterbereich hin. Als Interpretation hierfür wird für gewöhnlich die Bildung von magnetischen Domänen oder anderen Inhomogenitäten herangezogen. Daher konnte hier geschlossen werden, dass magnetische Inhomogenitäten in den Quarkkernen von Magnetaren existieren. Es wurde daraufhin argumentiert, dass aufeinander folgende Phasenübergänge, die von diskontinuierlichen Übergängen des magnetischen Feldes her rühren, eine große Menge an Energie frei setzen kann. Diese Energie würde wiederum den Stern aufheizen und dann durch Neutrino Strahlung abgegeben werden. Daher sollten Magnetare mit einem farbsupraleitenden Kern nach der Entleptonisierungs Phase eine große Menge an Neutrinos abstrahlen.

Etliche Fragen bezüglich farbsupraleitender Materie in Magnetaren bleiben bisher unbeantwortet. Man könnte zum Beispiel den Kühlmechanismuses der stark magnetisierten Kerne detailliert Untersuchen. Auch die Effekte der starken Magnetisierung auf die Globale Struktur wie Masse und Radius des Sternes sollten noch untersucht werden. Ein sehr wichtiges Detail, das bei der Berechnung von Masse und Radius eines Magnetars berücksichtigt werden muss, ist die starke Krümmung der Raumzeit, die die einfache sphärische Symmetrie des unmagnetisierten Sternes aufhebt. Aus diesem Grund können die Tolman- Oppenheimer- Volkoff Gleichungen, die auf sphärischer Symmetrie basieren, nicht verwendet werden um Masse und Radius des Sternes zu schätzen.

Geladen Mesonen sollten in niederenergetischer Näherung nur dann entkoppeln sobald $eB \gtrsim 12\,\phi_0^2$ wobei ϕ_0 die CFL Lücke (Gap) darstellt. Zufälligerweise entspricht dies der Region in der

auch die Oszillationen der Magnetisierung und der Lücke einen merklichen Effekt machen. Daher stellt sich die Frage inwiefern die magnetischen Oszillationen die niederenergetische Dynamik der mCFL Phase beeinflussen. Diese Fragen sollten, ebenso wie die Auswirkungen einer endlichen Masse des s-Quarks auf Farbsupraleiter in der mCFL Phase, in zukünftigen Studien untersucht werden.

Bei moderaten Dichten hat neutrale farbsupraleitende Materie mit zwei Quarkarten (Flavors) eine chromomagnetische Instabilität. Es wurde kürzlich darauf hin gewiesen, dass diese Instabilität durch die Formierung eines innhomogenen Kondensats geladener Gluonen und des entsprechenden induzierten magnetischen Feldes, beseitigt werden kann. Dies könnte für Erklärung der starken magnetischen Felder und anderer ungewöhnlicher Eigenschaften von Magnetaren nützlich sein. Die Feldstärken, die in diesem Ansatz verwendet wurden sind ähnlich denen die de Haas-van Alphen Oszillationen mit großer Amplitude hervorrufen. Daher sollten die Effekte der starken Magnetisierung der Quarkmaterie in der mCFL Phase auch in solchen Untersuchungen berücksichtigt werden. Es ist durchaus möglich, dass die kombinierten Effekte der de Haas-van Alphen Oszillationen und des Gluonkondensates auch das Problem der chromomagnetischen Instabilität von Farbsupraleitern lösen könnten.

Unsere Ergebnisse sind natürlich nur anwendbar, wenn das starke Magnetfeld, das auf der Oberfläche des Magnetars beobachtet wird, bis in den inneren Kern eindringt. Dies kann passieren, wenn die supraleitenden Protonen, die man in der äußeren Kruste erwartet, einen Typ II-Supraleiter bilden, sodass das äußere magnetische Feld in Form von Wirbeln vordringen kann. Es wurde dargelegt, dass die langen periodischen Schwingungen von isolierten Pulsaren nur erklärt werden können, wenn die äußere Kruste ein Typ I-Supraleiter und kein Typ II-Supraleiter ist. Die Ursache hierfür liegt in einer freien Präzessionsbewegung, die bei starker Kopplung nicht auftreten kann und als Standard-Erklärung für die Zeitvariation dient. Wenn es sich bei der äußeren Kruste von Neutronensternen tatsächlich um einen Typ I-Supraleiter handelt, dann könnten die Störungsmodelle, die auf den Wechselwirkungen zwischen den Neutronen-Wirbeln und den Protonen-Flussröhren beruhen, nicht länger angewendet werden.

In den späten 60er Jahren hat Tkachenko bewiesen, dass der niedrigste Energiezustand einer unendlichen Anordnung von Wirbeln in einem inkompressiblen Suprafluid auftritt, wenn die Wirbel ein zweidimensionales dreieckiges Gitter formen. Das Gitter unterstützt kollektive elastische Moden, die so genannten Tkachenko-Wellen, bei denen die Wirbellinien Parallelverschiebungen mit elliptischer Polarisation in der zu der Drehachse senkrechten Ebene vollziehen. Diese Moden können nicht innerhalb der Standard-Bekarevich-Khalatnikov-Hydrodynamik beschrieben werden, weil diese Theorie nur die Abhängigkeit der Rotationsenergie von der mittleren lokalen Wirbeldichte berücksichtigt. Die Energieerhöhung, die durch die Reibung des Wirbelgitters erzeugt wird und die wiederherstellende Kraft für diese Moden ist, wird jedoch vernachlässigt.

Ladungsneutrale Suprafluide im Inneren von Neutronensternen rotieren, indem sie eine Anordnung von einzeln quantisierten Wirbeln bilden. Die ungedämpfte Ausbreitung der zugehörigen Tkachenko-Wellen würde lokale Veränderungen der Wirbelliniendichte hervorrufen, die wiederum Änderungen des Suprafluid-Drehimpulses bewirken würden. Deshalb wird erwartet, dass dieser Effekt zu Veränderungen der Rotation und der Abbremsgeschwindigkeit des Sterns führen kann.

In dieser Arbeit wurde gezeigt, dass Typ I-Proton-Supraleitung nicht die einzige Lösung des Präzessionsrätsels ist, indem bewiesen wurde, dass die Langzeitveränderung des Spins von PSR

1828-11 mit Tkachenko-Schwingungen innerhalb von Suprafluid-Schalen erklärt werden kann. Unsere Analyse besagt, dass Tkachenko Moden mit schwach gekoppelten Theorien zwischen dem Suprafluid und dem normalen Fluid unabhängig von der Scherviskosität allgemein konsistent sind. Es wurde bewiesen, dass die Tkachenko-Wellen Schwingungsperioden haben können, die mit der niedrigsten beobachteten Periodizität von 256 Tagen von PSR 1828-11 übereinstimmt.

Die Existenz von Tkachenko Moden im stark gekoppelten Grenzfall hängt von der Scherviskosität normaler Materie ab. Für niedrige Viskositäten sind die Tkachenko Moden (bei starker Kopplung) auf Werte, die etwas kleiner sind als ihr korrespondierender nicht-dissipativer Grenzfall, renormiert. Das impliziert, dass die Tkachenko-Schwingungen bei starker Kopplung Perioden haben, die größer sind als die ihrer reibungsfreien Gegenstücke. In der Tat ist die Dämpfung, die durch gegenseitige Reibung verursacht wird, nicht immer stark genug, um ein oszillatorisches Verhalten zu verhindern. Daraus schließen wir, dass die Langzeit-Veränderung des Spins von PSR 1828-11 im Prinzip mit Tkachenko-Schwingungen in suprafluiden Schalen erklärt werden kann, wenn man bestimmte Werte für die gegenseitige Reibung und die normale Scherviskoität annimmt.

Unser Modell beruht auf bestimmten Näherungen. Wir haben die Zwei-Flüssigkeiten suprafluide Hydrodynamik angewendet, die modifiziert werden sollte, um die vielfachen Fluide im Kern des Neutronensterns zu berücksichtigen. Außerdem haben wir die Reibungseffekte, die auf die nicht verschwindende thermische Leitfähigkeit und Volumenviskositäten zurückzuführen sind, nicht betrachtet. Des weiteren müssen die zylindrische Symmetrie unseres Aufbaus und die Annahme gleichförmiger Dichte in realistischeren Betrachtungen von sphärisch suprafluiden Schalen mit Dichtegradienten überdacht werden.

Contents

Chapter 1

Introduction

The main purpose of this thesis is to explore the role played by gauge fields in providing new observable signatures that can attest to the existence of color superconductivity in the interior of compact stars. More specifically, we show that the inevitable thermal fluctuations of the non-Abelian gluon fields present in color superconductors can substantially increase their critical temperature, which has important consequences that could be observable. Moreover, it is shown that homogeneous color-superconducting matter becomes metastable in the presence of ultrastrong magnetic fields. This points towards the existence of magnetic domains or other types of magnetic inhomogeneities in the hypothesized quark cores of magnetars.

The first six sections of this thesis contain the basic physical ideas and concepts necessary for understanding the role played by gauge fields in the description of cold and dense quark matter. After a brief discussion in the first two sections concerning the main properties of quantum chromodynamics and its phase diagram, in Sec. 1.3 we explain the physics behind electronic superconductivity. The basics of the standard Bardeen-Cooper-Schrieffer theory of superconductivity, which provides a consistent microscopic explanation for the phenomenon of superconductivity, is given in this section. In addition, we include a discussion that not only introduces the usual mean field Ginzburg-Landau description of superconductivity but also explains how the effects of a thermally fluctuating electromagnetic field can be incorporated into the theory. It is shown how this can drastically change the character of the superconducting transition. These ideas will be important in Chapter 2 where we show, using the framework of Ginzburg-Landau theory, that thermal gluon fluctuations change the order of the color-superconducting transition from second into a strong first-order phase transition.

Most likely, the only place where color-superconducting quark matter can be observed by natural means is in the interior of compact stars. Theoretical aspects of color superconductivity are explained in quite some detail in Sec. 1.5 and a discussion about its possible observable signatures is given in Sec. 1.6. The results presented in this section are important for Chapter 2 and also for Chapter 3, which contains a thorough analysis on how the strong magnetic fields present in compact stars influence the properties of color-superconducting matter.

In Sec. 1.4 we discuss the phenomenon of helium superfluidity. A special emphasis is given towards understanding how vortices are created in rotating superfluids. This is directly connected to the subject of Chapter 4 where we show that the quasiperiodic timing variations observed in

pulsars can be explained by using the oscillatory modes of the lattice formed by vortices inside neutron superfluids in pulsars.

1.1 The Phase Diagram of Quantum Chromodynamics

Matter as observed in nature is composed of hadrons and leptons. Leptons are considered fundamental particles, while hadronic matter can be decomposed into more fundamental particles called quarks. In fact, all the phenomena observed so far in nature can be described in terms of the so-called standard model [1, 2], which contains quarks and leptons as the particles of matter and weak and strong gauge bosons that mediate their interactions. However, only 5% of the observed universe corresponds to ordinary matter made up of particles from the standard model. Dark matter and dark energy are supposed to account for the remaining matter in the universe and, in fact, dark matter has been recently observed experimentally through measurements of the Bullet Cluster, which was formed by the collision of two nearby clusters of galaxies approximately 150 million years ago [3]. Nobody yet knows what dark matter and dark energy are really composed of, although several intriguing proposals have been suggested [4].

The standard model has been able to explain and predict a series of phenomena with unmatchable accuracy and, in the next few years, new physics is expected to emerge at CERN's Large Hadron Collider (LHC) at Geneva, Switzerland [5]. At this new facility protons and antiprotons will collide at energies around 10 TeV, which is approximately ten times larger than those currently available at the Tevatron [6]. At such high energies matter as we know it may be revealed to be just a rough description of more fundamental entities such as strings [7] and even what we understand as spacetime may radically change [8]. At lower energies, however, the standard model can be trusted and a lot of attention has been put towards understanding ordinary matter at extreme conditions. In fact, the phase diagram of matter at extreme high temperatures and/or densities is illustrated in Fig. 1.1 [9].

Whether or not our universe was created after a spacetime singularity (the big bang) is still under debate but there is strong experimental evidence that suggests that the early universe's energy density and temperature were extremely large indeed. Perhaps the most striking evidence for the existence of a state of infinitely high temperature and density in the distant past is the ongoing Hubble expansion of our universe [10]. Furthermore, the observed microwave background spectrum (and its fluctuations) as well as the spectrum of density fluctuations provide fundamental information about the early stages of the universe. It is fair to say that these observations along with the equations of general relativity constitute the pillars of modern cosmology. They are the tools with which one can successfully describe the universe's evolution [11].

Looking at the phase diagram in Fig. 1.1, it is almost impossible not to wonder what matter was really like in the early universe. A fundamental property of the theory of strong interactions is that it is asymptotically free [12]. This means that the strong coupling constant that quantifies the interactions among quarks and gluons becomes small at large energies. It is then expected that in the early universe the temperature was so high that hadrons (colorless bound states of quarks and gluons) could not have been formed. Instead, weakly interacting deconfined quarks and gluons permeated the entire universe forming a thermalized state known as the quark-gluon plasma (QGP). Only after the universe had expanded and then cooled down to temperatures where its energy density dropped below approximately 1 GeV were the first hadrons formed.

When the universe's temperature was around 100 keV small atomic nuclei began to form. The unstable hadrons had already decayed and all the antiparticles had been annihilated leav-

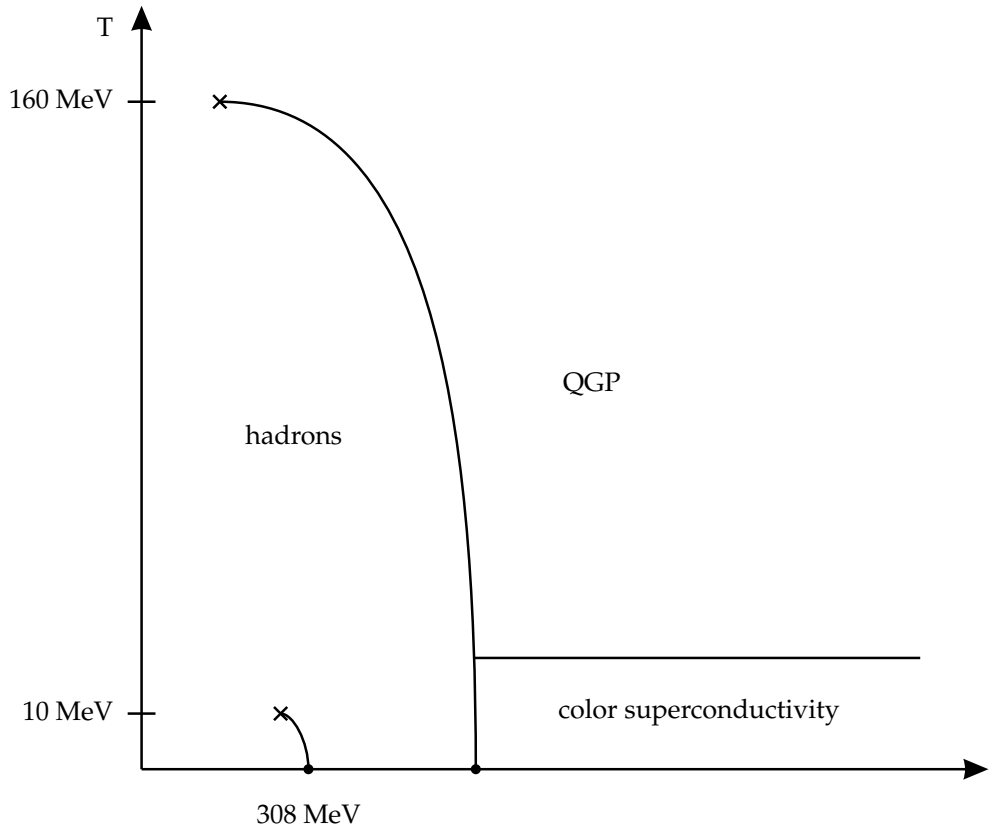

Figure 1.1: Schematic phase diagram of strongly interacting matter, from Ref. [9]. Note that μ is the quark chemical potential.

ing only protons, neutrons and electrons. The universe was still ionized and, thus, completely opaque to radiation. It only became transparent about 380000 years after the big bang when its temperature was around 3000 K and electrons and atomic nuclei combined forming electrically neutral atoms. The electromagnetic radiation that decoupled at that point was redshifted down to a temperature of about 2.7 K due to the expansion of the universe. This radiation corresponds to the cosmic microwave background. However, the extremely tiny baryon-antibaryon asymmetry observed in our universe after hadronization ($\sim 10^{-9}$) still needs to be understood.

In the last two decades the biggest challenge in nuclear physics has been to produce QGP in the laboratory by colliding heavy nuclei at ultrarelativistic energies [13]. The matter created in these collisions interpolates between the extremely hot and almost net-baryon free matter present in the early universe and the much colder and denser matter that might still exist nowadays in the inner core of compact stars such as neutron stars. Experiments conducted at Brookhaven's Relativistic Heavy Ion Collider (RHIC) located at Long Island, USA, with center-of-mass energies at $\sqrt{s} \sim 200$ AGeV created matter in the region close to the temperature axis in Fig. 1.1, around $(T, \mu) \sim (170, 10)$ MeV, and it is now widely believed that an equilibrated, strongly coupled QGP has been produced in these collisions [14]. Similar experiments will be performed at the LHC (ALICE project) in the next five years with center-of-mass energies

several times larger than those at RHIC [15]. In Fig. 1.1 we see that there is a line of first-order phase transitions that distinguishes QGP from hadronic matter. The line extends until the critical point where the transition changes to second order. The location of the critical endpoint depends on the values of the quark masses and current lattice calculations predict that it is located at $(T, \mu) \sim (160, 240)$ MeV [9].

At low temperatures and quark chemical potentials ordinary matter is in the hadronic phase where isolated quarks are never found. Nuclear matter as produced in the lab and also in stars is correctly described by using this phase. The ground state of (infinite) nuclear matter at zero temperature is at $\mu = 308$ MeV with a baryonic density of approximately 0.15 fm^{-3}. The tiny line in Fig. 1.1 that extends from the ground state to $T \sim 10$ MeV denotes the first-order phase transition line that ends at the critical point where there the transition is then of second order. This corresponds to the nuclear liquid-gas phase transition [16], where to the left of the nuclear matter line is the gaseous state and to the right is the liquid state. These states are indistinguishable above the critical end point.

The Compressed Baryonic Matter (CBM) experiment [17] to be performed in the next few years at GSI's (Gesellschaft für Schwerionenforschung) new facility FAIR (Facility for Antiproton and Ion Research) in Darmstadt, Germany will explore the region of high baryon densities in the phase diagram. Whether or not this experiment will be able to probe the cold and ultradense region where quark matter is a color superconductor is still unknown, although some important signatures may be observed [18]. Color superconductivity will be discussed in great detail in the following sections.

1.2 The Basics of QCD

Quantum chromodynamics is a renormalizable $[SU(N_c)]$ gauge theory (gauge symmetry groups are enclosed by square brackets) where N_c is the number of colors. Quarks are spin-1/2 particles that belong to the fundamental representation of $[SU(N_c)]$, whereas gluons are spin-1 gauge bosons defined in the adjoint representation of $[SU(N_c)]$. In general, QCD can be consistently formulated with an arbitrary number of colors N_c and quark flavors N_f, although $N_c = 3$ and $N_f = 6$ are found in nature.

The QCD Lagrangian density reads [1, 2, 9]

$$\mathcal{L}_{\rm QCD} = \bar{\psi}\,(i\gamma^\mu D_\mu - m)\,\psi - \frac{1}{4}\,F_a^{\mu\nu}\,F^a_{\mu\nu} + \mathcal{L}_{GF} + \mathcal{L}_{FP}\ , \tag{1.1}$$

where ψ are $4N_cN_f$-dimensional spinors, the Dirac conjugate spinor is defined as $\bar{\psi} \equiv \psi^\dagger\gamma_0$, γ^μ are Dirac matrices, and m is the current quark mass matrix, which is diagonal in flavor space, i.e., $m \equiv m_{ij}\,\delta_{ij}$ $(i, j = 1, ..., N_f)$. The known quark flavors are called up (u), down (d), strange (s), charm (s), bottom (b), and top (t). Their masses are ordered as follows: $m_u \simeq m_d \ll m_s \ll m_c \ll m_b \ll m_t$.

The covariant derivative $D_\mu = \partial_\mu - igA^a_\mu\,T_a$ couples the gluons, Yang-Mills bosons described by vector fields A^μ_a $(a = 1, ..., N_c^2 - 1)$, to fundamental fermions and the strength of this interaction is quantified by the strong coupling constant g. The $[SU(N_c)]$ generators are given by $T_a \equiv \lambda_a/2$ where λ_a are the Gell-Mann matrices. Moreover, the gluon field strength tensor is

defined as

$$F_a^{\mu\nu} \equiv \partial^\mu A_a^\nu - \partial^\nu A_a^\mu + g f_{abc}\, A_b^\mu\, A_c^\nu \ , \tag{1.2}$$

where f_{abc} are the structure constants of $[SU(N_c)]$ defined via $i f_{abc} T_c \equiv [T_a, T_b]$. The presence of nonlinear terms in A_a^μ in Eq. (1.2) implies that gluons also carry color charge and, thus, can self-interact. Therefore, even if we do not take into account the fermionic contribution in Eq. (1.1) the theory left over, known as pure Yang-Mills theory, is still an interacting theory. The terms $\mathcal{L}_{GF}$ and $\mathcal{L}_{FP}$ in Eq. (1.1) correspond to gauge fixing terms and to the contributions of Faddeev-Popov ghosts. These terms are necessary in order to have a well-defined gauge theory but they do not need to be discussed in detail here.

The physics behind the self-interactions among the Yang-Mills bosons can be readily understood once we recall what happens in ordinary electromagnetic theory. There the photon couples to charged fields even though it has no electric charge. The analog of the charge of a field in a non-Abelian gauge theory such as QCD is the representation that the fields belong to. Yang-Mills bosons couple to all fields transforming nontrivially under the $[SU(N_c)]$ gauge group. In fact, since the Yang-Mills bosons themselves transform under the group's adjoint representation they must interact with each other.

Quantum electrodynamics (QED) without fermions contains only a noninteracting photon [1, 2]. This theory is free and essentially trivial. Pure Yang-Mills theory, however, contains self-interaction and is highly nontrivial. The structure constants f_{abc} are completely determined by group theory, which means that the cubic and quartic self-interactions of the gauge bosons in Eq. (1.1) are completely determined by the non-Abelian symmetry.

In the limit of massless quarks it is sometimes convenient to decompose the quark spinors into right- and left-handed spinors

$$\psi \equiv \psi_R + \psi_L \ , \quad \psi_{R,L} \equiv \mathcal{P}_{R,L}\, \psi \ , \quad \mathcal{P}_{R,L} \equiv \frac{1 \pm \gamma_5}{2} \ , \tag{1.3}$$

where $\mathcal{P}_{R,L}$ are the chirality projectors. Moreover, it can be shown that when the quarks are massless the QCD Lagrangian is invariant under global chiral $U(N_f)_R \otimes U(N_f)_L$ transformations where

$$U_{R,L} \equiv \exp\left(i \sum_{a=0}^{N_f^2-1} \alpha_{R,L}^a\, T_a \right) \in U(N_f)_{R,L} \ , \tag{1.4}$$

$\alpha_{R,L}^a$ are the transformation parameters, and T_a are the generators of $U(N_f)_{R,L}$.

The chiral group $U(N_f)_R \otimes U(N_f)_L$ is isomorphic to $SU(N_f)_R \otimes SU(N_f)_L \otimes U(1)_V \otimes U(1)_A$ where the vector subgroup $U(1)_V$ corresponds to quark number conservation. The axial group $U(1)_A$ is explicitly broken by instantons, which corresponds to the chiral anomaly of QCD [19]. However, this symmetry might be effectively restored in matter because instantons are screened in hot (dense) media [20].

In the more realistic case where the quark current masses are nonzero the chiral symmetry of QCD is explicitly broken. In fact, the mass term in $\mathcal{L}_{\rm QCD}$ mixes quarks with different chiralities

$$\bar\psi^i\, m_{ij}\, \psi^j \equiv \bar\psi_R^i\, m_{ij}\, \psi_L^j + \bar\psi_L^i\, m_{ij}\, \psi_R^j \ , \tag{1.5}$$

where the projectors $\mathcal{P}_R$ and $\mathcal{P}_L$ are orthogonal and $\mathcal{P}_{R,L}\, \gamma_0 = \gamma_0\, \mathcal{P}_{L,R}$. If all the quark masses are equal the mass term in Eq. (1.5) preserves an $SU(N_f)_V$ symmetry, although the axial symmetries

are explicitly broken. In nature an approximate $SU(2)_V$ isospin symmetry is observed, which is a consequence of the approximate equality of the up and down current quark masses (the masses of the other quarks differ greatly).

In the QCD vacuum the $U(1)_A$ anomaly is present and the pattern of chiral symmetry breaking is $SU(N_f)_R \otimes SU(N_f)_L \rightarrow SU(N_f)_V$. There are $N_f^2 - 1$ broken generators and, consequently, $N_f^2 - 1$ Goldstone bosons. For $N_f = 2$ the Goldstone bosons correspond to the three pions, which are the lightest hadrons. However, pions are observed to have a small mass, which is a consequence of the fact that chiral symmetry is explicitly broken by the small, though nonzero, quark mass term in the QCD Lagrangian. Because of that pions are called pseudo-Goldstone bosons. For $N_f = 3$ the pseudo-Goldstone bosons account for the pseudoscalar meson octet, which includes pions, kaons, and the η meson. For a more detailed discussion see Ref. [9].

The equation of state of strongly interacting quark matter is determined using the grand canonical partition function [21, 22]

$$\mathcal{Z}(T,\Omega,\mu) = \int \mathcal{D}\bar{\psi}\,\mathcal{D}\psi\,\mathcal{D}A_a^\mu\ \exp\left\{\left[\int_X (\mathcal{L}_{QCD} + \mu\,\mathcal{N})\right]\right\}, \tag{1.6}$$

where the quark chemical potential μ is associated with the net quark number conservation and the number density operator is $\mathcal{N} \equiv \bar{\psi}\gamma_0\psi$. This partition function is defined in a compact Euclidean spacetime volume $\Omega \times 1/T$, where Ω and T are the system's volume and temperature, respectively. The boundary conditions are such that bosonic fields, such as the gluons, are periodic in the time direction, i.e., $A_a^\mu(0,\vec{x}) = A_a^\mu(1/T,\vec{x})$, while fermionic fields, such as the quarks, are antiperiodic, $\psi(0,\vec{x}) = -\psi(1/T,\vec{x})$ [21, 22]. Spacetime integrals are denoted as $\int_X = \int_0^{1/T} d\tau \int_\Omega d^3\vec{x}$.

Thermodynamical quantities such as pressure $p(T,\mu)$, entropy density $s(T,\mu)$, and quark number density $n(T,\mu)$ can be obtained from Eq. (1.6) as follows

$$p(T,\mu) = T\,\frac{\partial \ln \mathcal{Z}(T,\mu)}{\partial\Omega}\bigg|_{T,\mu}, \quad s(T,\mu) = \frac{\partial p(T,\mu)}{\partial T}\bigg|_{\mu}, \quad n(T,\mu) = \frac{\partial p(T,\mu)}{\partial \mu}\bigg|_{T}. \tag{1.7}$$

In particular, when $T \ll \mu$ the quark number density $n(T,\mu)$ for massless quarks is proportional to the third power of μ, $n \sim \mu^3$. The thermodynamical limit $\Omega \rightarrow \infty$ can be safely taken in Eq. (1.6) because $\ln \mathcal{Z}(T,\mu)$ is an extensive quantity ($\sim \Omega$) and, thus, the dependence of the pressure on the volume cancels out. In general, the expectation value of any given operator $\hat{\mathcal{O}}$ in the grand canonical ensemble is obtained by averaging, i.e.,

$$\langle\hat{\mathcal{O}}\rangle \equiv \frac{1}{\mathcal{Z}}\int \mathcal{D}\bar{\psi}\,\mathcal{D}\psi\,\mathcal{D}A_a^\mu\ \mathcal{O}\ \exp\left\{\left[\int_X (\mathcal{L}_{QCD} + \mu\,\mathcal{N})\right]\right\}. \tag{1.8}$$

In a quantum field theory the intensity of the coupling depends on the energy scale Q within which the experiments are performed. In fact, this is described by a renormalization group flow equation

$$Q\frac{\partial f}{\partial Q} = \beta(f), \tag{1.9}$$

where f is the coupling constant, and Q is an arbitrary energy scale. If the sign of the theory's β-function is positive (negative) the coupling increases (decreases) with Q. Since in nature

$N_f = 6$ we have that $\beta_{QCD} < 0$ and, thus, QCD is an asymptotically free theory [12]. The 3−loop formula for $\alpha_s = g^2/4\pi$ [23] is given by

$$\begin{aligned}\alpha_s(Q) &= \frac{4\pi}{\beta_0 \ln(Q^2/\Lambda^2_{\rm QCD})}\left[1 - \frac{2\beta_1}{\beta_0^2}\frac{\ln\left[\ln(Q^2/\Lambda^2_{\rm QCD})\right]}{\ln(Q^2/\Lambda^2_{\rm QCD})} + \frac{4\beta_1^2}{\beta_0^4 \ln^2(Q^2/\Lambda^2_{\rm QCD})}\right. \\ &\times \left.\left(\left(\ln\left[\ln(Q^2/\Lambda^2_{\rm QCD})\right] - \frac{1}{2}\right)^2 + \frac{\beta_2\beta_0}{8\beta_1^2} - \frac{5}{4}\right)\right], \qquad (1.10)\end{aligned}$$

where $N_c = 3$ and

$$\beta_0 = 11 - \frac{2}{3}N_f\ , \qquad \beta_1 = 51 - \frac{19}{3}N_f\ , \qquad \beta_2 = 2857 - \frac{5033}{9}N_f + \frac{325}{27}N_f^2\ . \qquad (1.11)$$

The value of the QCD scale $\Lambda_{\rm QCD}$ depends on the experiment used to measure α_s. When quarks are massless the classical QCD Lagrangian $\mathcal{L}_{QCD}$ has no dimensionful parameters. However, the quantization procedure introduces the dimensionful parameter $\Lambda_{\rm QCD}$. This process is sometimes known as dimensional transmutation [1, 2]. In fact, the typical size of a hadron can be estimated using standard values of $\Lambda_{\rm QCD}$ such as $\Lambda_{\rm QCD} \simeq 200$ MeV to be of the order of 1 fm.

The Lagrangian density in Eq. (1.1) contains all the elements necessary to describe the strong force. In the standard perturbative approach [21, 22] the system's thermodynamic quantities which are obtained from the partition function are computed as a perturbative series in powers of the strong coupling constant. After introducing Feynman rules for the propagators and the interaction vertices, one would naively expect that this perturbative series is an expansion in powers of g^2. However, it can be shown that this is only true at zero temperature [24]. For nonzero temperatures the expansion is in powers of g instead of g^2 because of the singular infrared properties of QCD at nonzero temperature imposed by the massless gluons.

Freedman and McLerran computed the series up to terms of the order g^4 at zero temperature [24]. In this case the theory has no infrared problems and the terms in the perturbative series are probably computable to all orders in g^2 [25]. As it will be shown in a following section, quark matter at zero temperature is color superconductive. Color superconductivity as well as ordinary electronic superconductivity are nonperturbative phenomena that cannot appear in perturbative calculations of the thermodynamic quantities.

For nonzero temperatures the perturbative expansion of the partition function in Eq. (1.6) has terms proportional to odd powers of g. These terms arise after resumming an infinite subset of diagrams describing the screening of long-range chromoelectric fields. In fact, the perturbative expansion breaks down because there are infinitely many diagrams at $O(g^6)$ [21]. This is known as the Linde problem of QCD [26]. However, all terms up to $O(g^6 \ln g)$ have been computed [27]. A truly nonperturbative calculation can only be performed numerically using lattice QCD [28].

In lattice QCD thermodynamic quantities are computed nonperturbatively on a hypercubic lattice in 4−dimensional Euclidean spacetime. As the lattice spacing $a \to 0$ Lorentz invariance is recovered (via a Wick rotation). For small values of μ lattice QCD results [28, 29] predict that the QGP-hadron gas transition is a crossover [30, 31]. However, so far these calculations are limited to the region where $T > \mu$ because of the so-called fermion sign problem [28, 29].

This problem appears because lattice simulations use Monte Carlo importance sampling and rely on the probabilistic interpretation of the weight in the path integral. However, this weight is given by the fermion determinant, which is complex at nonzero chemical potentials. Thus, lattice QCD still cannot be used to calculate the properties of matter as found, for example, in compact stars because there $T \ll \mu$. In this region of the phase diagram effective models are used to describe cold and dense quark matter [32, 33].

1.3 Eletronic Superconductivity in a Nutshell

When certain materials are cooled down below a certain critical temperature T_c they suddenly become superconductors. Historically, physicists had long suspected that the superconducting phase transition first observed by Onnes in 1911 [34] was somehow related to the superfluid transition, which involves the phenomenon of Bose-Einstein condensation. However, since electrons are fermions they would first have to pair forming bosons, which would then condense. This general picture is essentially correct; electrons form Cooper pairs whose condensation is responsible for superconductivity.

A microscopic model that could explain superconductivity was lacking until the late 50's when Bardeen, Cooper, and Schrieffer (BCS) were able to successfully explain and predict the properties of conventional superconductors [35]. The standard BCS theory was able to describe both qualitatively and quantitatively all the important properties of electronic superconductors known at that time. Basically, the theory says that superconductivity appears due to the formation of a gap in the quasiparticle excitation spectrum. This gap accounts for the fact that in the superconducting state one needs a finite amount of energy to excite an electron (more precisely, a quasiparticle [36]) at the Fermi surface. In constrast, in a metal even an infinitesimally small amount of energy can excite an electron at the Fermi surface.

According to Bardeen, Cooper and Schrieffer the material, which can be either a metal or an alloy, is described as an interacting system with electrons and phonons. Since electrons obey the Pauli exclusion principle at zero temperature all quantum states up to a certain energy, the so-called Fermi energy ε_F, are occupied. Energy states above ε_F, however, remain empty. In momentum space the boundary between occupied and empty states corresponds to the surface of a sphere, the Fermi sphere, with radius given by the Fermi momentum k_F. This configuration is stable as long as interactions are not taken into account.

In addition to the repulsive Coulomb interaction there is also an attractive force between the electrons in the material provided by the exchange of virtual phonons [37]. In practice, the phonon energy is limited from above by the Debye energy ω_D and due to Pauli blocking only electrons close to the Fermi surface can interact via phonon exchange. However, even an arbitrarily weak interaction between the electrons can lead to the formation of a new ground state, the superconducting state, where the electrons pair near the Fermi surface. This is the basic idea behind Cooper's theorem [38]. This new ground state is more stable because the total energy of the system is reduced by the amount corresponding to the sum of the binding energies of the electron pairs. Moreover, the single particle excitation energies are modified by the presence of a nonzero gap at the Fermi surface, which corresponds to the Cooper pair condensate.

In the presence of a nonzero gap ϕ the quasiparticle excitation spectrum E_k is given by

$$E_k = \sqrt{(\varepsilon_k - \mu)^2 + \phi(T,\mu)^2}, \tag{1.12}$$

where μ is the electron chemical potential, T is the temperature, and $\varepsilon_k = \vec{k}^2/2m$ is the energy of a free quasiparticle. The gap function ϕ is obtained in the standard BCS theory via the gap equation

$$\phi(T,\mu) = g^2 \int \frac{d^3\vec{k}}{(2\pi)^3} \frac{\phi(T,\mu)}{2E_k} \tanh\Big(\frac{E_k}{2k_BT}\Big), \tag{1.13}$$

where g is the coupling constant of the phonon-mediated attractive interaction among the electrons. Note that ϕ depends only on T and μ and not on the momentum $\vec{k}$. This only occurs because the attractive interaction between the electrons is considered to be point-like.

The integral in Eq. (1.13) diverges but it can be easily regularized by introducing a momentum cutoff, which is usually taken to be proportional to ω_D. The nontrivial solution of this equation ($\phi = 0$ is always a solution) at $T = 0$ reads

$$\phi_0 = 2\,\omega_D \exp\Big(-\frac{1}{N_0\, g^2}\Big), \tag{1.14}$$

where $N_0 = m\,k_F/2\pi^2$ is the electronic density of states at the Fermi surface. Another important result obtained within the BCS theory is the following relation between ϕ_0 and the critical temperature T_c

$$\frac{k_BT_c}{\phi_0} = \frac{e^\gamma}{\pi}, \tag{1.15}$$

where $\gamma \simeq 0.577$ is the Euler-Mascheroni constant. We will see later on that in color superconductivity the attractive interaction among the quarks is mediated by the gluons, which leads to a non-BCS dependence of the diquark gap on the strong coupling constant.

In 1986 Karl Müller and Johannes Bednorz found a radically new class of superconductors, which cannot be explained within the standard BCS theory, the so-called high-Tc or cuprate superconductors [39]. These materials share some common structural features such as the presence of relatively well separated copper-oxide planes. The superconducting phase transition temperatures that can be achieved in some compounds in this family are the highest among all known superconductors and can be as large as 125 K. This experimental discovery was so revolutionary that Karl Müller and Johannes Bednorz won the Nobel Prize of Physics already in 1987. Since then cuprate superconductors have been intensively studied but still no satisfactory theoretical explanation has been found.

1.3.1 Ginzburg-Landau Approach to Superconductivity

Seven years before the BCS theory was developed, Ginzburg and Landau had already realized that it was possible to describe superconductivity by expressing the free energy of the superconducting state as a function of ϕ, which in this case constitutes the order parameter of the transition [2, 40, 41]. Recall that in the ferromagnetic transition the magnetization $\vec{M}$ in a ferromagnet suddenly changes from zero to a nonzero value when the temperature drops below a certain critical temperature. Analogously, in a superconductor ϕ can be taken to be zero at high

temperatures and nonzero for temperatures below T_c. Their approach can be used to describe superconductors near to their critical temperature T_c.

In the Ginzburg-Landau theory ϕ is a complex field that depends on the spatial coordinates $\vec{x}$ and carries two units of electric charge e. In the presence of an external magnetic field $\vec{B}$ the Ginzburg-Landau free energy density reads

$$\mathcal{F}(\phi, \vec{A}) = \frac{(\vec{\nabla} \times \vec{A})^2}{2} + |\vec{D}\phi|^2 + a(T - T_c)|\phi|^2 + \frac{b}{2}|\phi|^4 + \dots , \tag{1.16}$$

where $\vec{D}(\vec{x}) = \vec{\nabla} - i\,2e\vec{A}(\vec{x})$ is the covariant derivative, $\vec{A}$ is the vector potential, and $\vec{B} = \vec{\nabla} \times \vec{A}$. Moreover, a and b are positive constants that can be derived from the microscopic theory and do not depend on the temperature. Note that the free energy is invariant under the $[U(1)]$ gauge transformation $\phi \to \exp(i\,2e\Lambda)\,\phi$ and $\vec{A} \to \vec{A} + \vec{\nabla}\Lambda$ where $\Lambda(\vec{x})$ is an arbitrary function. Also, one can show that the superconducting transition obtained in this mean-field approach is of second order.

A trademark of superconductivity is the Meissner effect in which an external magnetic field $\vec{B}$ that permeated the material before the superconducting transition is expelled from it as the temperature drops below T_c (see Fig. 1.2). It basically indicates that a configuration with a constant magnetic field inside the material is not favored energetically. The Meissner effect implies that the effective laws of electromagnetism inside the material should somehow change at T_c. Assuming that the system is homogeneous, the free energy $\mathcal{F}$ is minimized by $\phi = 0$ above T_c and by $\phi_0 \equiv |\phi| = \sqrt{-a(T - T_c)/b}$ below T_c. Therefore, below T_c the free energy is roughly

$$\mathcal{F} = \frac{(\vec{\nabla} \times \vec{A})^2}{2} + (2e\phi_0)^2\vec{A}^2 + \dots . \tag{1.17}$$

Now we have everything we need to explain the Meissner effect. The mass term for the gauge potential $\vec{A}$ indicates that the $[U(1)]$ gauge symmetry was spontaneously broken by the condensation of Cooper pairs below T_c. Note that we have fixed the gauge in Eq. (1.17). The electromagnetic $[U(1)]$ symmetry group has only one generator and, after fixing the gauge, the single Goldstone mode that appears as result of symmetry breaking is "eaten" by the photon, which in turn acquires a Meissner mass proportional to $(2e\phi_0)^2$.

Physically, it is observed that the magnetic field does not drop discontinuously from some nonzero value outside the superconductor to zero inside. In fact, the magnetic field leaks into the superconductor defining a length scale λ called the magnetic penetration depth. This length scale is determined by the competition between the energy in the magnetic field $\vec{B}^2 \sim \vec{A}^2/\lambda^2$ and the Meissner term $(2e\phi_0)^2\vec{A}^2$ in Eq. (1.17). Equating these contributions we obtain that $\lambda \sim (1/e\phi_0) = (1/e)\sqrt{-b/a\,(T_c - T)}$.

Similarly, the characteristic length scale over which the order parameter varies appreciably is known as the coherence length ξ, which is approximately given by $\xi \sim 1/\sqrt{-a\,(T_c - T)}$. The ratio $\kappa = \lambda/\xi$ plays a very important role in the theory of superconductivity. In fact, this parameter is used to classify superconducting materials into type I where $\kappa < 1/\sqrt{2}$ and type II where the reverse is true. These two groups behave differently in the presence of external magnetic fields.

Type-I superconductors cannot be penetrated by magnetic flux lines (Meissner effect). Ordinary superconductors, such as aluminum and niobium, are typical type-I superconductors.

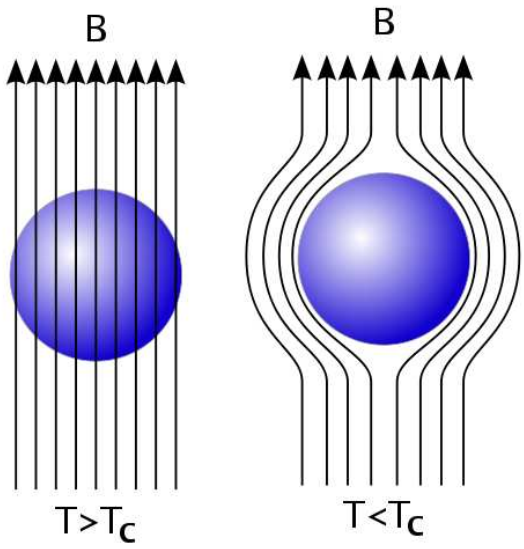

Figure 1.2: Magnetic field lines are excluded from a superconductor below its critical temperature.

On the other hand, a type-II superconductor is characterized by its gradual transition from the superconducting to the normal state. In a type-II superconductor, the coherence length is smaller than the London penetration depth, which means that magnetic flux lines can pierce the material in the form of vortices at strong enough external fields. These vortices can arrange themselves in a regular structure known as the Abrikosov vortex lattice [42].

Type-II superconductors are usually made of metal alloys or complex oxide ceramics, whereas type-I superconductors tend to be made of pure metals. While a type-I superconductor has its transition at a single critical temperature, a type-II superconductor has two critical temperatures that depend on the strength of the applied field. Above the lower temperature T_{c1} magnetic flux from external fields is no longer completely expelled and the superconductor exists in a mixed state consisting of normal and superconducting matter. Above the higher temperature T_{c2} superconductivity is completely destroyed and the system is again in the normal phase [43].

1.3.2 The Effect of Electromagnetic Fluctuations

In 1974 Halperin, Lubensky, and Ma [44] showed that the metal-superconducting phase transition becomes weakly first order once effects from the intrinsic fluctuating magnetic field are included. A similar analysis has been employed in the description of other important phenomena such as phase transitions in liquid crystals [45], transitions in the early universe [46], and the quantum Hall effect [47].

Halperin, Lubensky, and Ma used the free energy density functional $\mathcal{F}(\phi, \vec{A})$ in Eq. (1.16) to describe the interaction between the condensate ϕ of a type-I superconductor and the electromagnetic potential $\vec{A}$, which is taken to be in the Coulomb gauge, i.e., $\vec{\nabla} \cdot \vec{A} = 0$. Moreover, ϕ is assumed to be constant and the new free energy $F(\phi)$, which takes into account the thermal gauge field fluctuations, is defined by performing the functional integral over $\vec{A}$ as follows

$$e^{-F(\phi)/k_BT} = \int \mathcal{D}\vec{A}(\vec{r})\, e^{-\int d^3\vec{r}\ \mathcal{F}(\phi,\vec{A})/k_BT}. \tag{1.18}$$

Since $\mathcal{F}$ is quadratic in $\vec{A}$ the partition function above can be calculated exactly. It can be shown that

$$\frac{1}{2V}\frac{dF(\phi)}{d\phi} = a(T-T_c)|\phi| + b|\phi|^3 + 4e^2|\phi|\langle A^2\rangle_\phi, \tag{1.19}$$

where V is the volume of the system, and $\langle A^2\rangle_\phi$ is the expectation value of $\vec{A}^2(\vec{r})$ evaluated at a certain ϕ, which is

$$\langle A^2\rangle_\phi = 2k_BT_c\int_{k<\Lambda}\frac{d^3\vec{k}}{(2\pi)^3}\frac{1}{k^2+k_s^2}, \tag{1.20}$$

where Λ is the momentum cutoff. The momentum scale $k_s = 8e^2|\phi|^2$ is the inverse of the magnetic penetration depth. If ϕ is such that k_s is much smaller than Λ we have

$$\langle A^2\rangle_\phi = \frac{k_BT_c\,\Lambda}{\pi^2} - \sqrt{2}\,\frac{e\,k_BT_c}{\pi}|\phi|. \tag{1.21}$$

The first term in the equation above leads to a slight renormalization of the mean-field critical temperature T_c. The second term is more interesting because it leads to a term proportional to $|\phi|^3$ in $F(\phi)$ that has a negative sign. This term changes the order of the superconducting phase transition into first order because $F(\phi)$ has a minimum at $\phi \neq 0$ when T is still slightly larger than T_c.

We note in passing that the metal-superconducting phase transition has also been studied using Monte Carlo simulations of the Ginzburg-Landau model (see for instance Ref. [48]).

1.4 A Glimpse into Superfluidity

The element helium has two stable isotopes: ^{3}He and ^{4}He. In contrast to classical liquids that always crystallize at sufficiently low temperatures, these isotopes are known as quantum liquids because they remain liquified at temperatures very close to the absolute zero (they can solidify under pressure). This unique behavior appears because of the weak interactions among the atoms, which have a closed $1S$ electron shell, and the large zero-point oscillations produced by their small atomic mass [49].

Since ^{4}He atoms are bosons they tend to occupy the same single-particle state at very low temperatures, which leads to the formation of a Bose-Einstein condensate, and, consequently, superfluidity. ^{4}He superfluidity was observed in 1938 by Kapitza [50] and its singular properties have been studied in detail since then [51].

The ^{4}He superfluid transition is marked by a peak in specific heat at $T_\lambda = 2.17$ K, known as the $\lambda-$point, which behaves like $\ln|T-T_c|$ on both sides of the transition. This singularity is generally thought to represent the onset of Bose-Einstein condensation. In the superfluid state, ^{4}He displays remarkable hydrodynamic properties. For instance, it can flow through fine channels with no pressure drop, which seems to imply that it has zero viscosity. However, a direct measurement of the viscosity, using for example a rotating cylinder viscometer, shows that the viscosity is nonzero and has a value comparable with the viscosity above T_λ. This was explained

by Tisza [52] and Landau [53] using a two-fluid model in which ^{4}He consists of a mixture of two interpenetrating fluids: the superfluid with density ρ_s and velocity $\vec{v}_s$ and the normal fluid with density ρ_n and velocity $\vec{v}_n$. The superfluid consists of a perfect background liquid with zero entropy and viscosity and some type of phonon-like excitations. Also, the superfluid is taken to be irrotational, i.e.,

$$\vec{\nabla} \times \vec{v}_s = 0, \tag{1.22}$$

and the total density of the Bose liquid is given by $\rho = \rho_s + \rho_n$. The nonzero viscosity observed in the experiments is easily understood within the two-fluid model. In fact, since the normal fluid behaves as an ordinary fluid it provides the measured viscosity of ^{4}He.

The two-fluid description indicates that the system's motion can be decomposed into a center of mass motion (where the two components move in phase) and another type of propagation where the density at any point is essentially constant but the difference between the superfluid and normal fluid densities is not. This leads to a new kind of wave propagation known as second sound, which corresponds to temperature-dependent phonon density waves. These waves are excited by heat rather than pressure pulses. It should be emphasized, however, that the separation between normal and superfluid components used in the two-fluid model does not actually mean that the quantum liquid can be physically divided into two separate parts.

At low temperatures the only quasiparticles present in the system are the long-wavelength phonons and, thus, the excitation energy is $E_k \sim k$. The characteristic momenta of these excitations correspond to wavelengths that are large in comparison to the interatomic distance. In general, a linearly dispersing mode implies superfluidity. This can be seen from the following argument [2, 54].

Consider a mass M of fluid flowing down a tube with a certain velocity $\vec{v}$. The creation of an excitation with momentum $\vec{k}$ such that $M\vec{v} = M\vec{v}\,' + \vec{k}$ slows down the fluid to a velocity $\vec{v}\,'$. However, this is only possible if there is enough energy to be spared, i.e.,

$$\frac{1}{2}Mv^2 \geq \frac{1}{2}Mv'^2 + \omega(k). \tag{1.23}$$

After eliminating M we obtain that $v \geq \omega(k)/k$. For a linear dispersion relation this gives a critical velocity $v_c = \omega/k \equiv u$ (where u does not depend on k) below which the fluid cannot lose momentum, which then establishes the onset of superfluidity.

In a gas of noninteracting bosons one can excite any given boson with momentum $\vec{k}$ at the energy cost of only $k^2/2m$. There exists an infinite number of ungapped excitations in the quasiparticle spectrum. However, after superfluidity sets in there are fewer low energy excitations. Recall that the density of states at a given energy is $N(E) \propto k^{D-1}(E)\, dk/dE$. For example, when $D = 3$ we have $N(E) \propto \sqrt{E}$ for quadratically divergent modes, while $N(E) \propto E^2$ for linear modes at low energies. The unusual properties of superfluids result not from the presence of gapless excitations but rather from the scarcity of gapless excitations. There are just too few modes with which the superfluid can lose energy and momentum to.

For momenta larger than a certain k_r the spectrum is dominated by another kind of quasiparticles called rotons. The function E_k can be expanded in powers of $k - k_r$ in the region

around k_r

$$E_k = \Delta + \frac{(\vec{k} - \vec{k}_r)^2}{2m}, \tag{1.24}$$

where Δ and m are constants.

The number of phonons in a Bose liquid goes to zero as $T \to 0$. At low temperatures their density is very small and the system behaves as a non-interacting Bose gas. The thermodynamic quantities of this system at very low temperatures can then be easily calculated. For instance, the specific heat behaves as T^3, which is in accordance with experiments.

The lighter isotope ^{3}He has one less neutron than ^{4}He, so it is a fermion. Arbitrarily weak interactions between ^{3}He atoms provided by the van der Waals force will trigger the formation of atomic Cooper pairs leading to superfluidity. Superfluid ^{3}He was experimentally observed for the first time in 1972 at temperatures around $T_c = 2\,\mathrm{mK}$ [55], which is at least three orders of magnitude smaller than ^{4}He's T_λ. The rich phase structure of superfluid ^{3}He was studied by Leggett in 1975 [56]. Several aspects relevant for the description of ^{3}He's superfluid properties can be directly applied to understand spin-one color superconductivity [57].

The occurrence of superfluidity in fermionic systems may suggest that superfluidity is nothing but a different type of superconductivity where the Cooper pairs are chargeless. However, in superfluids the atomic interaction potential becomes repulsive for short mutual distances, which means that ^{3}He Cooper pairs have a total angular momentum of $L = 1$ (p-wave state). Thus, since the total Cooper pair wave function has to be antisymmetric we see in superfluid ^{3}He that the atoms pair in the $S = 1$ spin state, while ordinary electronic Cooper pairs have spin zero.

1.4.1 Rotating Superfluids

The superfluid is incompressible, i.e., $\vec{\nabla} \cdot \vec{v}_s = 0$ when v_s is much smaller than the speed of sound. In this case Eq. (1.22) implies that

$$\vec{v}_s = \frac{\vec{\nabla}\varphi}{m}, \qquad \nabla^2\varphi = 0. \tag{1.25}$$

This has some very important consequences. Consider a cylinder rotating around its symmetry axis with an angular velocity $\vec{\omega}$ and filled with superfluid helium (see Fig. 1.3). This can be obtained experimentally by starting with solid helium in a can under pressure larger than 25 atm at $T \sim 0$ K and rotating it. After the pressure is released the solid melts and then liquid helium is rotating with the angular momentum initially given to the solid. What is then the final state of helium?

Assuming that the superfluid is not spilling out of the cylinder, i.e., $\partial\varphi/\partial n = 0$ ($\vec{n}$ is the normal vector perpendicular to the surface) then φ is a constant and $\vec{v}_s$ vanishes for any $\vec{\omega}$. The assumption that the fluid is irrotational implies that the shape of the free liquid surface should be given by the equation

$$z = \frac{\omega^2 r^2}{2g}\frac{\rho_n}{\rho}, \tag{1.26}$$

where g is the acceleration due to gravity. Note that the factor ρ_n/ρ leads to a temperature dependent height $z = z(T)$. The validity of the equation above was tested by Osborne [58] who

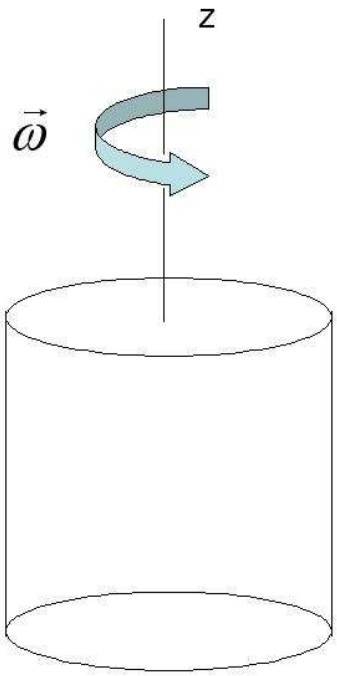

Figure 1.3: Rotating can filled with superfluid helium.

found instead that the free surface was that of an ordinary classical fluid

$$z_{cl} = \frac{\omega^2 r^2}{2g}, \tag{1.27}$$

which is independent of the temperature. In order to explain this discrepancy we have to reexamine Eq. (1.22). Cylindrically symmetric solutions of this equation are of the form

$$\vec{v}_s = \frac{C}{r}\hat{\theta}, \tag{1.28}$$

where C is a constant and $\vec{r} = (r, \theta)$ is a vector on the $x - y$ plane. If Eq. (1.22) is valid everywhere, including the origin, C must be zero. This contradicts the result in Eq. (1.27) and Feynman [60] showed that this apparent paradox could be solved by assuming that $\vec{\nabla} \times \vec{v}_s$ becomes singular at some isolated points in the fluid. This singularity is characterized by the circulation of the fluid

$$\Gamma = \oint d\vec{l} \cdot \vec{v}, \tag{1.29}$$

with which the corresponding symmetric solution becomes that of a rectilinear vortex parallel to the z axis

$$\vec{v}_s = \frac{k}{2\pi r}\hat{\theta}. \tag{1.30}$$

In this case the rotating superfluid contains a uniform array of parallel vortices distributed with a density of $2\omega/\Gamma$ per unit area (see Fig. 1.4). Note that the average superfluid velocity field is indistinguishable from a uniform rotation $\vec{v} = \vec{\omega} \times \vec{r}$ because both flow patterns give the same circulation around any macroscopic contour much larger than the intervortex spacing. Thus, adding the contribution from the superfluid one can obtain the correct result in Eq. (1.27).

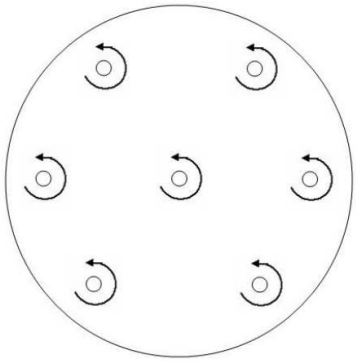

Figure 1.4: Rotating can seen from above with all vortices turning in the direction.

Onsager [59] and Feynman [60] independently showed that the circulation in superfluid helium defined in Eq. (1.29) is quantized in units of

$$\Gamma = \frac{2\pi}{m} = 0.997 \times 10^{-3}\text{cm}^2/\text{s}, \tag{1.31}$$

which was experimentally verified in the early 60's [61]. The energy per unit length of vortex line is given by

$$\varepsilon_v = \frac{1}{2}\int d^2\vec{r}\,\rho_s v_s^2 = \frac{\rho_s\Gamma^2}{4\pi}\int \frac{dr}{r} \simeq \frac{\rho_s\Gamma^2}{4\pi}\ln\frac{R}{\xi}, \tag{1.32}$$

where R is the radius of the cylinder and ξ is the radius of the vortex core. For $R \sim 1$ cm experiments indicate that $\xi \sim 1$ Å [49].

1.5 Color Superconductivity

The cold, ultradense inner core of neutron stars may be the only place in the universe where the ground state of strongly interacting baryonic matter is in a state with deconfined quarks and gluons [62]. Strongly interacting quark matter has been recently observed at RHIC [14] but the temperatures and densities involved are very different than those expected in compact stars. There the density can be several times larger than the nuclear saturation density. Studies using effective models for the strongly coupled limit of quantum chromodynamics [63, 64] as well as ab initio calculations performed in weak coupling [65, 66, 67, 68, 69, 70, 71, 72, 73, 74, 75, 76, 77] predict a phase transition between normal and color-superconducting (CSC) quark matter at high baryon densities and sufficiently low temperatures (for early papers on color superconductivity see Ref. [78] and for recent reviews see Ref. [79]). Therefore, it is expected that the inner region of compact stars may consist of color-superconducting matter. The presence of color superconductivity in compact stars still needs to be experimentally verified, however, a number of possible astrophysical signatures have been proposed in the last years [80, 81, 82]. Here we give a short review of some of the most important concepts and ideas behind the phenomenon of color superconductivity. For a very detailed discussion see Ref. [9].

The existence of color superconductivity in cold and dense quark matter can be rigorously proven at asymptotically high densities. The main argument stems from the fact that due to asymptotic freedom [12] when $\mu \gg \Lambda_{\rm QCD}$ the QCD coupling constant computed at the scale μ becomes small, $g(\mu) \ll 1$, and the dominant interactions between quarks is given by single-gluon exchange, which is attractive in the color-antitriplet channel. This can be seen directly from the scattering amplitude for single-gluon exchange in an $[SU(N_c)]$ gauge theory, which is proportional to

$$(T_a)_{ki}\,(T_a)_{lj} = -\frac{N_c+1}{4N_c}\,(\delta_{jk}\,\delta_{il} - \delta_{ik}\,\delta_{jl}) + \frac{N_c-1}{4N_c}\,(\delta_{jk}\,\delta_{il} + \delta_{ik}\,\delta_{jl})\ , \tag{1.33}$$

where i, j are the fundamental colors of the two quarks in the incoming channel, and k, l are their respective colors in the outgoing channel. The first term is antisymmetric, while the second is symmetric under the exchange of the color indices of either the incoming or the outgoing quarks. For $[SU(3)_c]$ Eq. (1.33) describes the coupling of two fundamental color triplets to an antisymmetric color antitriplet and a symmetric color sextet,

$$[\mathbf{3}]^c \times [\mathbf{3}]^c = [\bar{\mathbf{3}}]^c_a + [\mathbf{6}]^c_s\ . \tag{1.34}$$

The antitriplet contribution in Eq. (1.33) contains a minus sign, which means that this channel is attractive. On the other hand, the sextet channel has a positive sign and corresponds to a repulsive channel. Therefore, the quarks located at the Fermi surface experience an attractive interaction that, according to Cooper's theorem, causes an instability that can only be cured by the formation of diquark Cooper pairs. Since quarks have color degrees of freedom this phenomenon is called color superconductivity [78]. The diquark condensate Φ is the order

parameter that describes the transition, i.e., $\Phi = 0$ corresponds to the normal phase and $\Phi \neq 0$ to the color-superconducting phase.

Electromagnetism is an Abelian theory with spin-1 bosons. Without the lattice contribution present in superconducting materials, equally charged fermions would never experience an attractive interaction. Ordinary superconductivity arises because of the effective attractive interaction between electrons due to the exchange of lattice phonons. This interaction can be very complicated and, in fact, the exact microscopic mechanism necessary to explain high-T_c electronic superconductivity remains unknown. In contrast, color superconductivity appears as a direct consequence of asymptotic freedom, which is a well-known property of QCD.

The densities that can actually occur in the core of compact stars correspond to quark chemical potentials that are probably not much larger than 500 MeV and, therefore, $g \geq 1$. This then implies that single-gluon exchange is not the dominant interaction. Whether or not the matter in the core of compact stars is dense enough so that quark matter is a color superconductor is a question that still remains. Nevertheless, calculations in the framework of the Nambu-Jona-Lasinio (NJL) model [63, 64] show that color superconductivity does seem to occur also at moderate densities where QCD interactions are strongly coupled. In this case, the attractive interaction could be mediated by the exchange of instantons.

Since quarks have both color and flavor degrees of freedom the total number of ways in which two quarks can pair can be very large. The total wave function of a Cooper pair must be antisymmetric under the exchange of the paired quarks. Consequently, the possible color and flavor representations involved in the formation of the diquark state have to be chosen in order to satisfy the Pauli exclusion principle. This requirement helps to classify all possible diquark condensates [9, 83]. For ultrarelativistic particles only the total spin $J = L + S$ is a good quantum number. Thus, possible Cooper pair wave functions are classified according to their total spin J.

Current masses for the first three light quarks are $m_u \simeq 5$ MeV, $m_d \simeq 9$ MeV, and $m_s \simeq 100$ MeV [23]. The masses of the other three quarks are so large that they do not need to be taken into account to correctly describe the properties of matter in the central regions of compact stars. The symmetries defining the various color-superconducting phases depend on the masses and charges of the quarks. If the chemical potential is so large that up, down, and strange quarks can be considered as truly ultrarelativistic particles ($m/\mu \ll 1$) the ground state of quark matter corresponds to the color-flavor locked phase [84]. In this case the quarks pair in the $J = 0$ channel and this phase is characterized by the condensation of quark Cooper pairs in the color-antitriplet, flavor-antitriplet representation, which breaks down the normal phase's initial symmetry group $[SU(3)]_C \otimes SU(3)_L \otimes SU(3)_R \otimes U(1)_B \otimes U(1)_A$ into the diagonal $SU(3)_{R+L+C}$ subgroup. After considering that all the gluons acquire color Meissner masses we see that ten Goldstone bosons appear due to this symmetry breaking. The excitation spectrum in the CFL state is very similar to the one in the hadronic phase. In fact, it has been conjectured that since the symmetries of CFL quark matter are not different than those in $SU(3)_V$ flavor-symmetric hadronic matter, there is no need for a phase transition separating these two phases [85].

When discussing gauge symmetries it is important to remark that they cannot be truly spontaneously broken [86]. However, after fixing the gauge, spontaneous symmetry breaking can occur as it does in ordinary superconductivity (see Sec. 1.3.1). In the standard model of electroweak interactions the Higgs field breaks down the initial symmetry group $[SU(2)]_\ell \otimes$

$[U(1)]_Y$ into $[U(1)]_{em}$. Analogously, the presence of quark Cooper pairs breaks the $[SU(3)]_C$ color symmetry.

In the CFL phase the quark Cooper pair condensate has the form

$$\Phi_{ij}^{fg} = \epsilon_{ijk}\,\epsilon^{fgh}\,\Phi_k^h \tag{1.35}$$

where $\Phi_k^h = \delta_k^h\,\phi$. In the equation above, $i,j = 1,2,3$ and $f,g = 1,2,3$ denote color and flavor indices, respectively. The non-vanishing order parameter implies that both color ($[SU(3)]_C$) and flavor ($SU(3)_V$) symmetries are broken. A similar situation is found in superfluid ^{3}He [87] where Cooper pairs are formed with spin $S = 1$ and angular momentum $L = 1$. Accordingly, there the order parameter breaks the global $SO(3)$ symmetries corresponding to spin and angular momentum.

The CFL condensate has some very interesting properties. For instance, it is a baryon superfluid but not an electromagnetic superconductor. In fact, when it comes to the electromagnetic properties of quarks in the CFL phase the system is more adequately described as an isotropic electromagnetic insulator (although electron-positron pairs can be thermally excited and contribute to the total conductivity [88]). In conventional superconductivity the gauge symmetry of electromagnetism is spontaneously broken by the condensation of electron Cooper pairs. This process gives an effective mass to the photon that screens external magnetic fields (electromagnetic Meissner effect). On the other hand, in color superconductors the initial $[U(1)]_{em}$ symmetry, whose generator coincides with one of the vector-like generators of $SU(3)_L \otimes SU(3)_R$, is not really broken but "rotated" [84]. This new group, denoted here as $[\widetilde{U}(1)]_{em}$, is described by a massless linear combination of the photon and the eighth gluon and is analogous to the electromagnetic $[U(1)]_{em}$ symmetry that remains unbroken after the electroweak symmetry breaking. Using the convention adopted in Ref. [89], it can be shown [84, 90] that the "rotated" electric $\widetilde{Q}$-charges of the quarks are

s_b	s_g	s_r	d_b	d_g	d_r	u_b	u_g	u_r
0	0	-	0	0	-	+	+	0

(1.36)

in units of the $\widetilde{Q}$-charge $\widetilde{e} = e\cos\theta$ where θ is the mixing angle. In color-flavor space the associated charge operator $\widetilde{Q}$ is given by

$$\widetilde{Q} = Q_f \otimes 1_c - 1_f \otimes Q_c \tag{1.37}$$

where $Q_c = -\lambda_8/\sqrt{3} = \mathrm{diag}(-1/3, -1/3, 2/3)$.

Several other color-superconducting phases have been studied in the last years [9, 79]. For instance, when only up and down quarks are taken into account the most simple representation is the antisymmetric flavor singlet $[\mathbf{1}]_a^f$ representation of the $SU(2)_V$ flavor group. In this case, the simplest $J = 0$ quark Cooper pair condensate is given by

$$\Phi_{ij}^{fg} = \epsilon_{ijk}\,\epsilon^{fg}\,\Phi_k \tag{1.38}$$

where $i,j = 1,2,3$ are the color indices, while $f,g = 1,2$ are the corresponding flavor indices. The condensate in Eq. (1.38) describes the so-called 2-flavor color-superconducting (2SC) phase.

A system containing a single quark flavor cannot have Cooper pairs in the spin-zero channel. However, quarks can also pair in the $J = 1$ channel [91]. This channel corresponds to the symmetric $[\mathbf{3}]^J_s$ representation of the $SU(2)_J$ spin group. If one still assumes that the pairing occurs in the color $[\bar{\mathbf{3}}]^c_a$ channel, the Cooper pair wave function is overall antisymmetric. The condensate is a 3-vector in space which points in the direction of the spin of the Cooper pair. It has the form [69, 78, 92, 93]

$$\Phi^a_{ij} = \epsilon_{ijk}\,\Phi^a_k \tag{1.39}$$

where $a = x, y, z$ denotes the spatial component of the spin vector. Condensation breaks the local color $[SU(3)]_C$ symmetry and the global $SO(3)_J$ spin symmetry. This is similar to superfluid ^{3}He where the condensation of Cooper pairs breaks the group $SO(3)_S \otimes SO(3)_L$ as discussed above. Many different phases can be appear in this case. Two of the most important phases are the color-spin locked (CSL) phase, which has the order parameter

$$\Phi^i_j = \delta^i_j\,\Phi \tag{1.40}$$

and the polar phase where

$$\Phi^i_j = \delta_{j3}\,\delta^{iz}\,\Phi\ . \tag{1.41}$$

The order parameter of the CSL phase is very similar to the CFL order parameter in Eq. (1.35) because all quark colors participate in the pairing and the symmetry breaking pattern is also similar, $[SU(3)]_C \otimes SO(3)_J \times U(1)_V \otimes [U(1)_{em}] \to SO(3)_{C+J}$. All eight gluons become massive in the CSL phase. Moreover, CSL superconductors are also ordinary superconductors since the photon gains a mass [94].

The pattern of symmetry breaking that defines the polar phase is given by $[SU(3)]_C \otimes SO(3)_J \otimes U(1)_V \to [SU(2)]_C \otimes SO(2)_J \otimes \tilde{U}(1)$. The residual $[SU(2)]_C$ color symmetry is the local symmetry that corresponds to the three massless gluons that remain after symmetry breaking. The other five gluons become massive. Two true Goldstone bosons appear due to the breaking down of the rotational $SO(3)_J$ symmetry into $SO(2)_J$. Additionaly, we see that the baryon number is not broken but just "rotated". Furthermore, it can be shown that if there is only a single flavor present or if all flavors have the same electric charge a "rotated" electromagnetic $[\tilde{U}(1)]_{em}$ symmetry exists, while if there are at least two flavors with different charges the $[U(1)_{em}]$ symmetry is broken [9].

In general, the quark quasiparticle dispersion relations in the color-superconducting state are modified by the presence of a gap in the excitation spectrum. For massless quarks the dispersion relations are

$$E^a_{k,r}(\phi^a) = \left[(a|\vec{k}| - \mu)^2 + \lambda_r\,|\phi^a(T,\mu,\vec{k})|^2\right]^{1/2}\ . \tag{1.42}$$

Different sets of excitation branches are described by λ_r, $a = +$ ($a = -$) labels states with positive (negative) energies and the gap function ϕ^a depends on the temperature T, chemical potential μ, and momentum $\vec{k}$. A common approximation is to assume that the gap depends only on the temperature. The presence of an energy gap at the Fermi surface, $k = \mu$, means that in the superconducting state one has to give an extra amount of energy of the order of $2\,\phi$ in order to excite quasiparticle–quasiparticle-hole pairs on the Fermi surface. No extra energy is necessary in order to excite particle-hole pairs at the Fermi surface in a non-interacting system.

Therefore, we see that in general the superconducting state is energetically favored in comparison to the normal conducting state [49].

The CFL and CSL phases have two different excitation branches with two different gaps at the Fermi surface: $E^{+}_{\mu,1}(\phi) = 2\,\phi$ and $E^{+}_{\mu,2}(\phi) = \phi$. We can see that in these phases it costs twice the amount of energy to excite quasiparticle excitations from the first branch than from the second. In the 2SC and polar phases one of the two excitation branches is gapless, i.e., $E^{+}_{\mu,2} = 0$.

Since quarks have different electric charges, the pattern of symmetry breaking can also change in the presence of strong external magnetic fields. The physical upper limit for the magnetic field in a gravitationally bound star is $B \simeq 10^{18}$ G, which is obtained by comparing magnetic and gravitational energies. However, if quark stars are self-bound rather than gravitationally bound objects, this upper limit could be even higher [95]. In this case, the symmetries of the normal phase change because only s and d quarks have the same electric charge and for massless quarks the $SU(3)_L \otimes SU(3)_R$ initial symmetry changes into $SU(2)_L \otimes SU(2)_R$.

The typical energy scale defined by these strong fields is of the same order of magnitude as the color-superconducting gap present in the quasiparticle energy spectrum. Thus, one then naturally expects that strong magnetic fields should affect the diquark pairing. The first step in this direction was presented in Ref. [96] where it was observed that, since color-flavor locked (CFL) superconductors do not experience the electronic Meissner effect, a "rotated" strong magnetic field $\widetilde{H}$ that penetrates the system can affect the pairing and eventually lead to a new phase, the so-called magnetic color-flavor locked (mCFL) phase. The pattern of symmetry breaking that defines the mCFL phase is given by $[SU(3)]_C \otimes SU(2)_L \otimes SU(2)_R \otimes U(1)_B \otimes U(1)_A \otimes U(1)^{-}_{A} \to SU(2)_{R+L+C}$ where $U(1)^{-}_{A}$ corresponds to an anomaly-free current formed by a linear combination of s, d, and u axial currents [97]. Note that in this case there are only five Goldstone bosons as the result of symmetry breaking and all of them are chargeless. More details about mCFL superconductors are given in Chapter 3.

1.5.1 Resummation Schemes at Nonzero Temperature and Density

Temperature (density) corrections cannot generate new ultraviolet divergences that are different than those already present in the theory in the vacuum [21, 22]. However, as was already mentioned in Sec. 1.2, at nonzero temperatures naive perturbation theory breaks down due to the odd infrared behavior displayed by gauge theories. It can be shown [9] that loop calculations involve dressed gluon propagators that have terms of the form

$$\mathcal{D}(\omega, \vec{p}) \sim \frac{1}{\omega^2 - p^2 + \Pi(\omega, \vec{p})} \,, \tag{1.43}$$

where $\Pi(\omega, \vec{p})$ is the one-loop gluon self-energy (the specific details about the Lorentz and color structures of the gluon propagators are not particularly important in this discussion). The leading-order terms in the calculation of Π result from the contribution of states with momenta $k \sim T$ (or μ at $T = 0$) in the loop. Once the powers of the coupling constant arising from the vertices are taking into account we have $\Pi \sim g^2 T^2$ (or $\sim g^2 \mu^2$ at $T = 0$). Thus, as long as either ω or p are hard, i.e., of order T, the self-energy Π in the propagator (1.43) does not need to be included. However, when ω and p are soft, i.e., of order gT, Π is of the same order of magnitude as the other terms in the denominator and, therefore, cannot be neglected. In other words,

soft processes are described using the dressed propagator (1.43), while processes involving hard energy or momentum can be described by the simple bare propagator

$$D(\omega, \vec{p}) \sim \frac{1}{\omega^2 - p^2} \ . \tag{1.44}$$

This is the basic idea behind the hard-thermal-loop (HTL) resummation scheme [22, 100] and its equivalent at $T = 0$ and $\mu \neq 0$, which represents the hard-dense-loop (HDL) resummation scheme [101]. For a more detailed discussion about these methods see Refs. [9, 22].

It is now simple to see why the presence of the additional energy scale T (or μ, at $T = 0$) in the theory invalidates the naive perturbative scheme. Imagine that we have a process that involves a diagram with n vertices. Each vertex contributes with a factor of g. A straightforward application of perturbation theory would obtain that this diagram is of order $\mathcal{O}(g^n)$. However, let us consider the case where there is a loop in this diagram where the dominant contribution comes from the region of soft momenta, i.e., $k \sim gT$. The contribution of the propagator in Eq. (1.43) is then $\sim 1/(g^2T^2)$ instead of $\sim 1/T^2$. This means that two powers of g are actually canceled out and, therefore, the diagram is of order $\mathcal{O}(g^{n-2})$. Therefore, we see that power counting becomes problematic in these theories.

Finally, let us remark that in gauge theories also the vertices may need to be HTL (HDL) resummed in order to obtain the correct Ward identities.

1.5.2 The Color-Superconducting Gap in Weak Coupling

One way in which color superconductivity differs from BCS theory is the condensate's dependency on the coupling constant. In theories with short-range interactions, such as BCS theory, the gap's dependence on the coupling constant g is in the form of exponential of $1/g^2$. However, in QCD static color-magnetic interactions are not screened to any finite order in g [65, 66, 67, 69, 102] and, thus, the scattering of quarks near the Fermi surface is logarithmically enhanced by the emission of collinear, nearly static magnetic gluons. For a detailed discussion on the derivation of the gap equation in color superconductivity see Ref. [9]. It suffices here to consider the general form of the gap equation in weak coupling at $T = 0$

$$\phi = g^2\,\phi\left[\zeta\,\ln^2\left(\frac{\mu}{\phi}\right) + \beta\,\ln\left(\frac{\mu}{\phi}\right) + \alpha\right], \tag{1.45}$$

which is derived within the mean field approximation, and has the solution

$$\phi = 2\,b\,\mu\,\exp\left(-\frac{c}{g}\right)\left[1 + \mathcal{O}(g)\right] \ . \tag{1.46}$$

The exchange of almost static, long-ranged magnetic gluons gives the leading-order contribution to ϕ, which corresponds to the first term on the right-hand side of Eq. (1.45). This contribution is of leading order because, according to Eq. (1.46), $g^2\ln^2(\mu/\phi) \sim 1$. The coefficient ζ determines the constant c in the exponent in Eq. (1.46)

$$c = \frac{3\pi^2}{\sqrt{2}} \ , \tag{1.47}$$

which was first computed by Son [65]. The coefficient β determines the prefactor b in Eq. (1.46). The second term in Eq. (1.45) corresponds to a contribution of subleading order because $g^2 \ln(\mu/\phi) \sim g \ll 1$. This term appears due to the quark wave-function renormalization in dense quark matter [102, 103] and also because of the exchange of electric and non-static magnetic gluons [66, 67, 68, 69]. The coefficient α determines the $\mathcal{O}(g)$ corrections to the prefactor in the color-superconducting gap parameter in Eq. (1.46) [104]. The energy gap in the CFL phase at $T = 0$ reads [9]

$$\Delta(0) = 2^{-\frac{1}{3}} \pi e^{-\gamma} T_c \,, \tag{1.48}$$

whereas the critical temperature is given by

$$\ln \frac{T_c}{\mu} = -\frac{3\pi^2}{\sqrt{2}g} + \ln \frac{2048\sqrt{2}\pi^3}{9\sqrt{3}g^5} + \gamma - \frac{\pi^2+4}{8} + \mathcal{O}(g) \,, \tag{1.49}$$

and g is the QCD running coupling constant at the scale given by the chemical potential μ.

This formula correctly describes ϕ at asymptotically large densities where $\mu \gg \Lambda_{\rm QCD}$ and $g \ll 1$. Note that, although perturbation theory was used to obtain Eq. (1.46), ϕ cannot be expanded in powers of g. This nonperturbative dependence on the coupling constant is encoded in the gap equation (1.45).

In the core of neutron stars the quark chemical potential is very high but not asymptotically large, which means that quarks and gluons do not weakly interact. However, an extrapolation of the weak-coupling results above to reasonable densities produces gaps that are in agreement with those obtained within NJL-type models, which are between $10 - 100$ MeV.

1.5.3 Color Superconductivity Continued ...

We have discussed so far the idealized case where all the quarks involved in the pairing are massless. This is certainly a good approximation at asymptotically large densities where the quark chemical potential μ is very large in comparison to the quark masses m_q, i.e., $m_q/\mu \ll 1$. In this idealized case the CFL state is likely to be the true ground state of quark matter. However, this approximation definitively breaks down at the moderate, though large, densities present in the inner regions of neutron stars because there $\mu \sim 500$ MeV, which is not much larger than the strange quark mass $m_s \sim 100$ MeV. Taking into account the effects of nonzero quark masses on the pairing leads to several important consequences.

First, recall that a system containing only massless up, down, and strange quarks is already color and charge neutral. This can be immediately understood because such a system has an equal number of up, down, and strange quarks with the colors red, green, and blue, which ensures neutrality with respect to color and electric charge. Also, this configuration is automatically in $\beta-$equilibrium. However, once the particles are massive the number densities of up, down, and strange quarks are no longer equal, which in turn leads to the presence of nonzero electric and color charges in the system. Consequently, chemical potentials for electric and color charges have to be introduced to ensure overall electric and color neutrality [105]. Also, the Fermi surface corresponding to strange quarks becomes different than that of the lighter quarks (we are assuming that $m_u \simeq m_d \ll m_s$). The mismatch in the Fermi surface of different quark species can be shown to be proportional to the electric and color chemical potentials as well as

their mass difference [9]. In Ref. [106] the phase diagram of dense, locally neutral three-flavor quark matter was studied within the framework of the NJL model.

The fact that in this case different flavors have different Fermi surfaces directly affects the way the quarks can pair. Usual BCS-like Cooper pairs are formed by fermions located on the Fermi surface with momenta in opposite directions. The total momentum of the Cooper pair is zero. However, as the Fermi surface mismatch increases it becomes more and more difficult to form pairs with zero total momentum. In fact, color superconductivity persists as long as the gain in free energy due to condensation is larger than the energy necessary to find a matching fermion in the Fermi sea of the other species. When the mismatch is as large as the value of the gap on the Fermi surface the color-superconducting state becomes energetically disfavored in comparison to a state consisting of unpaired quarks [107]. The restoration of the normal conducting state is not the only possible outcome. In fact, the system can lower its energy by using some unconventional color-superconducting pairing that can include gapless excitations, spatial inhomogeneity, and also counter-propagating currents [108].

Examples of unconventional pairing scenarios can be found in Refs. [109, 110]. In condensed matter systems in the presence of an external magnetic field the electron energy depends on the spin projection (Zeeman effect) and, consequently, there are two different Fermi momenta for spin-up and spin-down electrons. A superconducting state may be formed in which the Cooper pairs carry nonzero total momentum leading to a spatially inhomogeneous order parameter. This pairing describes the so-called Larkin-Orchinnikov-Fulde-Ferrell (LOFF) phase [111]. Note that the LOFF state breaks translational invariance. In color superconductivity the LOFF pairing has also been suggested as an alternative to ordinary Cooper pairing [112].

Gapless phases have quasiparticle spectra where the gap parameter ϕ vanishes for certain values of the quasiparticle momentum k. The fact that 2SC superconductors can have gapless excitations was first pointed out by Shovkovy and Huang in Ref. [113] and the consequent stability problems created by the presence of these excitations were discussed in Ref. [114]. In fact, the 2SC phase is unstable because the Meissner screening masses of some gluons become imaginary [114]. In this case the instabilities occur when the ratio of the gap ϕ over the chemical potential mismatch ($\delta\mu$) is smaller than $\sqrt{2}$. Gapless color superconductivity also occurs in three-flavor quark matter. In fact, gapless CFL quark matter and its stability problems have been discussed in Refs. [115].

It has been proposed that the chromomagnetic instability in two-flavor quark matter can be fixed by the formation of a single plane-wave LOFF state [116, 117, 118, 119]. Moreover, a gluonic phase with vector condensation in the ground state has also been suggested [120, 121, 122, 123] and, in Ref. [124], it was shown that this phase is favored over the single plane-wave LOFF phase for a wide range of coupling strengths. Other alternatives include the use of a mixed phase [125]. Finally, in the case of three-flavor quark matter phases with spontaneously induced meson supercurrents [126] have also been discussed.

1.6 Detecting Color Superconductivity in Neutron Stars

Neutron stars were discovered almost four decades ago and since then there has been a wealth of experimental data that has elucidated the behavior of matter at high densities. The typical

density inside a neutron star is comparable to the nuclear saturation density, $\rho_{\rm nuclear} = 2.5 \times 10^{14}$ g cm^{-3}, which corresponds to a baryon number density of $n_0 \simeq 0.15$ fm^{-3}. At the center of the star the interparticle distances become as small as the intrinsic size of hadrons (roughly 1 fm) and, under these extreme conditions, new states of matter consisting of deconfined quark matter can arise. For a review of recent theoretical developments and observational constraints concerning the physics of neutron stars see Ref. [127].

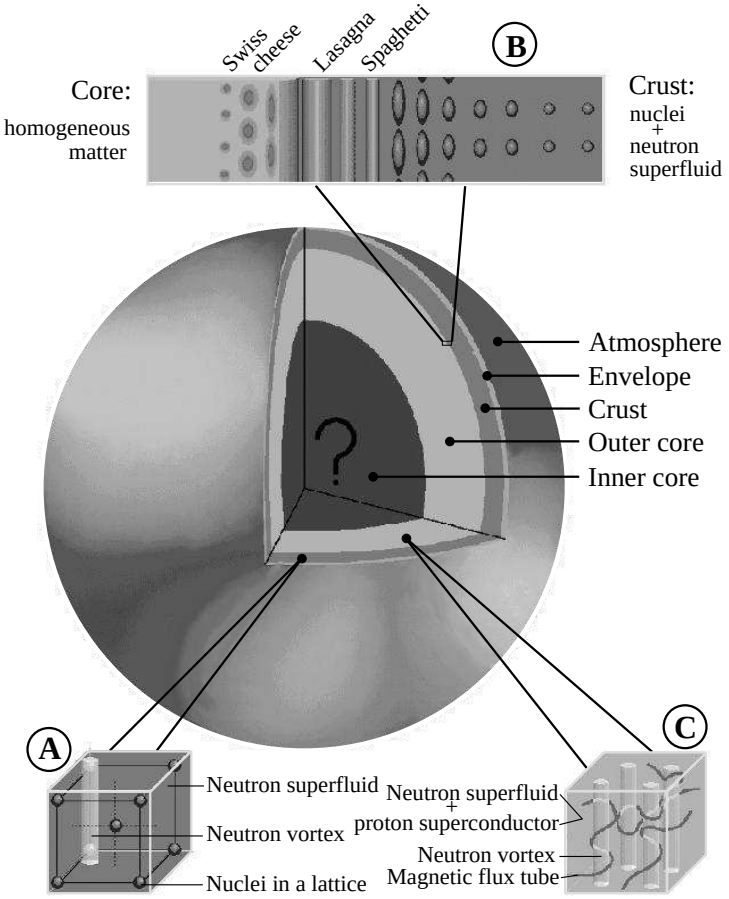

Figure 1.5: Theoretician's view of the inside of an ordinary neutron star, from Ref. [127].

Outside the star there are large magnetic (and electric) fields. A very thin hydrogen atmosphere is expected to exist at the star's surface, although a mix of heavy elements or even a condensed magnetic surface have also been proposed. The temperature and possibly the radius of neutron stars can be determined by the spectrum emitted from their surface [127]. Below the atmosphere there is a layer that is a few tens of meters thick that insulates the hot inner region from the surface. The star's crust has a width of approximately 1 km and it contains nuclei forming a lattice that is most likely immersed in a neutron superfluid (Figure 1.5, insert A).

Neutron stars are rotating self-gravitating objects and their rotation leads to the formation of vortices in the neutron superfluid, which can pin on the nuclei and then contribute to the creation

of spin glitches. The nuclear pasta phase (Figure 1.5, insert B) has increasingly elongated nuclei with the space in between filled by a neutron superfluid. The situation is reversed in the so-called Swiss cheese phase where bubbles of neutrons are immersed in an almost homogeneous proton-neutron liquid [127]. In the outer core (Figure 1.5, insert C) the neutron superfluid coexists with the proton fluid. Electrons are also present to maintain charge neutrality.

Recent developments concerning the interplay between neutron superfluidity and proton superconductivity can be found in Refs. [128, 129, 130, 131, 132]. The observed spin glitches of neutron stars are usually explained by the presence of an array of vortex lines formed due to the star's rotation. The vortex array expands when the star spins down and, thus, sudden jumps in the rotation frequency can be explained by the fact that the vortex lines are pinned to the crust of the star [128]. The situation becomes more complicated if one also includes the superconducting protons. If the protons form a type-II superconductor the neutron star magnetic field is confined to magnetic fluxoids through which the magnetic field may penetrate the core of the star. It has been claimed that this contradicts the observed long periodic oscillations attributed to the free precession of neutron stars [131]. However, in Refs. [130, 132] it has been suggested that in this case protons can form a type-I superconductor. While free precession is a plausible source of long-term variability in pulsar timing, in Chapter 4 we show that propagating Tkachenko modes (long wavelength shear modes of triangular lattices of singly quantized vortices) could provide an alternative explanation for the long-term pulsar spin variations [133].

Finally, there is a question mark at the inner core because its matter composition is still unknown. There the density is so high and the temperature is so low that deconfined color-superconducting quark matter may exist. However, the specific physical properties displayed by a color-superconducting core heavily depend on the phase considered.

The temperature of a newly born neutron star can be as large 10^{11} K (10 MeV). The star then cools down by mostly neutrino emission for approximately one million years and after this stage its temperature is approximately 10^5 K (10 eV) [134, 135], which is definitely lower than the estimated critical temperatures necessary for the onset of color superconductivity. The effects of color superconductivity on the cooling of neutron stars have been studied in the last few years [80]. However, with the current experimental data available the question of whether or not we have already observed the cooling of a star whose inner regions are composed of color-superconducting matter cannot be answered.

In white dwarfs simple Newtonian gravity can be applied in the computation of their masses and radii [95]. The mass and radius of neutrons stars, however, have to be computed within a fully general-relativistic setup. Spherically symmetric stars in hydrostatic equilibrium are described by the Tolman-Oppenheimer-Volkoff (TOV) equations [136], which have the matter equation of state as their main input. Their masses are within the range of $1.4 - 2.0$ solar masses [127], while their radii can be as large as 12 km. So far mass and radius measurements have not been able to confirm (or exclude) the presence of deconfined (color-superconducting) quark matter in compact stars. In general, the model parameters involved in the computation of the equation of state of both hadronic and quark matter can be chosen to produce stars with the required mass-radius relationship. In fact, it seems that pure hadronic stars, hybrid (quark matter core with hadronic crust) stars, and also bare quark stars can have masses and radii that are in agreement with the latest experimental constraints [137, 138].

For quickly rotating stars, effects from rotation on the spacetime metric have to be taken

into account [139]. Also, it is important to remark that neutron stars are called pulsars because of the electromagnetic radiation they emit due to rotation (see Fig. 1.6).

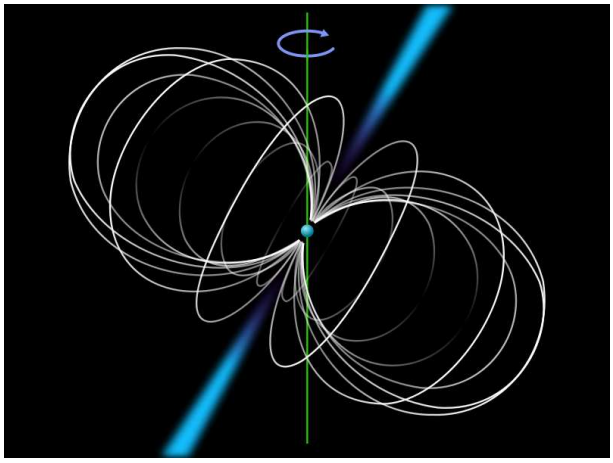

Figure 1.6: Schematic view of a pulsar. The sphere in the middle represents the neutron star, the curves indicate the magnetic field lines, and the protruding cones represent the emission beams. Note that the rotation axis and the magnetic axis are not aligned.

The measured quantities obtained from neutron star observations are basically the period P and the frequency $\dot{P}$ of rotation (see Fig. 1.7). Assuming that the radiation is emitted by a simple rotating dipole the star's magnetic field can be determined to be $B \sim 3.2 \times 10^{19} \, (P\dot{P})^{1/2}$ G. One can see in Fig. 1.7 that most neutron stars are radio pulsars with periods between $1 - 0.1$ seconds and magnetic fields of $10^{12} - 10^{13}$ Gauss. To have an idea of how large these fields are it suffices to say that they are thirteen orders of magnitude larger than the earth's surface magnetic field. One also observes a number of pulsars with $P < 0.1$ s and also a few with $P \geq 5$ s, which are the known anomalous X-ray pulsars and soft gamma repeaters (see Ref. [140] for a very detailed review). These stars with surface magnetic fields larger than 10^{14} G are also called magnetars. What basically distinguishes magnetars from ordinary neutron stars is that the main energy source for their radiative properties is their huge magnetic field [141]. Some general features shared by all magnetar candidates are:

- Very large surface magnetic fields, i.e., $B \geq 10^{14}$ G.
- Very young age, i.e., characteristic ages of $\tau_c \leq 10^4$ yrs.
- Very long rotation periods, i.e., $P \geq 5$ s .
- Very quick spinning down, i.e., $\dot{P} \geq 10^{-10}$.
- Emission of soft gamma ray bursts and also giant flares.

According to the standard magnetar model by Duncan and Thompson [141], the energy bursts of soft gamma ray repeaters are caused by solid fractures induced by strong magnetic fields in the crust of the star. Many properties of these objects are well described using the

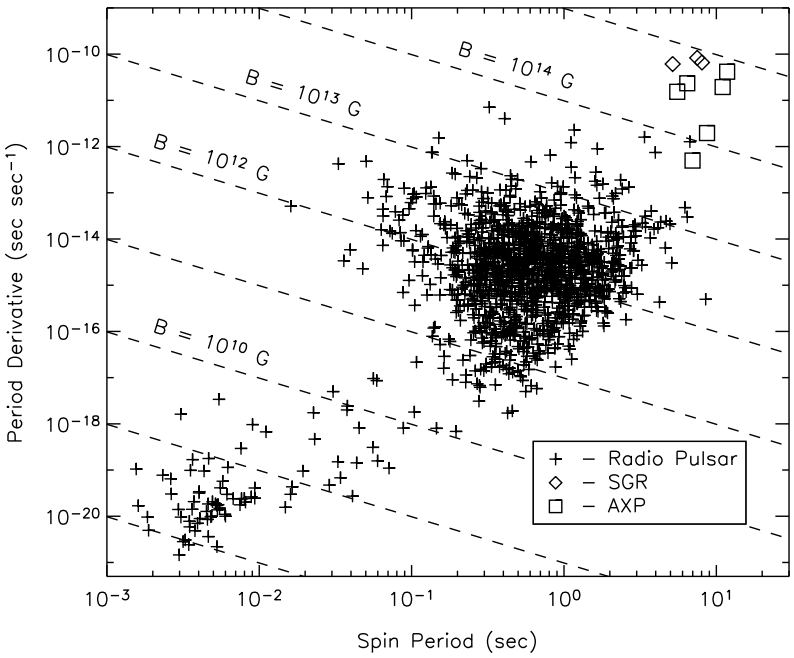

Figure 1.7: Period P versus period derivative $\dot{P}$ for radio pulsars (plus signs), Anomalous X-ray Pulsars (squares), and Soft Gamma Repeaters (diamonds). Contours of constant inferred magnetic field strength are drawn as diagonal dashed lines. See Ref. [140] for details.

hadronic magnetar model [140] but there are still some remaining issues, such as the quasi-periodicity of active phases, which require alternative ways of understanding them [142].

Also, recent studies have given support to the idea that old neutron stars could have previously been magnetars with magnetic fields that decayed over many years [143, 144]. This then suggests that magnetars could also have color-superconducting cores. Therefore, a detailed study of the effects of strong magnetic fields on color superconductors may be very important in understanding the physics of magnetars. We will come back to this important topic in Chapter 3 where we show that an ultramagnetized color-superconducting core can provide some new observables that may help to distinguish hadronic magnetars from magnetars with quark matter cores.

A spectacular way to detect quark matter in stars would be if quark stars, compact stars entirely made of deconfined quark matter and leptons [145], were observed. These stars could be self-bound stars, i.e., their stability is mostly due to strong interactions instead of gravity. Also, the density profile in these stars would be very different than in ordinary neutron stars because they could be uniform throughout their volume [139].

One of the main features of rotating, self-gravitating objects is that these objects develop instabilities as a result of the emission of gravitational waves. These instabilities can only be damped by viscosity [146]. The viscosity of nuclear and mixed phases of dense baryonic matter

has been calculated over the last three decades [147]. It has been shown in Refs. [148] that the viscosity of quark matter considerably differs from that of hadronic matter. This could then have some important phenomenological consequences.

Chapter 2

Gluonic Fluctuations in Color Superconductors

In this chapter we calculate the effects of gauge field fluctuations on the free energy density of a homogeneous color superconductor in the CFL phase. It will be shown that gluon fluctuations induce a strong first-order phase transition, in contrast to electronic superconductors where this transition is weakly first order. The critical temperature for this transition is larger than the one corresponding to the diquark pairing instability.

We obtain analytical formulas for the temperatures associated with the limits of metastability of the normal and superconducting phases as well as the latent heat associated with the first-order phase transition that are valid in weak coupling. We extend our analysis to intermediate densities and perform a numerical study on the first-order phase transition and the discontinuity of the diquark condensate at the critical point. We find that there are no local interactions between the diquark condensate and the gluons in color superconductivity. We published the results presented here in Ref. [75].

2.1 Introduction

In Sec. 1.3.1 we saw that the GL free energy density in an electronic superconductor has a local $[U(1)]$ symmetry in the presence of an external magnetic field. As long as thermal fluctuations are not taken into account the transition between the metallic and the superconducting state is of second order [41, 54]. Photon fluctuations contribute with a $|\phi|^3$ term in the free energy density that inevitably leads to a first-order phase transition [44].

Similarly, the physics of color superconductivity can be described near the transition temperature in terms of a GL free energy functional [71, 72], which depends on the expectation values of the order parameter and the gauge potential. Omitting the contribution from fluctuations, the GL free energy density for a CFL superconductor computed in weak coupling reads [71, 72] (see Appendix A)

$$\Gamma_{\rm cond} = \frac{6\mu^2}{\pi^2}\, t\, \Delta^2(T) + \frac{21\zeta(3)}{4\pi^4}\left(\frac{\mu}{T_c}\right)^2 \Delta^4(T), \tag{2.1}$$

where μ is the quark chemical potential and $t \equiv (T - T_c)/T_c$ is the reduced temperature. This

free energy exhibits a second-order phase transition at the critical temperature T_c given by

$$\ln \frac{T_c}{\mu} = -\frac{3\pi^2}{\sqrt{2}g} + \ln \frac{2048\sqrt{2}\pi^3}{9\sqrt{3}g^5} + \gamma - \frac{\pi^2+4}{8} + \mathcal{O}(g) \,, \tag{2.2}$$

where $g = g(\mu)$ is the strong coupling constant.

The gap parameter of the fermionic quasiparticle excitations is Δ (8-fold) and 2Δ (1-fold) [149]. One can check that the quadratic and quartic coefficients of $\Gamma_{\rm cond}$ for CSC are, respectively, 12 ($= 8\times 1^2 + 2^2$) and 24 ($= 8\times 1^4 + 2^4$) times larger than those for an electronic superconductor. It has been pointed out that fluctuations of the diquark condensate may induce a first-order transition because this theory has no infrared fixed point in the renormalization group flow of the coupling constants [73, 83, 150].

It follows from the GL theory of color superconductivity in weak coupling that the GL parameter is [151]

$$\kappa = \sqrt{\frac{72\pi^3}{7\zeta(3)\alpha_s}}\,\frac{T_c}{\mu} \,, \tag{2.3}$$

with $\alpha_s = g^2/(4\pi)$. Taking the limit $g \to 0$ we see that $\kappa \to 0$, which means that the CFL superconductor is most definitely type I.

The strength of a fluctuation-induced first-order transition is sensitive to the relationship among the three length scales involved in the problem: the coherence length near the transition ξ, the magnetic penetration depth near the transition, λ, and the coherence length at $T = 0$ $\xi_0 = 1/(2\pi T_c)$. Generally, a superconductor with $\lambda \gg \xi_0$ is said to be in the London limit. In this case the coupling between the gauge field and the order parameter is approximately local.

The opposite case, $\lambda \ll \xi_0$, corresponds to the Pippard limit where the coupling becomes highly nonlocal [54]. For a type-I electronic superconductor the Pippard limit is always realized at $T = 0$. However, near the transition temperature the penetration depth increases very rapidly and so does the ratio λ/ξ_0, which means that a crossover from the Pippard limit to the London limit is expected to occur near a second-order phase transition.

How does the first-order phase transition induced by gauge field fluctuations change this scenario? Are both limits still realized? In the case of known type-I electronic superconductors the first-order phase transition is sufficiently weak to warrant a crossover between the Pippard and the London limits. This crossover has been observed experimentally in strong type-I materials like aluminum [152].

However, the situation is completely different for a color superconductor. It was shown in Ref. [74] that $\lambda \ll \xi_0$ is maintained at the phase transition for asymptotically high baryon densities. As is shown below, this feature remains valid when the results of Ref. [74] are extrapolated to moderately high densities.

This chapter is organized as follows. In the next section, we discuss the generalized GL free energy density derived in Refs. [74, 75]. The relevant thermodynamic quantities of the first-order color-superconducting transition are derived for weak coupling in Sec. 2.3 and the extrapolation of the results to moderate densities is presented in Sec. 2.4. The technical details of the derivation of the generalized GL free energy density are discussed in Appendix A. In this chapter 4−vectors are denoted as $K \equiv K^\mu = (\omega, \vec{k})$ and the space-time integration is defined

as $\int_X = \int_0^{1/T} \int_\Omega d^3\vec{x}$ where T is the temperature and Ω the volume of the system. Moreover, Tr indicates the summation over all indices including momentum $\vec{k}$ and energy ω, while tr denotes the summation over all indices except momentum and energy. Furthermore, natural units $\hbar = k_B = c = 1$ are employed.

2.2 The Generalized GL Free Energy Density

It is widely known that when the temperature is sufficiently close to the critical temperature T_c the effects of fluctuations on the phase transition cannot be neglected [44]. This can be understood in the framework of GL theory where the free energy density of the fluctuations is roughly given by the thermal energy $k_B T$ within a volume l^3 where l is the characteristic length of the fluctuation. This volume corresponds to ξ^3 for the order parameter and λ^3 for the gauge potential. Since both lengths diverge as $|T - T_c|^{-1/2}$ the corresponding fluctuation energy density behaves as $|T - T_c|^{3/2}$. The condensation energy density, however, behaves as $|T - T_c|^2$. Therefore, when T becomes closer to T_c the fluctuation energy density will eventually dominate and the nature of the phase transition can be modified.

For a strong type-I superconductor ($\lambda \ll \xi$) the fluctuations of the gauge field largely exceed the fluctuations of the order parameter. Since CFL superconductors are extremely type I in weak coupling, it is then permissible to retain the fluctuations of the gauge field while neglecting those of the order parameter. We will show that a first-order phase transition occurs at $T_c^* > T_c$, while the temperature T_c determined by the diquark pairing instability (2.2) represents the lower bound for a supercooled normal phase without nucleation.

The effects of gauge field fluctuations can be added to the free energy of dense quark matter around T_c by using the Cornwall-Jackiw-Tomboulis (CJT) formalism [153]. The CJT effective action is especially useful in the case of spontaneous symmetry breaking, which is taken into account by introducing a bilocal source term in the QCD action.

Recall that the QCD partition function defined in Eq. (1.6) reads

$$\mathcal{Z} = \int \mathcal{D}A_a^\mu \, \mathcal{D}\bar{\psi} \, \mathcal{D}\psi \, \exp S \,, \tag{2.4}$$

where ψ and $\bar{\psi} = \psi^\dagger \gamma^0$ are the quark and adjoint quark fields, respectively. Gluon fields are described by adjoint fields A_a^μ. The action S is divided into several parts

$$S = S_A + S_F + g \int_X \bar{\psi}(X) \, T_a \gamma^\mu \psi(X) \, A_\mu^a(X) + S_{GF} + S_{FP}. \tag{2.5}$$

The purely gluonic action is

$$S_A = -\frac{1}{4} \int_X F_a^{\mu\nu} \, F_{\mu\nu}^a. \tag{2.6}$$

As before, the specific details of S_{GF} and S_{FP} do not need to be outlined in detail. S_F describes free, massless quarks in the presence of a chemical potential μ

$$S_F = \int_X \bar{\psi}(X) \, (i\partial \cdot \gamma + \mu\gamma^0) \, \psi(X). \tag{2.7}$$

In this chapter we consider only the interaction between the quarks and the gluons. This interaction is the one responsible for the formation of Cooper pairs. In the next chapter, however, effects from the unscreened "rotated" electromagnetic field on the pairing are explicitly taken into account.

In order to describe the pairing among the quarks it is convenient to introduce Nambu-Gor'kov spinors

$$\Psi = \begin{pmatrix} \psi \\ \psi_c \end{pmatrix}, \qquad \bar{\Psi} = \left(\bar{\psi}\ ,\ \bar{\psi}_c\right), \tag{2.8}$$

where $\psi_c = C\psi^T$ is the charge-conjugate spinor and C is the charge conjugation matrix defined as $C \equiv i\gamma^2\gamma^0$. In Nambu-Gor'kov space the fermionic action in Eq. (2.7) can be rewritten as

$$S_F = \frac{1}{2}\int_{X,Y} \bar{\psi}(X)\, S_0^{-1}(X,Y)\psi(Y). \tag{2.9}$$

The factor 1/2 accounts for the doubling of degrees of freedom in Nambu-Gor'kov space. The inverse free fermion propagator $S_0^{-1}(X,Y)$ in the equation above is

$$S_0^{-1} = \begin{pmatrix} [G_0^+]^{-1} & 0 \\ 0 & [G_0^-]^{-1} \end{pmatrix}, \tag{2.10}$$

where $[G_0^\pm]^{-1}(X,Y) = -i(i\partial_X \cdot \gamma \pm \mu\gamma^0)\,\delta^{(4)}(X-Y)$. In Nambu-Gor'kov space the interaction term takes the form

$$g\int_X \bar{\psi}(X)\, T_a\gamma^\mu\psi(X)\, A_\mu^a(X) = \frac{g}{2}\int_X \bar{\Psi}(X)\,\Gamma_a^\mu\Psi(X)\, A_\mu^a(X), \tag{2.11}$$

where we have defined the vertex

$$\Gamma_a^\mu = \begin{pmatrix} \gamma^\mu T_a & 0 \\ 0 & -\gamma^\mu T_a^T \end{pmatrix}. \tag{2.12}$$

Now a bilocal source term

$$\mathcal{K}(X,Y) = \begin{pmatrix} \sigma^+ & \varphi^- \\ \varphi^+ & \sigma^- \end{pmatrix}, \tag{2.13}$$

is added to the action S, which then becomes

$$S[\mathcal{K}] = S + \int_{X,Y} \bar{\Psi}(X)\,\mathcal{K}(X,Y)\,\Psi(Y). \tag{2.14}$$

The off-diagonal elements in $\mathcal{K}$, φ^-, and φ^+ are essential for color superconductivity because they describe the coupling of two (adjoint) quarks. The existence of Cooper pairs implies that the expectation value of these elements is different than zero. Moreover, the four entries of $\mathcal{K}$ are not independent. In fact, due to charge conjugation invariance we obtain that $\sigma^- = C[\sigma^+]^\dagger C^{-1}$. Also, since the total action has to be real-valued, one finds that $\varphi^- = \gamma^0[\varphi^+]^\dagger\gamma^0$. Finally, we arrive at the new QCD partition function

$$\mathcal{Z}[\mathcal{K}] = \int \mathcal{D}A_a^\mu\,\mathcal{D}\bar{\Psi}\,\mathcal{D}\Psi\,\exp S[\mathcal{K}], \tag{2.15}$$

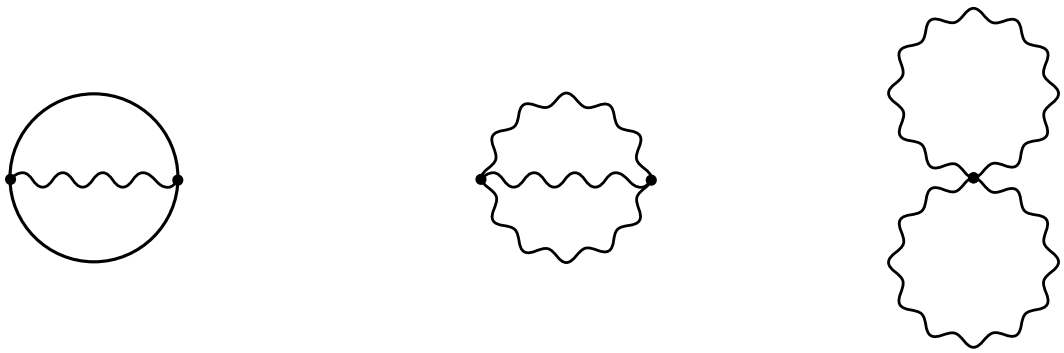

Figure 2.1: The two-loop approximation to Γ_2. Straight lines denote quark propagators and wavy lines denote gluon propagators.

which is the starting point for the application of the CJT formalism.

The CJT effective potential that is obtained from Eq. (2.15) [9] is

$$\Gamma[\bar{\mathcal{D}},\bar{\mathcal{S}}] = \frac{T}{2\,\Omega}\left\{\mathrm{Tr}\ln\bar{\mathcal{D}}^{-1} + \mathrm{Tr}(D^{-1}\bar{\mathcal{D}} - 1) - \mathrm{Tr}\ln\bar{\mathcal{S}}^{-1} - \mathrm{Tr}(S_0^{-1}\bar{\mathcal{S}} - 1) - 2\,\Gamma_2[\bar{\mathcal{D}},\bar{\mathcal{S}}]\right\}\ , \quad (2.16)$$

where $\bar{\mathcal{D}}$ and $\bar{\mathcal{S}}$ are the full gluon and quark propagators, D^{-1} and S_0^{-1} are the corresponding inverse tree-level propagators, and Γ_2 is the sum of all two-particle irreducible vacuum diagrams. We work in the two-loop approximation, i.e., Γ_2 contains only the diagrams shown in Fig. 2.1. The first diagram, which contains quark propagators, leads to a term of order $g^2\mu^4$ in Γ, while the other two diagrams (which contain only gluon propagators) lead to terms proportional to powers of T. Therefore, at small temperatures $T \sim T_c \sim \mu\,\exp(-1/g)$ one can drop the last two diagrams and consider only the first. In explicit form

$$\Gamma_2[\bar{\mathcal{D}},\bar{\mathcal{S}}] = -\frac{1}{2}\,\mathrm{Tr}\{\bar{\mathcal{D}}\,\Pi[\bar{\mathcal{S}}]\}\ , \quad (2.17)$$

where

$$\Pi[\bar{\mathcal{S}}] \equiv \frac{1}{2}\,\mathrm{Tr}(\hat{\Gamma}\,\bar{\mathcal{S}}\,\hat{\Gamma}\,\bar{\mathcal{S}}) \quad (2.18)$$

is a functional of the full quark propagator $\bar{\mathcal{S}}$ and the bare quark-gluon vertex $\hat{\Gamma}$. Note that the trace in Eq. (2.17) is over 4-momenta as well as Lorentz and adjoint color indices, while in Eq. (2.18) it is over 4-momenta as well as Nambu-Gor'kov, Dirac, flavor, and fundamental color indices. The minus sign in Eq. (2.17) accounts for the fermion loop and the factor 1/2 is due to the fact that this is a second-order correction to the CJT effective potential. Moreover, the factor 1/2 in Eq. (2.18) accounts for the extra fermionic degrees of freedom in Nambu-Gor'kov space.

The free energy density is given by the CJT effective potential at its stationary points, which are determined by

$$\left.\frac{\delta\Gamma}{\delta\bar{\mathcal{D}}}\right|_{\bar{\mathcal{D}}=\mathcal{D},\bar{\mathcal{S}}=\mathcal{S}} = 0\ , \quad \left.\frac{\delta\Gamma}{\delta\bar{\mathcal{S}}}\right|_{\bar{\mathcal{D}}=\mathcal{D},\bar{\mathcal{S}}=\mathcal{S}} = 0\ . \quad (2.19)$$

The first condition gives a Dyson-Schwinger equation for the gluon propagator

$$\mathcal{D}^{-1} = D^{-1} + \Pi[\mathcal{S}] \; . \tag{2.20}$$

Inserting this condition into Eq. (2.16), one observes that the second term cancels the last term, i.e., at the stationary point

$$\Gamma[\mathcal{D},\mathcal{S}] = \frac{T}{2\Omega}\left[\mathrm{Tr}\ln\mathcal{D}^{-1} - \mathrm{Tr}\ln\mathcal{S}^{-1} - \mathrm{Tr}(S_0^{-1}\mathcal{S}-1)\right] \; . \tag{2.21}$$

This expression corresponds to the free energy density at a given temperature T. In terms of the gluon and quark propagators in the normal phase, $\mathcal{D}_n(K)$ and $\mathcal{S}_n(K)$, the propagators in the superconducting phase are written as

$$\mathcal{S}(K) = \mathcal{S}_n(K) + \delta\mathcal{S}(K,\Delta) \; , \tag{2.22a}$$
$$\mathcal{D}^{-1}(K) = \mathcal{D}_n^{-1}(K) + \delta\Pi(K,\Delta) \; , \tag{2.22b}$$

where $\delta\Pi \equiv \Pi - \Pi_n$, i.e., $\mathcal{D}_n^{-1}$ *already* contains the HDL resummed gluon self-energy Π_n [9]. The gluon self-energy in the superconducting phase, Π, depends on the superconducting gap parameter Δ and, therefore, so does $\delta\Pi$. Similarly, the quark propagator in the normal phase $\mathcal{S}_n$ contains quark self-energy corrections and $\delta\mathcal{S}$ depends on Δ. Note that Δ is the value of the gap parameter obtained from a solution of the second Dyson-Schwinger equation (2.19). In the following, however, we shall consider Δ to be a free parameter. In order to obtain the physical value of the gap we then have to find the minimum of $\Gamma[\mathcal{D},\mathcal{S}]$ as a function of Δ.

Inserting Eqs. (2.22) into Eq. (2.21), we obtain

$$\Gamma = \Gamma_n + \Gamma_{\mathrm{cond}} + \Gamma_{\mathrm{fluc}} + \Gamma'_{\mathrm{fluc}} \; , \tag{2.23}$$

where

$$\Gamma_n = \frac{T}{2\,\Omega}\left[\mathrm{Tr}\ln\mathcal{D}_n^{-1} - \mathrm{Tr}\ln\mathcal{S}_n^{-1} - \mathrm{Tr}(S_0^{-1}\mathcal{S}_n - 1)\right] \; , \tag{2.24a}$$
$$\Gamma_{\mathrm{cond}} = \frac{T}{2\,\Omega}\left[\mathrm{Tr}(\mathcal{D}_n\delta\Pi) - \mathrm{Tr}(S_0^{-1}\delta\mathcal{S}) + \mathrm{Tr}\ln(1+\mathcal{S}_n^{-1}\delta\mathcal{S})\right] \; , \tag{2.24b}$$
$$\Gamma_{\mathrm{fluc}} = \frac{T}{2\,\Omega}\sum_{\vec{k},\omega=0}\mathrm{tr}\left\{\ln\left[1+\mathcal{D}_n(K)\delta\Pi(K,\Delta)\right] - \mathcal{D}_n(K)\delta\Pi(K,\Delta)\right\} \; , \tag{2.24c}$$
$$\Gamma'_{\mathrm{fluc}} = \frac{T}{2\,\Omega}\sum_{\vec{k},\omega\neq 0}\mathrm{tr}\left\{\ln\left[1+\mathcal{D}_n(K)\delta\Pi(K,\Delta)\right] - \mathcal{D}_n(K)\delta\Pi(K,\Delta)\right\} \; . \tag{2.24d}$$

The generalized GL free energy density is the difference in the CJT effective potential between the superconducting phase and the normal phase, $\Gamma - \Gamma_n$. It includes both the ordinary GL terms and the fluctuation terms. Note that we have added a term $\mathrm{Tr}(\mathcal{D}_n\delta\Pi)$ in Γ_{cond} and simultaneously subtracted it in $\Gamma_{\mathrm{fluc}}, \Gamma'_{\mathrm{fluc}}$. This term corresponds to the so-called exchange (free) energy density [21] and *must* be present in order to obtain the correct expression for Γ_{cond} [71, 72]. Therefore, we *have* to subtract it in the fluctuation part of the free energy density. Only with this subtraction $\Gamma_{\mathrm{fluc}} + \Gamma'_{\mathrm{fluc}}$ represents the well-known plasmon ring resummation

[21]. It is quite gratifying to see that the CJT formalism naturally contains all these different many-body contributions to the free energy density.

In Ref. [73] the exchange energy density was not subtracted from the plasmon ring contribution. This lead to an overall change of sign in the fluctuation energy density. As shown below [see Eq. (2.30)], the contribution of the fluctuation energy density is $\sim \ln(1+u) - u$, which is always negative, while in Ref. [73] it is $\sim \ln(1+u)$, which is positive for $u > 0$. Therefore, the authors of Ref. [73] concluded that gauge-field fluctuations raise the free energy density of the color-superconducting phase, which then decreases the transition temperature to the normal phase. In our case, however, the fluctuations decrease the free energy density, i.e., they stabilize the color-superconducting phase and, therefore, lead to a larger transition temperature.

This is physically plausible if one remembers that gauge-field fluctuations are also present in the normal phase, namely, in the first term in Eq. (2.24a). Since transverse gluons are massless in the normal phase, $\Pi_n(0) = 0$, long-wavelength fluctuations are enhanced over those in the color-superconducting phase where gluons are massive, $\delta\Pi \neq 0$. Thus, the fluctuation energy density in the normal phase is larger than in the superconducting phase.

The relevant fluctuation term is

$$\Gamma_{\rm fluc} = 8\,T \int \frac{d^3\vec{k}}{(2\pi)^3} \left\{ \ln\left[1 + \frac{m^2(T,k)}{k^2}\right] - \frac{m^2(T,k)}{k^2} \right\}, \tag{2.25}$$

while $\Gamma'_{\rm fluc}$ is of higher order (see Appendix A). The momentum-dependent Meissner mass reads

$$m^2(T,k) = \frac{1}{\lambda^2} f(k\xi_0), \tag{2.26}$$

with the chromomagnetic penetration depth given by

$$\frac{1}{\lambda^2} = \frac{7\zeta(3)}{24\pi^4} \frac{g^2\mu^2\Delta^2}{T_c^2}, \tag{2.27}$$

and

$$f(y) = \frac{6}{7\zeta(3)} \sum_{s=0}^{\infty} \int_0^1 dx \frac{1-x^2}{(s+\frac{1}{2})[4(s+\frac{1}{2})^2 + y^2x^2]}\,. \tag{2.28}$$

Carrying out the integration in Eq. (2.25) and combining the result with Eq. (2.1), we find

$$\Gamma = \frac{6\mu^2}{\pi^2}\, t\,\Delta^2(T) + \frac{21\zeta(3)}{4\pi^4} \left(\frac{\mu}{T_c}\right)^2 \Delta^4(T) + 32\pi\, T_c^4\, F\left(\frac{\xi_0^2}{\lambda^2(T)}\right) \tag{2.29}$$

where the function F is defined as

$$F(z) = \int_0^\infty dx\, x^2 \left\{ \ln\left[1 + \frac{z}{x^2} f(x)\right] - \frac{z}{x^2} f(x) \right\}\,. \tag{2.30}$$

Anticipating the result $t \sim \mathcal{O}(g)$, cf. Eq. (2.42), in the derivation of Eq. (2.29), we replaced $TT_c^3 \equiv T_c^4(1+t)$ by T_c^4 in front of the last term. Keeping the full expression only leads to order $\mathcal{O}(g)$ corrections in the results presented in Sec. 2.3. Similarly, the higher-order terms of $\Gamma'_{\rm fluc}$

lead to order $\mathcal{O}(g)$ corrections in the second term in Eq. (2.29), cf. Appendix A. Therefore, the impact on the results in Sec. 2.3 is also only of order $\mathcal{O}(g)$.

The London limit corresponds to small arguments in Eqs. (2.28) and (2.30). We have

$$f(y) = 1 - \frac{31}{140}\frac{\zeta(5)}{\zeta(3)}y^2 + \mathcal{O}(y^4), \tag{2.31}$$

and

$$F(z) \simeq -\frac{\pi}{3}z^{\frac{3}{2}}. \tag{2.32}$$

In the Pippard limit the arguments of $f(y)$ and $F(z)$ become large and we end up with

$$f(y) = \frac{3\pi^3}{28\zeta(3)y}\left[1 - 16\,\frac{\ln 2y + \gamma}{\pi^3 y} + \mathcal{O}(y^{-3})\right], \tag{2.33}$$

and

$$F(z) \simeq -\frac{\pi^3}{28\zeta(3)}z\Big[\ln\Big(\frac{3\pi^3}{28\zeta(3)}z\Big) + \text{const}\Big]. \tag{2.34}$$

Here we have retained the first corrections for both limits of the function $f(y)$ in order to assess the deviation from each limit at the CSC phase transition.

Before concluding this section, let us clarify once more several differences between our formulation and that of Ref. [73]. First, since in their treatment the term $-m^2(T,k)/k^2$ in Eq. (2.25), which arises from the subtraction of the exchange energy density, is missing their formal power series expansion for the fluctuation energy density in terms of Δ starts already at quadratic order. This then leads to a renormalized critical temperature T_c'. However, since we include the term in question there is no such renormalization of T_c. Moreover, the authors of Ref. [73] find that the difference between T_c and T_c' is of order $\mathcal{O}(g^2)$. Since the two-loop approximation employed in the derivation of Eq. (2.29) is not sufficiently accurate to provide all corrections of this order, such $\mathcal{O}(g^2)$ corrections cannot be reliably computed. Furthermore, the authors of Ref. [73] approximated the momentum-dependent Meissner mass by a constant and simply cut off the momentum integration in Eq. (2.25). This corresponds to the London limit of Eqs. (2.28) and (2.30) where the fluctuation energy density is of the form of Eq. (2.32). The shift in the transition temperature compared to that of Eq. (2.2) is then only of order $\mathcal{O}(g^2)$ [73] and not of order $\mathcal{O}(g)$ as found here and in Refs. [74, 75].

2.3 The First-Order CSC Transition in Weak Coupling

A generic first-order phase transition can be described by three characteristic temperatures: the transition temperature T_c^*, the maximum temperature of the (metastable) superheated superphase $T_{\rm sh}$, and the minimum temperature of the (metastable) supercooled normal phase $T_{\rm sc}$ [41]. These temperatures are related in the following way

$$T_{\rm sc} < T_c^* < T_{\rm sh}\ , \tag{2.35}$$

and they can be obtained from the generalized GL free energy density (2.29). The lower margin of a supercooled normal phase corresponds to

$$\left.\frac{\partial^2\Gamma}{\partial\Delta^2}\right|_{\Delta=0} = 0, \tag{2.36}$$

and, using Eq. (2.29), we have

$$T_{\rm sc} = T_c \ , \tag{2.37}$$

which relates $T_{\rm sc}$ with the onset temperature for diquark pairing. On the other hand, the transition occurs at

$$\frac{\partial\Gamma}{\partial\Delta} = 0 \ , \qquad \Gamma = 0 \ , \tag{2.38}$$

for a value of $\Delta \equiv \Delta_{c^*} \neq 0$. This implies that

$$t_c^* \ + \ \frac{7\zeta(3)}{4\pi^2}\frac{\Delta_{c^*}^2}{T_c^2} + \frac{7\zeta(3)}{18\pi^3}g^2F'\left(\frac{\xi_0^2}{\lambda_{c^*}^2}\right) = 0 \ , \tag{2.39a}$$

$$t_c^* \ + \ \frac{7\zeta(3)}{8\pi^2}\frac{\Delta_{c^*}^2}{T_c^2} + \frac{7\zeta(3)}{18\pi^3}g^2\frac{\lambda_{c^*}^2}{\xi_0^2}F\left(\frac{\xi_0^2}{\lambda_{c^*}^2}\right) = 0 \ . \tag{2.39b}$$

Eliminating t_c^* in the equations above we have

$$\mathcal{F}\left(\frac{\xi_0^2}{\lambda_{c^*}^2}\right) = \frac{216\pi^7}{7\zeta(3)g^4}\left(\frac{T_c}{\mu}\right)^2 \ , \tag{2.40}$$

where $\mathcal{F}(z) = -F'(z)/z + F(z)/z^2$. Solving Eq. (2.40) for $\Delta_{c^*}^2$ with the aid of Eq. (2.34), we obtain

$$\Delta_{c^*}^2 = \frac{\pi^2}{63\zeta(3)}\, g^2T_c^2 \ . \tag{2.41}$$

The transition temperature is obtained by substituting Eq. (2.41) into either one of Eqs. (2.39). This substitution gives

$$T_c^* = \left(1 + \frac{\pi^2}{12\sqrt{2}}\, g\right) T_c \ . \tag{2.42}$$

These results were first derived in Ref. [74]. The penetration depth at the transition is

$$\frac{1}{\lambda_{c^*}^2} = \frac{g^4}{216\pi^2}\mu^2 \ , \tag{2.43}$$

which yields the ratio

$$\frac{\xi_0^2}{\lambda_{c^*}^2} = \frac{g^4\mu^2}{864\pi^4T_c^2} \gg 1 \ . \tag{2.44}$$

Thus, the Pippard limit is valid for the entire CSC phase at sufficiently large chemical potentials.

We now determine $T_{\rm sh}$. The free energy density Γ as a function of Δ has a local maximum between $\Delta = 0$ and the minimum Δ_{c^*} at $T = T_c^*$ in the superconducting phase. As T increases, the local minimum remains unchanged until it coalesces with the local maximum where

$$\frac{\partial\Gamma}{\partial\Delta} = 0 \ , \qquad \frac{\partial^2\Gamma}{\partial\Delta^2} = 0 \ , \tag{2.45}$$

for a value of $\Delta \equiv \Delta_{\rm sh} \neq 0$. It then follows that

$$t_{\rm sh} + \frac{7\zeta(3)}{4\pi^2}\frac{\Delta_{\rm sh}^2}{T_c^2} \quad + \quad \frac{7\zeta(3)}{18\pi^3} g^2 F'\left(\frac{\xi_0^2}{\lambda_{\rm sh}^2}\right) = 0 \,, \tag{2.46a}$$

$$F''\left(\frac{\xi_0^2}{\lambda_{\rm sh}^2}\right) \quad = \quad -\frac{432\pi^7}{7\zeta(3)g^4}\Big(\frac{T_c}{\mu}\Big)^2 \,. \tag{2.46b}$$

Moreover, Eq. (2.46b) together with Eq. (2.34) yield

$$\Delta_{\rm sh}^2 = \frac{\pi^2}{126\zeta(3)} g^2 T_{c^*}^2 = \frac{1}{2}\Delta_{c^*}^2 \,. \tag{2.47}$$

Subtracting Eq. (2.39b) from Eq. (2.46a) and using Eq. (2.34), we find that

$$t_{\rm sh} - t_c^* = \frac{g^2}{72}(1 - \ln 2) \,, \tag{2.48}$$

which results in

$$T_{\rm sh} = \left[1 + \frac{g^2}{72}(1 - \ln 2)\right] T_c^* \,. \tag{2.49}$$

Note that T_c^* is one order of g closer to $T_{\rm sh}$ than to $T_{\rm sc}$. The ratio

$$\frac{\xi_0^2}{\lambda_{\rm sh}^2} = \frac{g^4\mu^2}{1728\pi^4 T_c^2} \tag{2.50}$$

implies that in weak coupling even the metastable CSC state is in the Pippard limit. Although the diagrammatics behind the generalized GL free energy density (2.29) determine T_c only up to the subleading order, the leading-order differences among the three characteristic temperatures do not change if higher-order corrections to T_c are included.

Another observable associated with the first-order phase transition is the latent heat $L = T_c\,\Delta S$ where ΔS is the change in entropy density at the transition. We have

$$\Delta S = -\Big(\frac{\partial\Gamma}{\partial T}\Big)_{\Delta=\Delta_c^*} = \frac{2g^2}{21\zeta(3)}\mu^2 T_c \,, \tag{2.51}$$

which gives

$$L = \frac{2g^2}{21\zeta(3)}\mu^2 T_c^2 \equiv \frac{6\mu^2}{\pi^2}\,\Delta_{c^*}^2 \,. \tag{2.52}$$

Now we calculate the strength of the first-order phase transition as was defined in Ref. [44]

$$t_{\rm HLM} = \frac{L}{\Delta c_v} \,, \tag{2.53}$$

where Δc_v is the jump in specific heat at the second-order phase transition, which neglects the fluctuations. If we ignore the third term in Eq. (2.29) we recover the ordinary GL theory from which we find $\Delta c_v = 24\,\mu^2 T_c/[7\zeta(3)]$. Thus, we have

$$\frac{t_{\rm HLM}}{T_c} = \frac{g^2}{36} \,. \tag{2.54}$$

Eq. (2.54) implies that the strength of the first-order phase transition weakens (logarithmically) with increasing chemical potential, which is in agreement with the fact that the second-order phase transition is recovered at asymptotically large densities. Note that for electronic superconductors $t_{\rm HLM}/T_c \sim 10^{-6}$ [44], which is much smaller than the right-hand side of Eq. (2.54) for realistic values of $g \sim 1$.

2.4 Numerical Results

Strictly speaking, the weak-coupling results in the previous section are only valid at ultrahigh baryon densities such that $\mu \gg \Lambda_{\rm QCD}$. For quark matter that may exist inside a compact star μ is expected to be slightly higher than $\Lambda_{\rm QCD}$, which means that the weak-coupling expansion becomes problematic. Nevertheless, we assume that the generalized GL free energy density remains numerically reliable down to realistic quark densities. Even if this is not the case, the qualitative statement for the absence of the London limit in CSC may still survive according to the argument given at the end of this section.

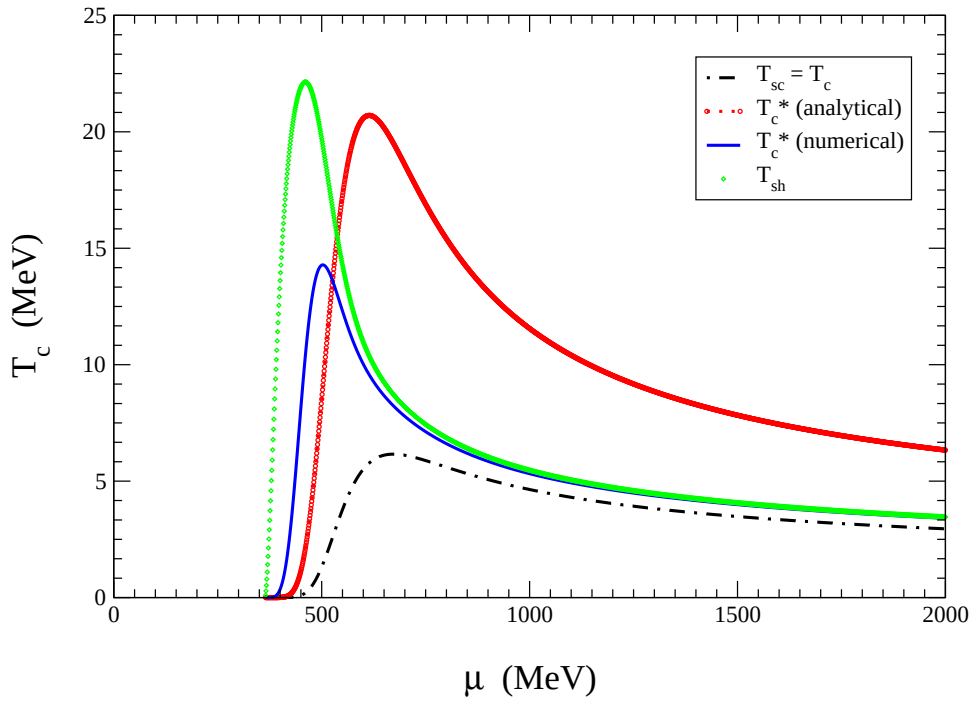

Figure 2.2: Comparison between the different temperatures involved in the discussion of the fluctuation-induced first order phase transition.

We solved Eqs. (2.40) and (2.46b) numerically in order to find Δ_{c^*} and $\Delta_{\rm sh}$ as functions of the chemical potential. The transition temperature T_c^* is obtained using Δ_{c^*} in either one of

Eqs. (2.39) and the temperature $T_{\rm sh}$ is obtained from the first equation in Eq. (2.46a). We used the 3-loop formula for $\alpha_s = g^2/4\pi$ [23] previously shown in Eqs. (1.10) and (1.11) with three colors and three flavors. Moreover, we have taken $\Lambda_{QCD} = 364$ MeV in our calculations in order to obtain the correct value of α_s at the scale of the Z-boson mass.

Figure 2.2 shows the three temperatures $T_{\rm sc}$, T_c^*, and $T_{\rm sh}$ as functions of the chemical potential along with the weak-coupling formula (2.42). Note that T_c^* is still closer to $T_{\rm sh}$ than to $T_{\rm sc}$ down to few hundreds of MeV. A comparison between the critical temperature T_c^* evaluated

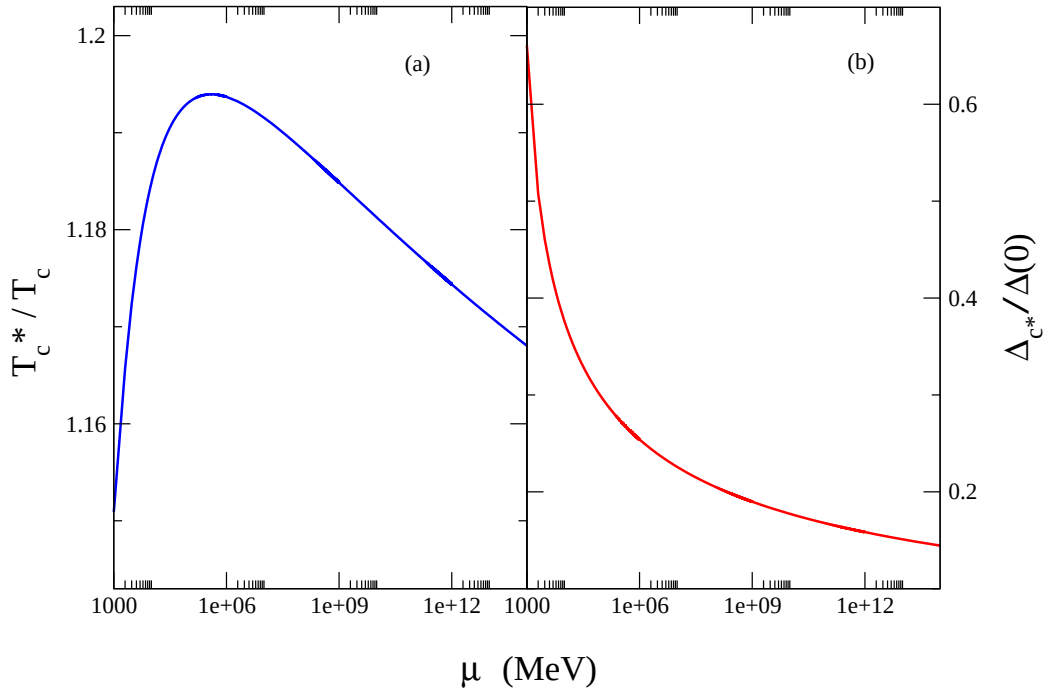

Figure 2.3: (a) Comparison between the critical temperatures at high densities. (b) Discontinuity of the gap at the transition.

numerically and T_c is shown in Fig. 2.3 (a) and the discontinuity of the gap at T_c^*, relative to its value at $T = 0$ previously shown in Eq. (1.48), is shown in Fig. 2.3 (b). Both plots indicate that

$$\lim_{\mu\to\infty} \frac{T_c^*}{T_c} = 1 \,, \qquad \lim_{\mu\to\infty} \frac{\Delta_{c^*}}{\Delta(0)} = 0 \,, \tag{2.55}$$

which is expected from asymptotic freedom, i.e., $\lim_{\mu\to\infty} g(\mu) = 0$. However, because of Eq. (1.10) the convergence is logarithmically slow.

Now we will address the question of whether or not the London limit is realized near T_c^* for color superconductors in the range of chemical potentials explored here. From Fig. 2.4 we see that the ratio $\xi_0/\lambda_{c^*} \gg 1$, which means that only the Pippard limit of magnetic interactions is

present in color superconductivity. Even for the minimum value of the ratio ξ_0/λ_{c^*}, which is around $\mu = 700$ MeV, the Pippard expansion of $m^2(k,T)$ in Eq. (2.33) works better than the London expansion displayed in Eq. (2.31). This is also the case for the metastable CSC state up to $T_{\rm sh}$ as is shown in Fig. 2.5.

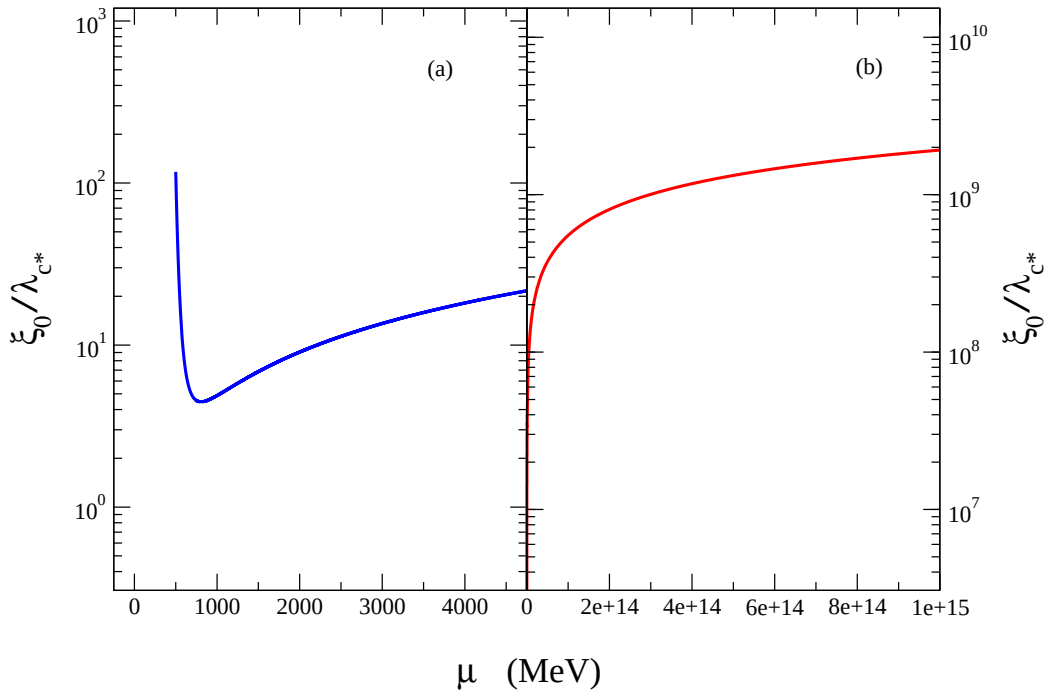

Figure 2.4: (a) ξ_0/λ_{c^*} at small chemical potentials. (b) The same ratio at very large chemical potentials.

It is instructive to express the right-hand side of Eq. (2.40) in terms of the GL parameter (2.3) and compare it with the corresponding equation for a metallic superconductor. The generalized GL free energy density in an electronic superconductor was given in Ref. [74]. The terms we want to compare are

$$\mathcal{F}\Big(\frac{\xi_0^2}{\lambda_{c^*}^2}\Big) = \frac{3\pi^2\kappa^2}{16\alpha_s} \tag{2.56}$$

for color superconductors and

$$\mathcal{F}\Big(\frac{\xi_0^2}{\lambda_{c^*}^2}\Big) = \frac{\pi^2\kappa^2}{16\alpha_e v_F} \tag{2.57}$$

for electronic superconductivity. A large value on the right-hand side of Eq. (2.56) or Eq. (2.57) points towards the London limit at the first-order phase transition. Since $\alpha_e \ll \alpha_s$ and $v_F \sim \alpha_e$, the right-hand side of Eq. (2.57) is much larger than that in Eq. (2.56) when the same GL

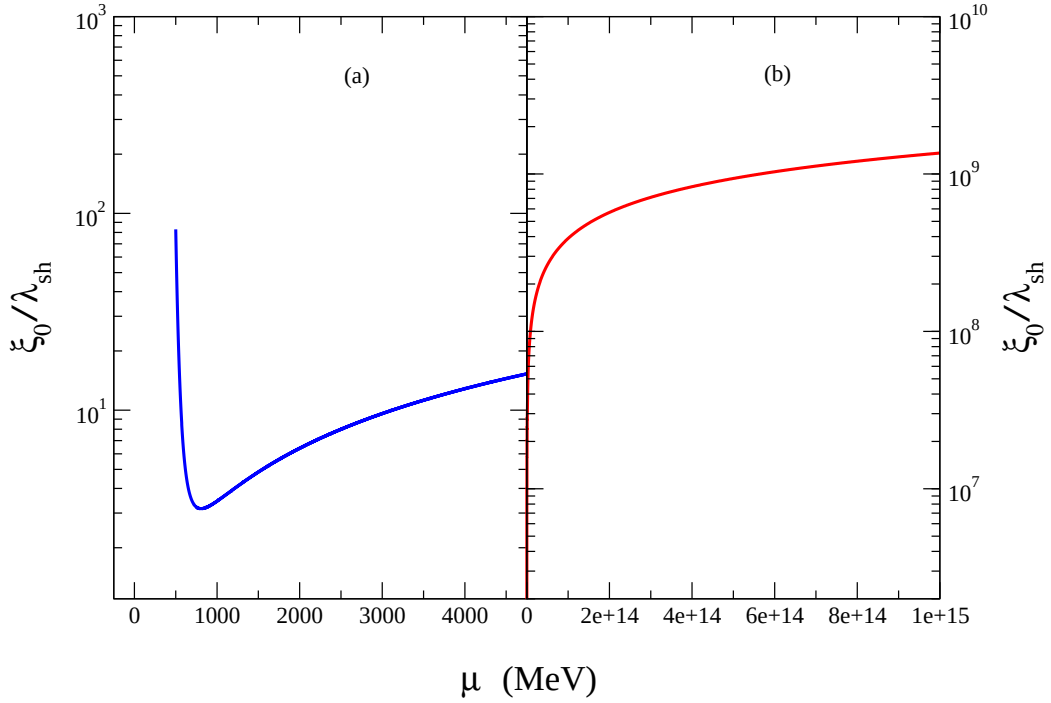

Figure 2.5: (a) $\xi_0/\lambda_{\rm sh}$ at small chemical potentials. (b) The same ratio at very large chemical potentials.

parameter is used. In other words, the London limit is more likely to be realized in metallic superconductors.

It was shown in Ref. [44] within a one-loop renormalization-group calculation using the ϵ expansion that no stable infrared fixed point can exist for a theory involving local interactions between Abelian gauge fields and order parameters unless the number of order parameter components N is artificially extended to $N > N_c = 365$. This is far beyond the case of relevance for electronic superconductivity. This result is then interpreted as signaling the presence of a first-order transition. Therefore, for electronic superconductors gauge-field fluctuations are always expected to change the order of the phase transition into first order, irrespective of further details about the transition.

For color superconductors, however, the effective action, which contains only the order parameter and the gauge fields as well as the specific form of their interactions, is not known. Therefore, the general result derived in Ref. [44] may not be applicable. However, the results we obtained for the CFL phase seem to suggest that fluctuation-induced first-order phase transitions are indeed present in color superconductivity. Furthermore, due to the absence of the London limit we expect that, once gauge-field fluctuations and first-order phase transitions are taken into account, local interactions between the diquark condensate and the gluons are never realized in color superconductors, regardless of which phase is considered. This would constitute

a striking new physical effect that would only come about in color superconductivity.

The crossover from nonlocal to local interactions near the critical temperature in superconducting metals of strong type-I has been recently observed [152]. What we found in the present study rules out the possibility of observing such a crossover in color superconductors.

Chapter 3

Color-Flavor Locked Superconductor in Strong Magnetic Fields

In this chapter we study the effects of strong magnetic fields on the properties of CFL superconducting quark matter within an NJL model. We find that both the energy gaps that describe color-superconducting pairing as well as the magnetization are oscillating functions of the magnetic field. Also, we observe that the oscillations of the magnetization can be so strong that homogeneous quark matter becomes unstable for a range of parameters. It is suggested that this points towards the existence of magnetic domains or other types of magnetic inhomogeneities in the hypothesized quark cores of magnetars. We presented most of the results discussed here in Ref. [89].

3.1 Introduction

Strong magnetic fields exist on the surface of compact stars, e.g., $B \lesssim 10^{12}$ G for ordinary neutron stars [156] while for magnetars they can be as large as $B \simeq 10^{16}$ G [157]. Often one can take the conductivity of the matter inside neutron stars to be essentially infinite because the dissipation time scales are very long in comparison to the other time scales of interest [95]. In this case the magnetohydrodynamic equations [95] predict that the magnetic force field lines are "frozen in" the fluid, which implies that the magnetic flux $\int_S \vec{B}\cdot d\vec{S}$ through any closed surface S moving with the fluid is constant. Assuming that the field lines do penetrate the central regions of the star, the conservation of magnetic flux indicates that the magnetic field strength in the small, inner core of magnetars can be at least as large as $B \simeq 10^{18}$ G. This large value already corresponds to the physical upper limit for the magnetic field in a gravitationally bound star [95].

We have seen in Sec. 1.6 that the superdense, cold core of ordinary neutron stars most likely consists of some sort of color-superconducting quark matter. There is no reason why the same idea cannot be applied to magnetars. The energy scale defined by a field of approximately 10^{18} G is roughly of the order of 100 MeV, which is comparable to the color-superconducting gap present in the quasiparticle energy spectrum and the strange quark mass. Since quarks are charged particles it is then expected that such a strong magnetic field should affect their

pairing. In Ref. [96] the effects of an extremely strong magnetic field on the pairing of a CFL superconductor were investigated.

In this chapter we study how a moderately strong magnetic field (namely, $eB/\mu^2 \lesssim 1$ where μ is the quark chemical potential) changes the properties of color-flavor locked superconducting quark matter. This is expected to model the conditions that exist in the inner core of magnetars where the density of matter can be ten times higher than the nuclear saturation density. For simplicity's sake we assume that under these conditions matter is sufficiently dense so that effects of non-vanishing quark masses (including the strange quark mass) can be neglected. Also, using the property of enforced neutrality of the color-flavor locked phase [159], we assume that no electrons are needed in the magnetized version of the phase. Applying the same arguments as in Ref. [159], we expect that this is justified as soon as all quark quasiparticles remain gapped. In our analysis, therefore, the chemical potentials of up, down, and strange quarks are equal. Admittedly, we neglect possible nonzero color chemical potentials that might be needed to enforce the color Gauss law [160]. However, such chemical potentials are expected to be small for the range of parameters considered here, i.e., $eB/\mu^2 \lesssim 1$.

In order to determine the thermodynamic properties of the mCFL phase we solve the corresponding gap equations for a range of magnetic fields. As expected, the magnetization of mCFL quark matter displays de Haas-van Alphen oscillations and it can be as large as the applied magnetic field for a wide range of parameters. This is in contrast to the magnetization of dense hadronic matter, which is usually considered to be negligible [161]. The large magnetization in magnetar models with (either normal or color-superconducting) quark matter cores could lead to physical properties that are distinctively different from models with only hadronic matter.

In the next section we discuss the most important features concerning mCFL color superconductors and also illustrate the derivation of the free energy and the corresponding gap equations (details of our calculations are explicitly given in Appendices B and C). In Sec. 3.3 we show how to regularize the gap equations within the proper time method and in Sec. 3.4 we show our numerical results. Throughout this chapter 4-vectors are denoted by capital letters, e.g., $K^\mu = (k_0, \vec{k})$. The space-time integration is defined as $\int_X = \int_0^{1/T} \int_\Omega d^3\vec{x}$ where T is the temperature and Ω the volume of the system. Moreover, we use the standard system of units where $\hbar = c = k_B = 1$.

3.2 The Free Energy of the mCFL Phase

In cold, dense quark matter color superconductivity is expected to occur due to attractive interactions between quarks located on the Fermi surface. At very low temperatures and extremely high densities one can safely neglect the effects of nonzero quark masses and, in this case, the CFL phase is expected to be the true ground state of quark matter [84]. This phase is characterized by the condensation of quark Cooper pairs in the color-antitriplet, flavor-antitriplet representation, which breaks the initial symmetry group $[SU(3)]_C \otimes SU(3)_L \otimes SU(3)_R \otimes U(1)_B \otimes U(1)_A$ down into the diagonal $SU(3)_{R+L+C}$ subgroup (note that $U(1)_A$ is an approximate symmetry in dense matter). After taking into account that all the gluons become massive through the Higgs mechanism one finds that ten Nambu-Goldstone bosons appear due to the breaking of global symmetries [162, 163]. Following the same convention as in the QCD vacuum these bosons

are the $\pi^{\pm}$, π^0, $K^{\pm}$, K^0, $\bar{K}^0$, η, η' mesons, and φ, which is a massless field related to baryon symmetry breaking.

We have seen in Sec. 1.5 that in spin-zero color superconductors the initial $[U(1)]_{em}$ symmetry is not really broken but "rotated" [84]. The new group $[\widetilde{U}(1)]_{em}$ corresponds to a massless linear combination of the vacuum photon and the eighth gluon. For convenience, recall that the "rotated" electric $\widetilde{Q}$-charges of the quarks are (see Sec. 1.5)

s_b	s_g	s_r	d_b	d_g	d_r	u_b	u_g	u_r
0	0	-	0	0	-	+	+	0

and the pattern of symmetry breaking that defines the mCFL phase is $[SU(3)]_C \otimes SU(2)_L \otimes SU(2)_R \otimes U(1)_B \otimes U(1)_A \otimes U(1)_A^- \Longrightarrow SU(2)_{R+L+C}$ where $U(1)_A^-$ corresponds to an anomaly-free current formed by a linear combination of the s, d, and u axial currents [97]. There are only six Nambu-Goldstone bosons (i.e., π^0, K^0, $\bar{K}^0$, η, η', and φ) due to symmetry breaking and all of them are neutral with respect to the $\widetilde{Q}$-charge. As expected, the masses of the charged Nambu-Goldstone bosons of the CFL phase (i.e. $\pi^{\pm}$ and $K^{\pm}$) have terms that are proportional to $\sqrt{eB}$ [168].

It is convenient at this point to discuss the energy scales that appear in our study in more detail. The relevant mass scales in the problem are the quark chemical potential μ, the temperature T, and the magnetic length $l = 1/\sqrt{eB}$. For very high, although still realistic densities, $\mu \simeq 500$ MeV. If the magnetar's interior fields are indeed as large as 10^{18} G the corresponding magnetic energy scale approaches the QCD scale, i.e., $\sqrt{eB} \lesssim 77$ MeV. The relevant dimensionless parameter in the problem is the ratio eB/μ^2, which is smaller than one even for the largest realistic fields. Thus, from a phenomenological point of view it would suffice to study only the regime of small eB/μ^2. However, our analysis extends also to larger fields which correspond to $eB/\mu^2 \simeq 1$.

Note that at such extremely high fields the magnetic length can be comparable or even smaller than the average interquark distance. Then, all usual assumptions about the color superconductor's in-medium electromagnetic properties should be reanalyzed. In fact, in this limit the most important effect caused by the field might be the so-called magnetic catalysis of chiral symmetry breaking, as in the vacuum [97, 98, 99]. The corresponding new ground state is characterized by different condensates. Its symmetry, though, is similar to the symmetry in the mCFL phase except for the baryon number symmetry that remains unbroken [97].

We use a massless three-flavor quark model with a local NJL-type interaction to describe the mCFL phase. The free energy density $\mathcal{F}$ of this system composed of quarks in the presence of an external magnetic field $\vec{H}$ is a functional that depends on the gap functions, the chemical potential, the temperature, and the induced magnetic field $\vec{B}$. The fields $\vec{H}$ and $\vec{B}$ have different physical meaning and need to be distinguished. For instance, in an idealized model for the inner core of a color-superconducting magnetar, $\vec{H}$ would correspond to the field present in the outer layers of the star. Inside the core one has to take into account the magnetization of the medium and in this case $\vec{B}$ has to be used. We assume that both $\vec{H}$ and $\vec{B}$ are uniform fields that point in the $\hat{z}$-direction. This approximation is valid as long as the fields do not change appreciably within the relevant length scales defined throughout the computation of the system's thermodynamic quantities such as the quark number density. This is indeed the case here because the characteristic length scale associated with the problem is of the order of one

fermi. Note that we do not specify here whether the magnetic field has toroidal and/or poloidal components.

The partition function of the system is given by

$$\begin{aligned} \mathcal{Z} &= \mathcal{N}_0\, e^{-\frac{\Omega}{T}\left(\mathcal{F}+\frac{B^2}{8\pi}\right)} \\ &= \int \mathcal{D}\bar{\psi}\mathcal{D}\psi\, \exp\left\{\int_X \left[\mathcal{L}-\frac{B^2}{8\pi}\right]\right\}, \end{aligned} \tag{3.1}$$

where $\mathcal{N}_0$ is the normalization constant. The Lagrangian density reads

$$\mathcal{L} = \bar{\psi}(i\partial\!\!\!/ + e\widetilde{Q}A\!\!\!/ + \mu\gamma_0)\psi + \sum_{\eta=1}^{3}\frac{G}{4}(\bar{\psi}P_\eta\psi_c)(\bar{\psi}_c\bar{P}_\eta\psi), \tag{3.2}$$

where A^μ describes the gauge field of the in-medium electromagnetism $[\widetilde{U}(1)]_{em}$. The quark spinor ψ^a_α carries color $a = (b, g, r) = (1, 2, 3)$ and flavor $\alpha = (s, d, u)$ indices and the charge-conjugate spinors are defined as in Chapter 2, i.e., $\psi_c = C\bar{\psi}^T$ and $\bar{\psi}_c = \psi^T C$ where $C = i\gamma^2\gamma^0$ is the charge conjugation matrix.

We consider only the pairing in the antisymmetric channels and, thus, $(P_\eta)^{ab}_{\alpha\beta} = i\gamma_5\,\epsilon^{ab\eta}\epsilon_{\alpha\beta\eta}$ (no sum over η) and $\bar{P}_\eta = \gamma_0 P_\eta^\dagger\gamma_0$. The index η labels the pairing channels, i.e., $\eta = 1$, 2, and 3 correspond to ud, us, and sd pairings, respectively.

For each channel we introduce a complex scalar field ϕ_η, which has expectation value Δ_η. The four-fermion interaction is bosonized via a Hubbard-Stratonovich transformation, which then gives a Yukawa-type interaction

$$\frac{G}{4}(\bar{\psi}P_\eta\psi_c)(\bar{\psi}_c\bar{P}_\eta\psi) \to \frac{\phi_\eta}{2}(\bar{\psi}_c\bar{P}_\eta\psi) + \frac{\phi^*_\eta}{2}(\bar{\psi}P_\eta\psi_c) - \frac{|\phi_\eta|^2}{G}. \tag{3.3}$$

In the following we neglect diquark fluctuations, which is equivalent to setting $\phi_\eta = \Delta_\eta$. Moreover, using the standard Nambu-Gor'kov spinor

$$\Psi = \begin{pmatrix}\psi \\ \psi_c\end{pmatrix} \tag{3.4}$$

and the gap matrix $\Phi^+ = \sum_{\eta=1}^{3}\Delta_\eta P_\eta$, the Lagrangian density can be rewritten as

$$\mathcal{L}(X) = -\sum_{\eta=1}^{3}\frac{|\Delta_\eta|^2}{G} + \frac{1}{2}\bar{\Psi}(X)\,\mathcal{S}^{-1}(X)\Psi(X) \tag{3.5}$$

where

$$\mathcal{S}^{-1}(X) = \begin{pmatrix}[G^+_{0(\widetilde{Q})}]^{-1} & \Phi^- \\ \Phi^+ & [G^-_{0(-\widetilde{Q})}]^{-1}\end{pmatrix} \tag{3.6}$$

and the following shorthand notation is used: $[G^\pm_{0(\widetilde{Q})}]^{-1} = [i\partial\!\!\!/ + e\widetilde{Q}A\!\!\!/(X) \pm \mu\gamma_0]$ and $\Phi^- = \gamma_0(\Phi^+)^\dagger\gamma_0$.

The mCFL pairing is characterized by the residual $SU(2)_{R+L+C}$ global symmetry, which means that the corresponding gap matrix is invariant under simultaneous flavor ($1 \leftrightarrow 2$) and color ($1 \leftrightarrow 2$) exchanges. Consequently, this implies that $\Delta \equiv \Delta_1 = \Delta_2$ and $\phi \equiv \Delta_3$. The CFL gap structure is recovered when $\Delta = \phi$.

All diquark pairs are chargeless with respect to the "rotated" electromagnetic symmetry. The pairs can be composed of either quarks with opposite $\widetilde{Q}$-charges or $\widetilde{Q}$-neutral quarks (in the following, when discussing quark charges, we always have in mind the $\widetilde{Q}$-charges even if this is not explicitly emphasized). The gap function ϕ has contributions only from pairs of neutral quarks while Δ is formed by pairs of quarks with opposite charges and pairs of neutral quarks. In the presence of a strong magnetic field one would naively expect that pairs made of quarks with opposite charges have smaller coherence lengths in comparison to the pairs formed only by neutral quarks, i.e., Δ should be larger than ϕ. In a following section we show that this is the case in the limit of very strong fields. However, for moderate fields this is not generally true.

The Gibbs free energy density $\mathcal{G}$ of the mCFL phase is

$$\mathcal{G} = \frac{B^2}{8\pi} - \frac{HB}{4\pi} + \mathcal{F} - \mathcal{F}_{\rm vac} \tag{3.7}$$

where

$$\mathcal{F} = \frac{2\Delta^2}{G} + \frac{\phi^2}{G} - \Gamma(T, \mu, \Delta, \phi, B). \tag{3.8}$$

The last term in the equation above is the one-loop contribution of quarks, i.e.,

$$\Gamma(T, \mu, \Delta, \phi, B) = \frac{1}{2} \ln \det \mathcal{S}^{-1}. \tag{3.9}$$

The free energy of the vacuum is given by $\mathcal{F}_{\rm vac} = -\Gamma_{\rm vac} \equiv -\Gamma(0,0,0,0,0)$.

In equilibrium $\mathcal{G}$ is evaluated at its stationary point with respect to Δ, ϕ, and B and it describes all the system's thermodynamic properties. The CFL free energy has to be recovered when H vanishes. The stationary point is found from the solutions of the equations

$$\Delta = \frac{G}{4}\Big(\frac{\partial \Gamma}{\partial \Delta}\Big), \tag{3.10a}$$

$$\phi = \frac{G}{2}\Big(\frac{\partial \Gamma}{\partial \phi}\Big), \tag{3.10b}$$

$$B = H + 4\pi M \tag{3.10c}$$

where M is the magnetization of the system, which is given by $M = (\partial\Gamma/\partial B)|_{\rm stationary}$. At the stationary point the gaps depend explicitly on the induced field B. This field incorporates the magnetic properties of the medium described by the magnetization M.

We consider only the zero-temperature limit $T = 0$ in our discussion because typical temperatures in stellar cores are much less than 1 MeV [144]. According to Eq. (B.33) in Appendix B the one-loop quark contribution to the free energy reads

$$\begin{aligned} \Gamma(0, \mu, \Delta, \phi, B) &= 3\,P(\phi) + P(\Delta_1) + P(\Delta_2) \\ &+ 4\,F(\Delta) \end{aligned} \tag{3.11}$$

where $\Delta_{1/2} = \frac{1}{2}(\sqrt{\phi^2 + 8\Delta^2} \pm \phi)$. The neutral quark contributions are given by the three terms containing P-functions

$$P(\phi) \;=\; \mathrm{tr}_{B=0}\left[E_0^+(\phi) + E_0^-(\phi)\right] \tag{3.12}$$

where the trace is defined as $\mathrm{tr}_{B=0}[\ldots] = \int \frac{d^3\vec{p}}{(2\pi)^3}[\ldots]$ and $E_0^{\pm}[\phi] = \sqrt{(p \mp \mu)^2 + \phi^2}$ with $p \equiv \sqrt{p_3^2 + \vec{p}_\perp^{\,2}}$. The one-loop contributions from charged quarks are given in terms of the following function:

$$F(\Delta) \;=\; \mathrm{tr}_B\left[E_B^+(\Delta) + E_B^-(\Delta)\right]. \tag{3.13}$$

The trace is here defined as a sum over the Landau levels with an integral over the longitudinal momentum, i.e.,

$$\mathrm{tr}_B[\ldots] = \frac{eB}{8\pi^2}\sum_{n=0}^{\infty}\alpha_n \int_{-\infty}^{\infty} dp_3[\ldots] \tag{3.14}$$

with $\alpha_n = 2 - \delta_{n0}$. The quasiparticle dispersion relation of charged quarks is

$$E_B^{\pm}[\Delta] = \sqrt{(\varepsilon_B \mp \mu)^2 + \Delta^2} \tag{3.15}$$

where $\varepsilon_B = \sqrt{p_3^2 + 2eBn}$.

Using the well-known Euler-McLaurin summation formula [54]

$$\sum_{n=0}^{\infty}\frac{\alpha_n}{2}f(n) = \int_0^{\infty} dx\, f(x) - \frac{1}{12}f'(0) + \cdots, \tag{3.16}$$

we see that, formally, $\lim_{B\to 0} F(x) = P(x)$. Therefore, after taking the limit $\Delta = \phi$ and $B = H = 0$ we recover the free energy of the CFL phase in the absence of an external field.

3.2.1 Regularizing the mCFL Free Energy

The traces in the definition of the P and F functions involve integrations and sums over the quasiparticle energies throughout the whole phase space, which means that these functions diverge in the ultraviolet. In order to obtain the physically meaningful free energy density of the system these functions must be regularized. In effective quark models, such as the NJL model used here, it is common to restrict the phase space by introducing a sharp finite cutoff in momentum space. However, because of the special properties of the system in a magnetic field, such a prescription is not very useful. Utilizing a sharp cutoff when an energy spectrum with discrete Landau levels is considered would introduce unphysical discontinuities in many thermodynamical quantities.

In this study, therefore, we regularize the traces in Eqs. (3.12) and (3.13) by introducing a smooth cutoff function h_Λ (where Λ is a constant with dimensions of energy). The cutoff function should approach one at small energies ($\varepsilon \ll \Lambda$) and vanish at large energies ($\varepsilon \gg \Lambda$). Providing that h_Λ falls off sufficiently fast in the ultraviolet region, the regularized functions

$$P_\Lambda(\phi) \;=\; \int \frac{d^3\vec{p}}{(2\pi)^3} h_\Lambda\left[E_0^+(\phi) + E_0^-(\phi)\right] \tag{3.17}$$

and

$$F_\Lambda(\Delta) = \frac{eB}{8\pi^2}\sum_{n=0}^{\infty}\alpha_n\int_{-\infty}^{\infty}dp_3\,h_\Lambda\,\left[E_B^+(\Delta)+E_B^-(\Delta)\right] \tag{3.18}$$

are free from divergences. Note that we used $\varepsilon = p$ in Eq. (3.17) and $\varepsilon = \varepsilon_B$ in Eq. (3.18).

After using several different choices for h_Λ we opted to employ the Gaussian-like form, i.e.,

$$h_\Lambda = \exp\left(-\varepsilon^2/\Lambda^2\right) \tag{3.19}$$

in our numerical calculations. A sharp cutoff could be implemented with the function $h_\Lambda = \theta\left(\Lambda-\varepsilon\right)$ [where $\theta\left(x\right)$ is the step function]. While this would produce no apparent abnormalities in the behavior of $P_\Lambda(\phi)$, it leads to unphysical discontinuities in $F_\Lambda(\Delta)$ and, consequently, in the free energy as a function of the magnetic field.

In the numerical calculations in Sec. 3.4 we use the cutoff function in Eq. (3.19) with $\Lambda = 1$ GeV. It should be mentioned here that we have also checked the cutoff independence of our results by varying the value of Λ (while keeping it sufficiently large) and simultaneously readjusting the diquark coupling constant G so as to keep the CFL gap at $B = 0$ unchanged.

Using the regularized functions $P_\Lambda(\phi)$ and $F_\Lambda(\Delta)$ the gap equations (3.10a) and (3.10b) become

$$\Delta = \frac{G}{4}\left[R_1P_1(\Delta_1)+R_2P_1(\Delta_2)+4\Delta F_1(\Delta)\right], \tag{3.20a}$$

$$\phi = \frac{G}{2}\left[3\phi P_1(\phi)+U_1P_1(\Delta_1)+U_2P_1(\Delta_2)\right], \tag{3.20b}$$

where the functions P_1 and F_1 are defined as follows

$$P_1(\phi) \equiv \frac{1}{\phi}\frac{dP_\Lambda(\phi)}{d\phi}, \tag{3.21a}$$

$$F_1(\Delta) \equiv \frac{1}{\Delta}\frac{dF_\Lambda(\Delta)}{d\Delta}. \tag{3.21b}$$

In the gap equations above we also introduced the notation

$$R_{1/2} = 2\Delta\left(1\pm\frac{\phi}{\sqrt{\phi^2+8\Delta^2}}\right), \tag{3.22a}$$

$$U_{1/2} = \pm\frac{\left(\phi\pm\sqrt{\phi^2+8\Delta^2}\right)^2}{4\sqrt{\phi^2+8\Delta^2}}. \tag{3.22b}$$

The gap equations derived here are slightly different than those obtained in Refs. [96, 164]. However, as shown in Sec. 3.3, our solutions for the gap functions are in agreement with the analytical formulas obtained in Refs. [96, 164] at asymptotically high fields.

3.2.2 Lifshitz-Kosevich Approach

In the core of magnetars the magnetic field could be so large that $T^2 \ll eB \leq \mu^2$. Under these conditions some thermodynamical quantities, such as the magnetization, contain terms that oscillate with large amplitudes as a function of B [54]. To single out the oscillatory parts of the thermodynamic quantities it is sometimes convenient to perform the sum over the levels using the Poisson summation formula

$$\sum_{n=0}^{\infty} \alpha_n \, \rho(n) = 2 \int_0^{\infty} dn \, \rho(n) + 4 \, Re \left\{ \sum_{k=1}^{\infty} \int_0^{\infty} dn \, \rho(n) \, \exp(i2\pi k \, n) \right\}. \tag{3.23}$$

This idea was employed by Lifshitz and Kosevich in Ref. [165] in their analysis of the de Haas-van Alphen effect. In this section we use their method to show that the mCFL gap functions should be oscillating functions of the magnetic field.

Only F_Λ is important in this analysis because P_Λ does not depend explicitly on the Landau levels. We can then compute the sum over Landau levels in Eq. (3.18) and obtain

$$F_\Lambda(\Delta) = P_\Lambda(\Delta) + \sum_{k=1}^{\infty} Re\{F_\Lambda^k(\Delta)\} \tag{3.24}$$

where

$$F_\Lambda^k(\Delta) \equiv \frac{eB}{\pi^2} \int_0^{\infty} dp_3 \int_0^{\infty} dn \, h_\Lambda \, \left[E_B^+(\Delta) + E_B^-(\Delta)\right] \, \exp(i2\pi k \, n), \tag{3.25}$$

whereas n is now a continuous variable. The first term on the right-hand side in Eq. (3.24) provides the contribution that is independent of the magnetic field. Now we change the integration variable from n into ε using $n = (\varepsilon^2 - p_3^2)/2eB$, which gives

$$F_\Lambda^k(\Delta) = \frac{1}{\pi^2} \int_0^{\infty} dp_3 \int_{\frac{p_3}{\sqrt{2eB}}}^{\infty} d\varepsilon \; \varepsilon \, h_\Lambda \, \left[E_0^+(\Delta) + E_0^-(\Delta)\right] \, \exp(-i\pi k \, p_3^2/eB) \, \exp(i\pi k \, \varepsilon^2/eB). \tag{3.26}$$

The important values in the integral over p_3 are concentrated at $p_3^2 \simeq eB$. The oscillatory part of the integral, however, comes from the region where $\varepsilon \simeq \mu$ (see the discussion below). Thus, when $eB \ll \mu^2$ the lower limit of the integral over ε can be taken as zero [54]. This approximation is adopted in the following. The integral over p_3 can be performed and we obtain

$$F_\Lambda^k(\Delta) = \frac{1}{2\pi^2} \left(\frac{eB}{k}\right)^{1/2} \int_0^{\infty} d\varepsilon \; \varepsilon \, \exp(i\pi k \, \varepsilon^2/eB - i\pi/4) \, h_\Lambda \, \left[E_0^+(\Delta) + E_0^-(\Delta)\right]. \tag{3.27}$$

Performing the integral above by parts, we obtain

$$\begin{aligned} F_\Lambda^k(\Delta) \;&=\; \frac{1}{4i\pi^3} \left(\frac{eB}{k}\right)^{3/2} \exp(-i\pi/4) \left\{ h_\Lambda \left[E_0^+(\Delta) + E_0^-(\Delta)\right] \, \exp(i\pi k \, \varepsilon^2/eB) \Big|_0^{\infty} \right. \\ &-\; \int_0^{\infty} d\varepsilon \, \exp(i\pi k \, \varepsilon^2/eB) \left[\frac{dh_\Lambda}{d\varepsilon} \, \left(E_0^+(\Delta) + E_0^-(\Delta)\right) \right. \\ &-\; \left. \left. h_\Lambda \left(\frac{\varepsilon + \mu}{E_0^+(\Delta)} + \frac{\varepsilon - \mu}{E_0^-(\Delta)} \right) \right] \right\}. \end{aligned} \tag{3.28}$$

Reorganizing the terms, we end up with

$$\begin{aligned} F_\Lambda^k(\Delta) &= -\frac{\exp(-i\pi/4)}{2\pi^3}\left(\frac{eB}{k}\right)^{3/2}\sqrt{\mu^2+\Delta^2} - \frac{1}{4i\pi^3}\Big(\frac{eB}{k}\Big)^{3/2}\exp(-i\pi/4) \\ &\times \int_0^\infty d\varepsilon\,\exp(i\pi k\,\varepsilon^2/eB)\Big\{h_\Lambda\Big[\frac{\varepsilon+\mu}{E_0^+(\Delta)}+\frac{\varepsilon-\mu}{E_0^-(\Delta)}\Big] \\ &+ \frac{dh_\Lambda}{d\varepsilon}\left[E_0^+(\Delta)+E_0^-(\Delta)\right]\Big\}. \end{aligned} \tag{3.29}$$

The function $dh_\Lambda/d\varepsilon$ has its largest values around Λ and, as long as $\Lambda/\mu \gg 1$, the last term in the integral in Eq. (3.29) can be omitted because it is for the most part canceled by the vacuum subtracting term $\mathcal{F}_{vac}$. Therefore, the function F_Λ^k contains only two terms

$$\begin{aligned} F_\Lambda^k(\Delta) &= -\frac{\exp(-i\pi/4)}{2\pi^3}\left(\frac{eB}{k}\right)^{3/2}\sqrt{\mu^2+\Delta^2} - \frac{1}{4i\pi^3}\Big(\frac{eB}{k}\Big)^{3/2}\exp(-i\pi/4) \\ &\times \int_0^\infty d\varepsilon\,\exp(i\pi k\,\varepsilon^2/eB)\;h_\Lambda\Big[\frac{\varepsilon+\mu}{E_0^+(\Delta)}+\frac{\varepsilon-\mu}{E_0^-(\Delta)}\Big]. \end{aligned} \tag{3.30}$$

The cutoff function in the integral above is not really necessary. This can be shown by rewriting the last term in Eq. (3.30) using an extra integral over Δ'

$$\begin{aligned} F_\Lambda^k(\Delta) &= -\frac{\exp(-i\pi/4)}{2\pi^3}\left(\frac{eB}{k}\right)^{3/2}\sqrt{\mu^2+\Delta^2} + \frac{1}{4i\pi^3}\Big(\frac{eB}{k}\Big)^{3/2}\exp(-i\pi/4) \\ &\times \int_0^\infty d\varepsilon\,\exp(i\pi k\,\varepsilon^2/eB)\int_0^\Delta d\Delta'\,\Delta'\Big[\frac{\varepsilon+\mu}{E_0^{+\,3}(\Delta')}+\frac{\varepsilon-\mu}{E_0^{-\,3}(\Delta')}\Big]. \end{aligned} \tag{3.31}$$

Since the integrand converges at least linearly there is no need to include the cutoff function in Eq. (3.31). This expression can be simplified even further by introducing the variable $\xi = \varepsilon - \mu$, which gives

$$\begin{aligned} F_\Lambda^k(\Delta) &= -\frac{\exp(-i\pi/4)}{2\pi^3}\left(\frac{eB}{k}\right)^{3/2}\sqrt{\mu^2+\Delta^2} + \frac{1}{4i\pi^3}\Big(\frac{eB}{k}\Big)^{3/2}\exp(ik\pi\mu^2/eB - i\pi/4) \\ &\times \int_0^\Delta d\Delta'\,\Delta'\int_{-\infty}^\infty d\xi\,\xi\,\frac{\exp(i2\pi k\,\xi\mu/eB)}{(\xi^2+\Delta^2)^{3/2}}, \end{aligned} \tag{3.32}$$

where we used that the relevant part of the integral is defined within the range where $\xi/\mu \ll 1$, which allows us to neglect the contribution coming from the quasi-antiparticles. Moreover, we have extended the lower limit of integration from $-\mu$ to $-\infty$, which is a valid approximation in the limit $eB \ll \mu^2$ [54]. The integral over ξ in Eq. (3.32) can be solved analytically in terms of the modified Bessel function of the second kind $K_1(x)$ [166]. The final result for F_Λ is

$$\begin{aligned} F_\Lambda(\Delta) &= P_\Lambda(\Delta) + \frac{\sqrt{2}}{4\pi^3}\zeta(3/2)\,\mu^3\sqrt{\mu^2+\Delta^2}\left(\frac{eB}{\mu^2}\right)^{3/2} + \sum_{k=1}^\infty \frac{\mu^4}{4\pi^4}\left(\frac{eB}{k\,\mu^2}\right)^{5/2} \\ &\times \cos(k\pi\mu^2/eB - \pi/4)\Big[1 - \frac{2\pi\Delta\,k\mu}{eB}\,K_1\left(\frac{2\pi k\,\Delta\,\mu}{eB}\right)\Big]. \end{aligned} \tag{3.33}$$

This expression clearly shows that $F_\Lambda(\Delta)$ receives an oscillatory contribution due to the cosine term with a period proportional to μ^2/eB (although several harmonics may also contribute). Thus, we see that since $F_\Lambda(\Delta)$ oscillates so does $F_1(\Delta)$ (see its definition in Eq. (3.21b)). This also implies that the gap functions will experience similar magnetic oscillations. However, note that for large values of k and small magnetic fields $eB/\mu^2 \ll 1$ the asymptotic expansion of $K_1(x) \simeq \exp(-x)\,(\pi/2x)^{1/2}$ indicates that for large gaps the oscillations are strongly suppressed.

Even though we have made several approximations in the derivation of Eq. (3.33), we expect that the magnetic oscillations are indeed present in the system. In fact, it is shown in Sec. 3.4 that our full numerical solutions for the gap equations display magnetic oscillations.

3.3 Proper Time Regularization of the Gap Equations

A fully quantitative study of the mCFL gap equations can only be done numerically, which is done in Sec. 3.4. In order to obtain a deeper insight into this problem here, we also perform an analytical analysis of the mCFL gap equations. For this it is convenient to use the proper time formalism originally introduced by Schwinger [167].

We use the following proper time representation

$$\mathrm{tr}\left(\frac{1}{A}\right) = \frac{1}{\sqrt{\pi}}\int_0^\infty \frac{d\tau}{\sqrt{\tau}}\,\mathrm{tr}\left(e^{-A^2\tau}\right) \tag{3.34}$$

to obtain the following expressions for the functions $P_1(\phi)$ and $F_1(\phi)$ in the gap equations

$$\begin{aligned} P_1(\phi) &= \frac{\mu^2}{4\pi^2}\int_{(\mu/\Lambda)^2}^\infty \frac{ds}{s^2}\,(1+2s)\,e^{-s(\phi/\mu)^2} \\ &= \frac{1}{4\pi^2}\left[\Lambda^2 e^{-\phi^2/\Lambda^2} + (2\mu^2-\phi^2)\mathrm{Ei}\left(-\frac{\phi^2}{\Lambda^2}\right)\right], \end{aligned} \tag{3.35}$$

$$F_1(\phi) = \frac{\mu^2}{4\pi^2}\int_{(\mu/\Lambda)^2}^\infty \frac{ds}{\sqrt{s}} e^{-s(\Delta/\mu)^2} f\,(y,s)\,, \tag{3.36}$$

where we defined the dimensionless proper time parameter s as $s = \mu^2\tau$, $\mathrm{Ei}(x)$ is the exponential integral function [166], and the following new function was introduced

$$\begin{aligned} f(y,s) &= \frac{y}{2\sqrt{\pi}}\sum_{n=0}^\infty \alpha_n \int_0^\infty dz\,\left[e^{-\left(\sqrt{z^2+yn}+1\right)^2 s}\right. \\ &\quad \left. + e^{-\left(\sqrt{z^2+yn}-1\right)^2 s}\right], \end{aligned} \tag{3.37}$$

with $y \equiv 2eB/\mu^2$. Note that in the limit of weak and strong fields this function behaves as

$$f(y,s) \simeq \frac{y}{2\sqrt{s}}\coth\left(\frac{ys}{2}\right), \quad \text{for} \quad y \gg 1, \tag{3.38}$$

$$f(y,s) \simeq \frac{1+2s}{s^{3/2}} + \frac{y^2}{12} r_s, \quad \text{for} \quad y \ll 1. \tag{3.39}$$

The term r_s is obtained from the weak-field expansion of $f(y,s)$ as follows

$$\begin{aligned} r_s &= \frac{s}{\sqrt{\pi}}\int_0^\infty dz\left[e^{-s(z+1)^2}+e^{-s(z-1)^2}\right. \\ &\quad \left.+\frac{1}{z}\left(e^{-s(z+1)^2}-e^{-s(z-1)^2}\right)\right] \\ &= \sqrt{s}\left[1-\sqrt{\pi s}\,e^{-s}\,\mathrm{Erfi}(\sqrt{s})\right], \end{aligned} \tag{3.40}$$

where $\mathrm{Erfi}(z)$ is the imaginary error function [166].

3.3.1 Analytical Solutions of the Gap Equations

The first important limit that has to be considered is the CFL superconducting limit, which is defined for zero magnetic fields. This changes Eq. (3.11) into

$$\Gamma(0,\mu,\Delta,\phi,0) = 3P(\phi)+P(\Delta_1)+P(\Delta_2)+4P(\Delta) \tag{3.41}$$

where we used $\lim_{B\to 0} F(\Delta) = P(\Delta)$. The gap equations are then

$$\Delta = \frac{G}{4}\left[R_1\,P_1(\Delta_1)+R_2\,P_1(\Delta_2)+4\Delta\,P_1(\Delta)\right], \tag{3.42}$$

and

$$\phi = \frac{G}{2}\left[3\phi\,P_1(\phi)+U_1\,P_1(\Delta_1)+U_2\,P_1(\Delta_2)\right]. \tag{3.43}$$

These equations have only one nontrivial solution: $\Delta=\phi=\phi_0$ where ϕ_0 is the CFL gap function. In fact, using the ansatz $\Delta=\phi=\phi_0$ we find that the two equations coincide with each other, which gives

$$\phi_0 = \frac{2G\,\phi_0}{3}\left[2P_1(\phi_0)+P_1(2\phi_0)\right]. \tag{3.44}$$

This is the gap equation of the CFL phase. The corresponding free energy is also reduced to the CFL free energy. We now find an analytical solution for the equation above. Excluding the trivial solution $\phi_0=0$ and using the analytical representation for the P_1-function in Eq. (3.35), the gap equation takes the form

$$\begin{aligned} 1 &= \frac{G}{3\pi^2}\left[\Lambda^2\left(\frac{1}{2}e^{-4\phi_0^2/\Lambda^2}+e^{-\phi_0^2/\Lambda^2}\right)+(2\phi_0^2-\mu^2)\right. \\ &\quad \left.\times\mathrm{Ei}\left(-\frac{4\phi_0^2}{\Lambda^2}\right)+(\phi_0^2-2\mu^2)\mathrm{Ei}\left(-\frac{\phi_0^2}{\Lambda^2}\right)\right]. \end{aligned} \tag{3.45}$$

Assuming that $\phi_0/\mu \ll 1$ and $\phi_0/\Lambda \ll 1$ this equation becomes

$$1 \simeq \frac{G}{\pi^2}\left\{\frac{\Lambda^2}{2}-\mu^2\left[\gamma+\ln(2^{2/3}\phi_0^2/\Lambda^2)\right]\right\} \tag{3.46}$$

where γ is the Euler-Mascheroni constant. The solution for ϕ_0 is

$$\phi_0 = \frac{\Lambda}{2^{1/3}}\exp\left(-\frac{\pi^2}{2\,G\,\mu^2}+\frac{\Lambda^2}{4\mu^2}-\frac{\gamma}{2}\right). \tag{3.47}$$

Note that the exponent in Eq. (3.47) contains the typical BCS factor $\exp(-1/NG)$ where G is the diquark coupling constant and N is the density of states of the quarks that contribute to the pairing. The density of states of a single quark is $N_0 = \mu^2/2\pi^2$, which can be seen from Eq. (B.29). Therefore, in this case we have that $N = 4N_0$.

3.3.2 mCFL Phase in Ultrastrong Fields

It is also possible to solve the gap equations in Eqs. (3.20a) and (3.20b) analytically when only the lowest Landau level (LLL) is populated. This corresponds to the case where $eB/\mu^2 \gg 1$. Assuming that $\Delta \gg \phi$ in this limit, we obtain that

$$\Delta_{1/2} \simeq \sqrt{2}\,\Delta \pm \frac{\phi}{2}, \qquad R_{1/2} \simeq 2\Delta \pm \frac{\phi}{\sqrt{2}}, \qquad U_{1/2} \simeq \pm\frac{\sqrt{2}\Delta}{2} + \frac{\phi}{2}\,. \tag{3.48}$$

The gap equations then are

$$\Delta = G\left[\Delta\, P_1(\sqrt{2}\,\Delta) + \Delta\, F_1(\Delta)\right] \tag{3.49}$$

and

$$\phi = \frac{G}{2}\left[3\phi\, P_1(\phi) + \phi\, P_1(\sqrt{2}\,\Delta) + \sqrt{2}\,\phi\, P_2(\sqrt{2}\,\Delta)\right]. \tag{3.50}$$

In the LLL approximation we have

$$F_1(\Delta) = -\frac{eB}{4\pi^2}\,\mathrm{Ei}(-\Delta^2/\Lambda^2) \tag{3.51}$$

and

$$P_2(\sqrt{2}\Delta) = -\frac{1}{2\sqrt{2}\pi^2}\,\left[\mu^2\, e^{-2\Delta^2/\Lambda^2} - \Delta^2\,\mathrm{Ei}(-2\Delta^2/\Lambda^2)\right]. \tag{3.52}$$

Note that the gap equations are now decoupled. In fact, Eq. (3.49) can be solved to find Δ and this result can be used in Eq. (3.50) to determine ϕ. The equation for Δ is

$$1 \simeq \frac{G}{4\pi^2}\left\{\Lambda^2 - (eB + 2\mu^2)\left[\gamma + \ln(\Delta^2/\Lambda^2)\right] - 2\mu^2\,\ln 2\right\}, \tag{3.53}$$

where the same approximations used in the derivation of Eq. (3.47) have also been applied. Eq. (3.53) has the solution

$$\Delta = \Lambda\,\exp\left[-\frac{2\pi^2}{G(eB + 2\mu^2)} - \frac{\gamma}{2} + \frac{\Lambda^2 - 2\mu^2\,\ln 2}{2\,(eB + 2\mu^2)}\right]. \tag{3.54}$$

The exponent in Eq. (3.54) displays the typical BCS factor $\exp(-1/NG)$ and

$$N = \frac{\mu^2}{\pi^2} + \frac{eB}{2\pi^2} = 4N_0 + 4N_{LLL} \tag{3.55}$$

is the total density of states of the four quasiquarks that contribute to the pairing. However, the situation now is different than that found in CFL superconductors because the quasiquarks can

be neutral or charged. Again, the density of states of a single neutral quasiquark is $N_0 = \mu^2/4\pi^2$. On the other hand, for the lowest Landau level the density of states of charged quasiquarks of a single spin state is $N_{LLL} = eB/8\pi^2$.

The gap equation for ϕ can be similarly solved and we find

$$\phi = \Lambda \left(\frac{\Lambda}{\sqrt{2}\,\Delta}\right)^{1/3} \exp\left(-\frac{\pi^2}{3G\mu^2} + \frac{\Lambda^2}{6\mu^2} - \frac{\gamma}{3} - \frac{1}{12}\right). \tag{3.56}$$

Our analytical results for the gaps are consistent with the assumption $\Delta \gg \phi$ when $eB/\mu^2 \gg 1$, which was made in the beginning of this section. Moreover, they have the same physical properties as those found in Ref. [96, 164].

3.4 Numerical Results

The free parameters of the model (G and Λ) are set to yield a CFL gap ϕ_0 of either 10 MeV or 25 MeV at $\mu = 500$ MeV when $B = 0$. (All numerical results shown below correspond to the choice of the coupling constant and the cutoff parameter: $G = 4.32$ GeV^{-2} or $G = 5.15$ GeV^{-2} and $\Lambda = 1$ GeV.) In Fig. 3.1 we plotted the ratio between the mCFL and CFL gaps as functions of eB/μ^2. As was mentioned in the last section, we have checked the model dependence of our results by changing the parameters Λ and G. When $eB/\mu^2 \gtrsim 0.3$ the gap Δ, which receives contributions from pairs of neutral quarks and also pairs with opposite charges, differs considerably from ϕ where only neutral quarks enter into the pairing. For smaller fields ($eB/\mu^2 \lesssim 0.1$) the mCFL gaps are practically the same as ϕ_0.

For ultrastrong fields ($eB/\mu^2 \gtrsim 2$) Δ is much larger than ϕ. This is consistent with the analytical solutions for the mCFL gap equations found in Sec. 3.3.1 and in Refs. [96, 164]. There the authors considered fields so large that only the lowest Landau level contributed to the dynamics. As argued in the previous section, since these fields should already probe the dynamics of the vacuum the effects from magnetic catalysis should be taken into account [97, 98, 99]. Moreover, assuming $\mu = 500$ MeV, the corresponding field strengths appear to be of the order of $B \simeq 8.5 \times 10^{19}$ G, which may be too large to be found in compact stars [169].

In Fig. 3.1 we see that the gaps display magnetic oscillations with respect to eB/μ^2, which is in agreement with the discussion in Sec. 3.2.2. These oscillations share the same physical origin as the de Haas-van Alphen oscillations observed in metals. They appear as a consequence of the oscillatory structure in the density of states, which is imposed by the quantization of the energy levels associated with the orbital motion of charged particles [54].

At zero temperature most electronic properties of metals depend on the density of states on the Fermi surface. Therefore, an oscillatory behavior as a function of B should appear in any quantity that depends on the density of states on the Fermi surface. In the case of an mCFL color superconductor it is the quark density of states on the Fermi surface that is relevant. Since the gaps in the excitation spectrum depend on the quark density of states and every physical quantity that we are interested in depends on the gaps, some type of magnetic oscillations should appear. The presence of nonzero gaps, however, smears out the Fermi surface so that the oscillatory structure is considerably reduced. This then explains the smoothness of the oscillations and their dependence on the magnitude of the gaps, which are seen in Fig. 3.1.

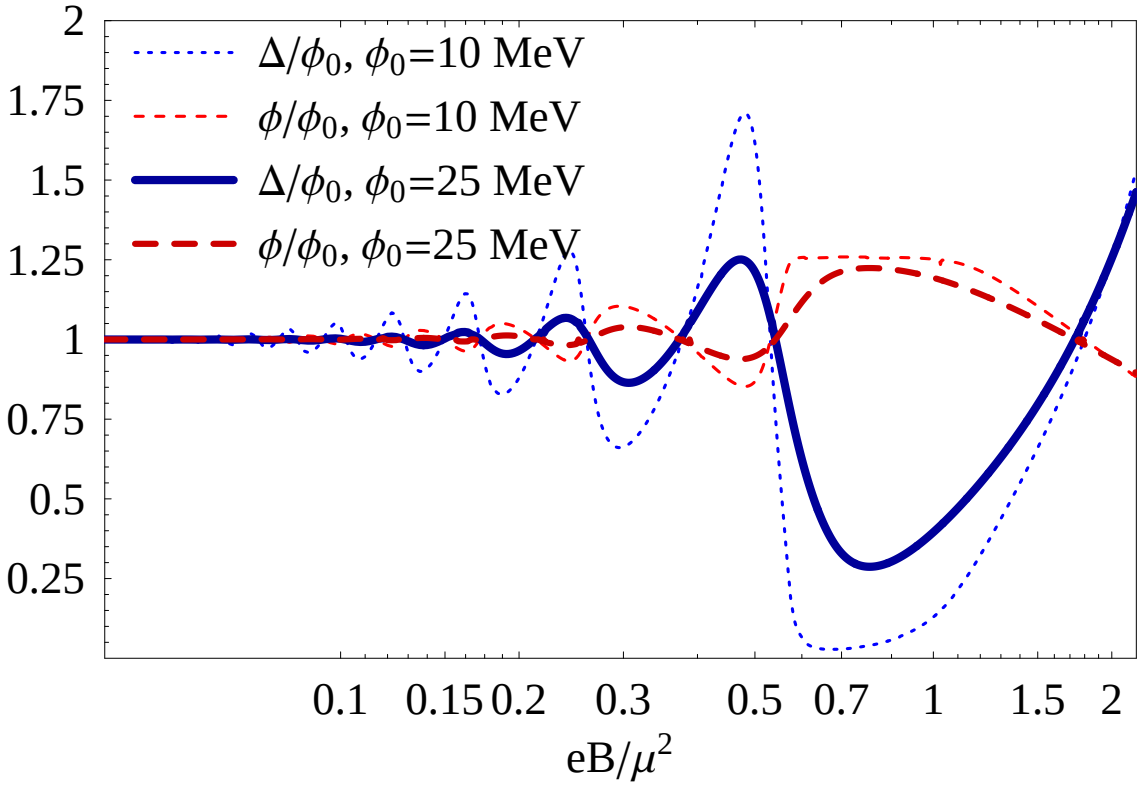

Figure 3.1: Ratios Δ/ϕ_0 and ϕ/ϕ_0 versus eB/μ^2 for two sets of parameters that yield $\phi_0 = 10$ MeV and $\phi_0 = 25$ MeV.

3.4.1 Magnetic Properties of mCFL Quark Matter

In the presence of strong magnetic fields the magnetization M affects the properties of the mCFL phase. As mentioned in the introduction, this might be relevant to explain the magnetic properties of magnetars with color-superconducting quark cores. A phenomenon that is quite often observed in magnetic systems is the formation of magnetic domains [54]. In metals, the large magnitude of the de Haas-van Alphen oscillations in the magnetization can create regions where $(\partial H/\partial B)_\mu < 0$ and/or $HB < 0$. These correspond to unstable or metastable states. The condition for thermodynamic stability $(\partial H/\partial B)_\mu > 0$ implies that $4\pi\,|\chi(\mu, B)| < 1$ where $\chi(\mu, B) = (\partial M/\partial B)_\mu$ is the differential susceptibility. When the differential susceptibility exceeds $1/4\pi$, depending on the geometry of the system, a transition into a magnetic domain configuration may occur. The presence of magnetic domains in the crust of a neutron star was discussed by Blandford and Hernquist in Ref. [170].

In Ref. [161] it was shown that the magnetization of hadronic matter is negligible even for magnetar conditions, i.e., $4\pi\,M/B \ll 1$ for $B \lesssim 10^{19} G$. In the case of color-superconducting matter, however, the situation is very different. In Fig. 3.2 we plotted this ratio versus eB/μ^2 for an mCFL superconductor. The magnetization is extremely large in this case and it displays de Haas-van Alphen oscillations that have very large magnitudes. Note that the existence of

nonzero energy gaps makes the Fermi surface look fuzzy and the magnetization's oscillations in mCFL quark matter are much smoother than those of the magnetization of cold, unpaired quark matter [171].

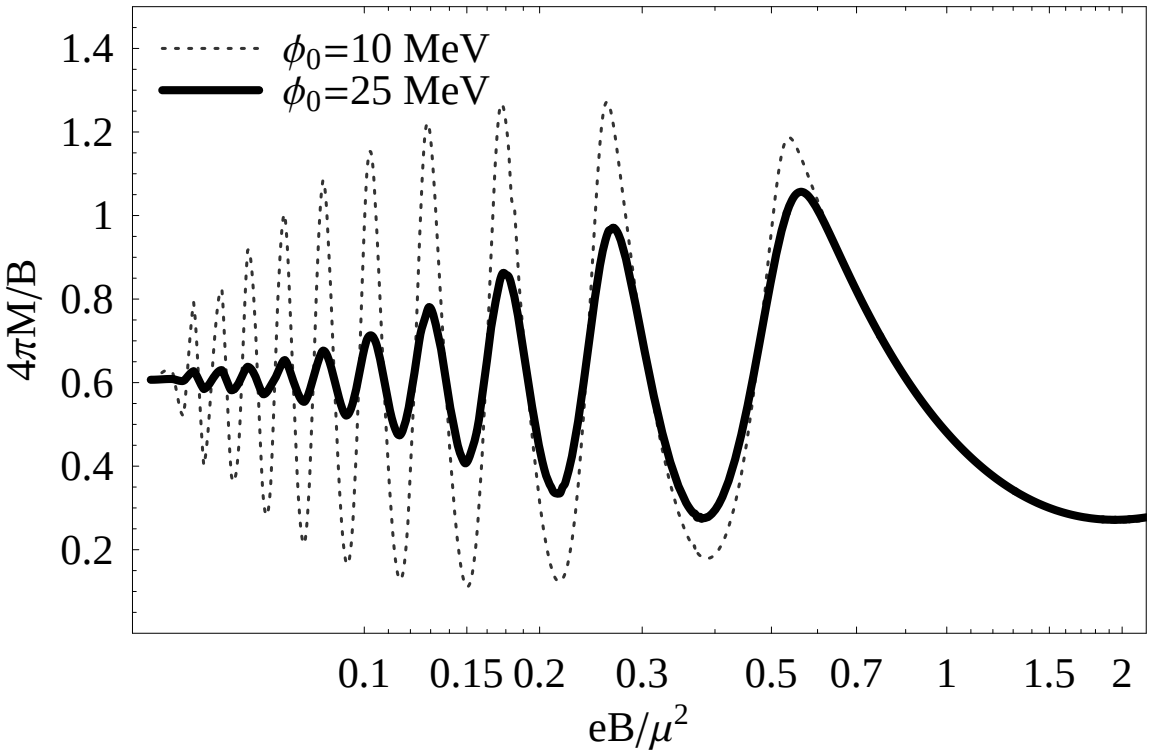

Figure 3.2: Ratio $4\pi\, M/B$ versus eB/μ^2 for two sets of parameters that yield $\phi_0 = 10$ MeV and $\phi_0 = 25$ MeV.

Our results for the H-B curve are shown in Fig. 3.3. Several regions of thermodynamic instabilities are obtained for $eB/\mu^2 \lesssim 1$. The metastable regions in Fig. 3.3, which correspond to $(\partial H/\partial B)_\mu < 0$, can be filtered out by either using a Maxwell construction or a mixed phase where microscopic domains with nonequal magnetization values coexist. This could lead to various physical consequences. As the field H increases the system could undergo successive phase transitions with discontinuous changes of the induced magnetic field B [54]. On the other hand, when mixed phases are formed the relative size of domains with different magnetization values would change with H so as to keep the average induced magnetic field B continuous. In either case, since the magnitude of the fields involved is enormous the system could potentially release an immense amount of energy. Further studies are needed to see whether this finding could have any important implications for magnetars.

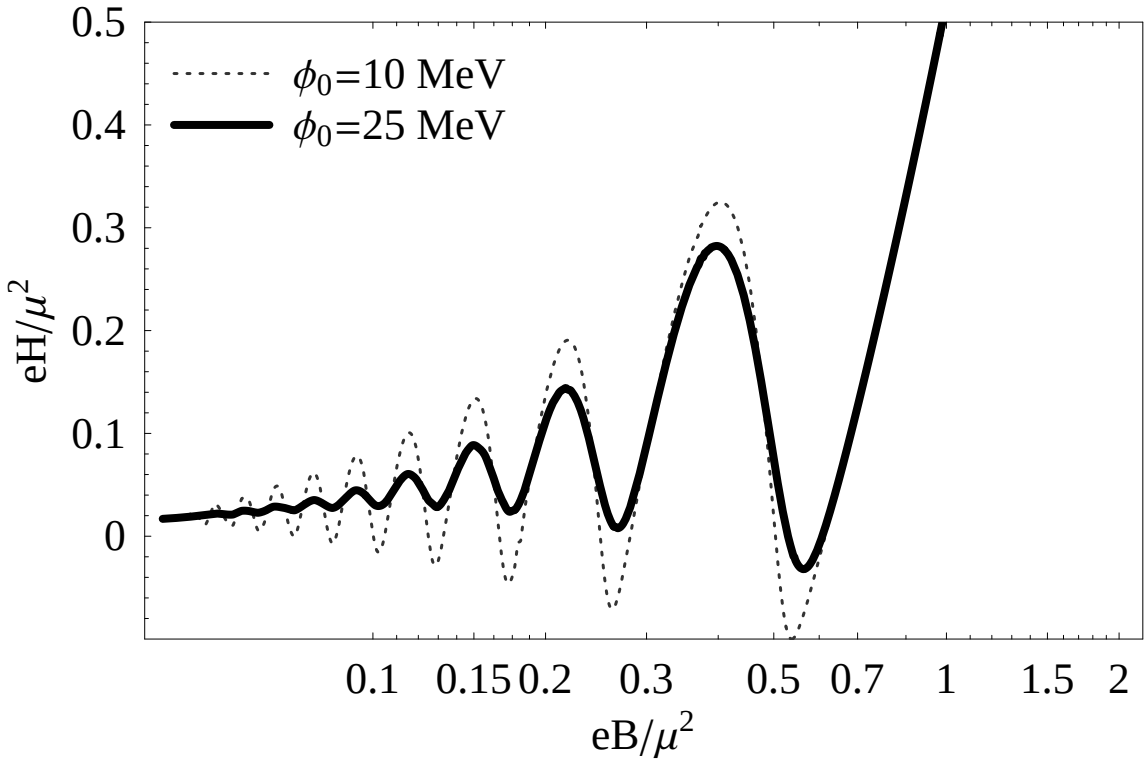

Figure 3.3: External field eH/μ^2 versus eB/μ^2 for two sets of parameters that yield $\phi_0 = 10$ MeV and $\phi_0 = 25$ MeV.

Chapter 4

Tkachenko Modes as Sources of Quasiperiodic Pulsar Spin Variations

In this chapter we study the long-wavelength shear modes (Tkachenko waves) of triangular lattices formed by vortices in neutron star interiors taking into account the mutual friction between the superfluid and the normal fluid as well as the shear viscosity of the normal fluid. The set of Tkachenko modes that propagate in the plane orthogonal to the spin vector are weakly damped if the coupling between the superfluid and the normal fluid is small. In strong coupling, however, their oscillation frequencies are lower and undamped for small and moderate values of the shear viscosity. The periods of these modes are consistent with the observed $\sim 100 - 1000$ day variations of spin for PSR 1828-11. We presented the results discussed in this chapter in Ref. [133].

4.1 Introduction

Pulsars are rotating neutron stars that generate lighthouse-like beams of radio emission from their magnetic poles. The measured pulse allows for the determination of their rotation rates with great precision. Most pulsars have stable pulsar shapes and are steadily slowing down [174]. However, observations in the past few decades revealed several types of timing irregularities in a subclass of isolated compact stars.

The observation of pulsar glitches provides a striking example of a timing anomaly. They correspond to abrupt increases in the pulsar rotational frequency and its derivative. The slow relaxation of these quantities after the glitch has been considered as a signal for the presence of superfluidity inside neutron stars [175]. Neutron superfluidity is expected to take place in dense hadronic matter due to the attractive component of the nuclear force, which leads to the formation of neutron Cooper pairs. At low densities the pairing can occur in the relative $^1S_0$ channel and at high densities the $^3P_2 - {}^3F_2$ channel is favored [176]. In addition, protons are expected to pair in the S-wave channel due to their low concentration.

Even though pulsar glitches attest to the existence of superfluidity in stars, they cannot be used in determining how large the coupling between the superfluid and the normal fluid component is. During the last decade mounting evidence has emerged for the existence of

long-period oscillations in a handful of pulsars [177]. An outstanding example of this kind of phenomenon is observed in PSR 1828-11 [178]. Its timing residuals are modulated with periods of 256 and 511 days, while a 1009-day periodicity is inferred with less confidence. These timing residuals coincide with periodic modulations of the pulse shape, which indicates that the pulsar undergoes some sort of precessional motion with the periods quoted above [179].

However, free precession is incompatible with the existence of a superfluid in the pulsar's interior if the superfluid is strongly coupled to the normal fluid [180]. The parameter that quantifies the coupling depends on the superconducting/superfluid properties of the fluid(s) and the non-superconducting material which resists the vortex motion. Microscopic calculations predict a wide range of values for this parameter. However, if free precession is established beyond a reasonable doubt it will exclude strongly coupled theories. Nevertheless, while free precession is a plausible source for the long-term variability in pulsar timing, here we follow a different route [181] by exploring the propagation of Tkachenko modes as the source of long-term pulsar spin variations.

In the late 60's Tkachenko showed that the lowest energy state of an infinite array of vortices in an incompressible superfluid occurs when the vortices form a two-dimensional triangular lattice [182]. The lattice supports collective elastic modes, called Tkachenko waves, in which the vortex lines undergo parallel displacements with elliptic polarization in the plane perpendicular to the rotation axis. These modes cannot be described within standard Bekarevich-Khalatnikov hydrodynamics [183] because this theory includes only the dependence of the rotational energy on the mean local vortex density and it neglects the energy increase produced by the shear of the vortex lattice, which is the restoring force for these modes.

Charge neutral superfluids in neutron star interiors rotate by forming an array of singly quantized vortices. The undamped propagation of the corresponding Tkachenko waves would cause local changes in the density of the vortex lines that generate variations in the superfluid's angular momentum. Therefore, it is expected that this can lead to changes in the rotation and spin-down speeds of the star. Using this idea, Ruderman [184] pointed out that Tkachenko modes provided a possible explanation for the quasiperiodic timing residuals observed in the Crab pulsar, which have periods of hundreds of days.

In this chapter we study the propagation of Tkachenko modes in neutron star superfluids and calculate the damping of these modes by mutual friction and the shear viscosity of normal matter. These factors are clearly important for the continuous propagation of the Tkachenko modes, which would certainly lead to observable effects. Provided that the observed variations are indeed caused by the shear modes of the lattice we can ask the question: what do the quasi-sinusoidal timing variations tell us about the microscopic physics governing superfluids in neutron stars?

This chapter is organized as follows; in Sec. 4.2 we review the equations of superfluid hydrodynamics that include the combined effects of vortex tension, mutual friction, and shear viscosity. Sec. 4.3 is devoted to the derivation of the characteristic equation for the Tkachenko and inertial modes and in Sec. 4.4 we present our numerical results for their frequency. Throughout this chapter the cgs unit system is employed.

4.2 Superfluid Hydrodynamics with Vortex Tension

There are several length scales in this problem, namely, the vortex core radius $\sim 10^{-12}$ cm, the intervortex spacing $\sim 10^{-3}$ cm, and the characteristic size of the region where neutron superfluidity can be found $\sim 10^{5}$ cm (we refer to these three different scales as micro, meso, and macroscopic scales). A meaningful hydrodynamic description requires averaging over the mesoscopic scales. To describe the deformations of the vortex lattice one needs an additional dynamical variable, the local deformation of the vortex lattice $\boldsymbol{\epsilon}(\mathbf{r})$, which must be incorporated in the Bekarevich-Khalatnikov superfluid hydrodynamics [183]. A hydrodynamic description of superfluids that includes lattice deformations has been studied by a number of authors [185, 186, 187]. In this thesis we use the Chandler-Baym version of superfluid hydrodynamics [187] to study the Tkachenko modes and their damping from mutual friction and shear viscosity. For the sake of self-consistency, we repeat some of the steps in Chandler-Baym's derivation of the fundamental superfluid hydrodynamic equations below.

We start off by noting that at nonzero temperature the system is composed of vortices as well as normal fluid and superfluid components. These dynamical components are coupled to each other due to the hydrodynamic equations that contain the usual viscosities [188] and the mutual friction forces arising from the interactions between the normal fluid excitations and the vortex lines. The basic role played by these forces is to couple the velocities of the normal fluid and vortex lines. This coupling damps the transverse modes and the sound modes.

In the laboratory frame, the fluid motions are naturally separated into the center-of-mass motion (first sound) and second sound which corresponds to temperature-dependent relative oscillations between the superfluid and the normal component. These motions are conveniently described in terms of the total mass current $\vec{j} = \rho_N \vec{v}_N + \rho_S \vec{v}_S$ and the relative velocity $\vec{q} = \vec{v}_N - \vec{v}_S$ where ρ_S (ρ_N) and $\vec{v}_S$ ($\vec{v}_N$) are the superfluid (normal fluid) density and velocity, respectively. In addition, one needs an equation for the time variations of the lattice deformation $\vec{\epsilon}(\vec{r})$. Note that the tiny effects arising due to the inertia of the vortex lines are neglected. The total mass density ρ is

$$\rho = \rho_S + \rho_N, \tag{4.1}$$

with which we can write the continuity equation

$$\frac{\partial \rho}{\partial t} + \vec{\nabla} \cdot \vec{j} = 0, \tag{4.2}$$

which is always valid regardless whether the fluid is viscous or not.

It can be shown [187] that the conservation of vorticity leads to the superfluid acceleration equation

$$\frac{\partial \vec{v}_S}{\partial t} + \vec{\omega} \times \frac{\partial \vec{\epsilon}}{\partial t} = -\vec{\nabla} \left(\frac{\vec{v}_S^{\,2}}{2} + h \right), \tag{4.3}$$

where $\vec{\omega} = \vec{\nabla} \times \vec{v}_S$ and h is a dissipative term present also in nonrotating superfluid hydrodynamics [183], which is given by

$$h = -\zeta_3 \vec{\nabla} \cdot \left(\vec{j} - \rho \vec{v}_N \right) - \zeta_4 \vec{\nabla} \cdot \vec{v}_N, \tag{4.4}$$

where ζ_3 and ζ_4 correspond to bulk viscosity coefficients.

The other hydrodynamic equations are the conservation of momentum and the acceleration equation for the vortex lines. The momentum conservation law (Euler's equation) is

$$\frac{\partial j_i}{\partial t} + \partial_k \left(\pi_{ik} - \gamma_{ik} + \tau_{ik}\right) = 0, \tag{4.5}$$

where $i, k = 1, 2, 3$ and

$$\pi_{ik} = \rho_S \, v_{Si} \, v_{Sk} + \rho_N \, v_{Ni} \, v_{Nk} + P_0 \, \delta_{ik} \tag{4.6}$$

is the stress tensor in superfluid hydrodynamics, which is a generalization of the usual formula in ordinary fluid dynamics. In Eq. (4.6) P_0 corresponds to the pressure in the fluid at rest. The tensor π_{ik} describes the mechanical transport of the different particles in the fluid and also the pressure forces acting in the fluid. These are reversible processes that account for the transfer of momentum inside the fluid [188]. On the other hand, the inclusion of viscous terms in the dynamics leads to an irreversible transfer of momentum from points where the velocity is large to those where it is small. The viscous tensor is

$$\tau_{ik} = -\eta \left(\partial_i v_{Nk} + \partial_k v_{Ni} - \frac{2}{3}\delta_{ik} \, \vec{\nabla} \cdot \vec{v}_N\right) - \delta_{ik}[\zeta_1 \vec{\nabla} \cdot \left(\vec{j} - \rho \vec{v}_N\right) + \zeta_2 \vec{\nabla} \cdot \vec{v}_N], \tag{4.7}$$

where η is the shear viscosity and ζ_1 and ζ_2 are bulk viscosity coefficients [183, 188]. The different terms in τ_{ik} arise because of the requirement that the total entropy of the system must always increase. Note that τ_{ik} depends only on the spatial derivatives of the normal velocity because internal friction is supposed to occur in a fluid only when different fluid particles have different velocities. In other words, dissipation due to internal friction appears when there is a relative motion between distinct parts of the fluid.

An implicit assumption taken for granted when writing Eq. (4.7) is that the velocity gradients are small and, thus, the momentum transfer due to viscosity depends only on the first derivatives of the velocity. We have also assumed that when the system is not rotating it is isotropic, which means that its properties can be described by scalar quantities such as η and the bulk viscosity coefficients. Moreover, thermal conduction effects are not taken into account.

The vortex elastic stress tensor γ_{ik} is defined as

$$\gamma_{ik} = \mu_S \left(\partial_k \epsilon_i + \partial_i \epsilon_k - 3\delta_{ik} \, \vec{\nabla} \cdot \vec{\epsilon}\right) - 2\Omega\lambda \, \delta_{iz} \frac{\partial \epsilon_k}{\partial z}, \tag{4.8}$$

where $\mu_S = \rho_S \hbar \Omega / 8 m_N$ is the shear modulus of the triangular vortex lattice calculated by Tkachenko [182], m_N is the mass of the neutron, Ω is the pulsar rotation frequency, and

$$\lambda = \frac{\hbar \rho_S}{8 m_N} \ln\left(\frac{b}{a}\right) \tag{4.9}$$

is the vortex tension. In the definition of λ we have that a is the coherence length and $b = (\pi\hbar/\sqrt{3} m_N \Omega)$ is the vortex radius of the triangular lattice.

The line acceleration equation can be written as

$$\rho_S \, \vec{\omega} \times \left(\vec{v}_S - \frac{\partial \vec{\epsilon}}{\partial t}\right) = \vec{\sigma} - \vec{D}, \tag{4.10}$$

where $\vec{\sigma}$ is the vortex elastic force density defined as

$$\vec{\sigma} \equiv \mu_S \left[2\vec{\nabla}_\perp (\vec{\nabla}_\perp \cdot \vec{\epsilon}) - \nabla_\perp^2 \vec{\epsilon} \right] - 2\Omega\lambda \frac{\partial^2 \vec{\epsilon}}{\partial^2 z}, \tag{4.11}$$

where $\vec{\nabla}_\perp$ is the gradient in the x-y plane and $\vec{D}$ is the mutual friction force.

In the rotating frame the linearized versions of the fundamental superfluid hydrodynamic equations for the net mass current, the relative velocity, and the superfluid velocity are

$$\frac{\partial \vec{j}}{\partial t} + \left(2\vec{\Omega} \times \vec{j} \right) + \vec{C} + \vec{\sigma} + \vec{\nabla} P + \rho \vec{\nabla} \phi = 0, \tag{4.12}$$

$$\frac{\partial \vec{q}}{\partial t} + \left(2\vec{\Omega} \times \vec{q} \right) - \frac{\vec{\sigma}}{\rho_S} - \vec{f} = 0, \tag{4.13}$$

$$\frac{\partial \vec{v}_S}{\partial t} + \left(2\vec{\Omega} \times \frac{\partial \vec{\epsilon}}{\partial t} \right) + \frac{\vec{\nabla} P}{\rho} + \vec{\nabla} \phi = 0, \tag{4.14}$$

where $P = P_0 - \rho(\vec{\Omega} \times \vec{r})^2/2$. The force density $\vec{C}$ is defined as the gradient of the viscous tensor τ_{ik} with the bulk viscosity coefficients set to zero, i.e.,

$$C_i = -\eta \, \partial_k \left(\partial_i v_{Nk} + \partial_k v_{Ni} - \frac{2}{3} \delta_{ik} \vec{\nabla} \cdot \vec{v}_N \right). \tag{4.15}$$

Note that we included the contribution from the Newtonian gravitational potential ϕ to the momentum conservation law because the neutron superfluid feels the presence of the star's gravitational field. This potential satisfies the equation

$$\nabla^2 \phi = \nabla^2 (\phi_S + \phi_N) = 4\pi G (\rho_S + \rho_N), \tag{4.16}$$

where G is the Newton's constant and ϕ_S and ϕ_N are the gravitational potentials of the superfluid and the normal fluid, respectively. The final equation that describes the mutual friction force is

$$\vec{f} = \beta \rho_S \left[\vec{n} \times \left[\vec{\omega} \times \left(\frac{\partial \vec{\epsilon}}{\partial t} - \vec{v}_N \right) \right] \right] + \beta' \rho_S \left[\vec{\omega} \times \left(\frac{\partial \vec{\epsilon}}{\partial t} - \vec{v}_N \right) \right], \tag{4.17}$$

where $\vec{n} \equiv \vec{\omega}/\omega$ and β and β' are the phenomenological mutual friction coefficients.

4.3 Tkachenko and Inertial Modes

We consider plane-wave perturbations with respect to the equilibrium which corresponds to uniform rotation. We use a Cartesian system of coordinates where the z-axis is directed along the axis of rotation, i.e., $\vec{\Omega} = (0, 0, \Omega)$. The vectors $\vec{j}$ and $\vec{q}$ can be decomposed into transverse and longitudinal parts, which are defined as $\vec{j} = \vec{j}_t + \vec{j}_l$ and $\vec{q} = \vec{q}_t + \vec{q}_l$. The transverse parts which are of interest here satisfy the condition

$$\vec{\nabla}_\perp \cdot \vec{j}_t = \vec{\nabla}_\perp \cdot \vec{q}_t = 0. \tag{4.18}$$

The perturbation equation for the transverse components of the vectors $\vec{j}$ and $\vec{q}$ derived from Eqs. (4.12), (4.13), and (4.14) are (hereafter the subscript t is omitted)

$$\frac{\partial j_i}{\partial t} + (2\epsilon_{lmn}\Omega_m j_n + \sigma_l + k_m\tau_{lm})P_{il} = 0, \tag{4.19}$$

$$\frac{\partial q_i}{\partial t} + (2\epsilon_{lmn}\Omega_m q_n - \frac{\sigma_l}{\rho_S} - f_l)P_{il} = 0, \tag{4.20}$$

$$\frac{\partial v_i}{\partial t} + 2\epsilon_{lmn}\Omega_m \frac{\partial \epsilon_n}{\partial t} P_{il} = 0. \tag{4.21}$$

In the equations above we used a projector $P_{il} = \delta_{il} - k_i k_l/k^2$ where $\vec{k}$ is the wave vector. Our coordinate system is such that the wave vector lies on the $z-x$ plane $\vec{k} = (k \sin\ \theta,\ 0,\ k \cos\ \theta)$ where θ is the angle formed by the vectors $\vec{\Omega}$ and $\vec{k}$.

Writing the time perturbations as $j_i(t) \sim j_i\ e^{2\Omega p t}$ (a similar definition is used for the other vectors) we obtain, after some algebra, the characteristic equation $\det\ ||K_{ij}|| = 0$ where

$$K_{ij} = \begin{pmatrix} p - \tilde{\eta}\alpha d & (\gamma_S h - 1) & -\tilde{\eta}\gamma_S \alpha d & -\gamma_S\gamma_N h \\ d + \gamma_S g & p - \tilde{\eta} & \gamma_S\gamma_N g & -\tilde{\eta}\gamma_S \\ -\hat{\beta} g & -\hat{\beta}^* h & p + \hat{\beta}(d + \gamma_N g) & -\hat{\beta}^*(1 - \gamma_N h) \\ -\hat{\beta}^* g & \hat{\beta} h & \hat{\beta}^*(d + \gamma_N g) & p + \hat{\beta}(1 - \gamma_N h) \end{pmatrix}. \tag{4.22}$$

We used the following shorthand notations in the definition of the matrix K_{ij}: $\gamma_{N/S} = \rho_{N/S}/\rho$, $d^{1/2} = \cos\ \theta$, $\hat{\beta}^* = 1 - \hat{\beta}'$, $\tilde{\eta} = \eta k^2/(2\Omega\rho)$, $\alpha = (4-d)/3$, $\hat{\beta} = \gamma_N^{-1}\beta$, and $\hat{\beta}' = \gamma_N^{-1}\beta'$. Moreover, we have that

$$g = \frac{k^2}{4\Omega^2\rho_S}\left[\mu_S - d(\mu_S - 2\Omega\lambda)\right], \tag{4.23}$$

$$h = \frac{k^2}{4\Omega^2\rho_S}\left[\mu_S - d(\mu_S + 2\Omega\lambda)\right]. \tag{4.24}$$

Note that the coefficients g and h are independent of the density because $\mu_S \sim \rho_S$ and $\lambda \sim \rho_S$. The density appears only through the normalization of the shear viscosity $\tilde{\eta} \sim \rho^{-1}$. The eigenmodes of the matrix in Eq. (4.22) provide the oscillatory modes in the general case where the shear viscosity of normal matter and the mutual friction between normal and superfluid components are included. In the non-dissipative limit ($\beta = \beta' = \eta = 0$) the modes separate into two independent sets that describe the inertial and Tkachenko modes. The (real) eigenfrequencies of these modes in units of 2Ω are

$$p_I = \pm i\, d^{1/2}, \quad p_T = \pm i\left[(d+g)\,(1-h)\right]^{1/2}, \tag{4.25}$$

where the indices I and T refer to inertial and Tkachenko modes, respectively.

4.4 Numerical Results

If the Tkachenko modes are generated within superfluid shells with the width of $R_c \sim 10$ km their corresponding wave vectors are of the order of $k_{\rm min} = 2\pi/R_c \sim 6.28 \times 10^{-6}$ cm, which sets the lower limit on the wave vector. Since the hydrodynamic description breaks down at length scales $\sim 10b$ ($b \sim 10^{-3}$ cm is the intervortex distance) the wave vector is bounded from above by the value $k_{\rm max} = 73.3$ cm^{-1}. We are interested in the small wave-vector limit $k \sim k_{\rm min}$, which describes vortex density waves across the entire superfluid shell.

The parameters g and h are of the order of $s = (\hbar^2 k_{\rm min}^2/2m_n)(8\hbar\Omega)^{-1}$. For instance, when $k = k_{\rm min}$ and $\Omega_\star = 15.51$ Hz (the rotation frequency of PSR 1828-11) we obtain that $s = 10^{-14}$. Therefore, for $s \ll 1$ the eigenmodes corresponding to Tkachenko waves in the dissipationless limit are given by $p_T = \pm i\,[(d+g)]^{1/2}$. In the limit $d \ll g$ where the wave vectors are highly collinear to the spin vector we obtain that $p_T = \pm i\sqrt{g}$ and, in the opposite limit $d \gg g$, the Tkachenko modes become identical to the inertial modes, i.e., $p_T = p_I$.

Fig. 4.1 displays the period of the Tkachenko modes without dissipation as a function of their wave vector. Only the long-wavelength perturbations have periods of the order of 100 days, which are then relevant for observations. In this limit the periods rapidly decrease for perturbations with finite d. The period $P(k_{\rm min}, d = 0) = 331$ days for $\Omega_\star = 15.51$ Hz suggests that the shortest period observed in PSR 1828-11, which corresponds to 256 days, should be identified with the fundamental oscillation mode. Oscillations with larger periods should then be identified with the higher-order harmonics of this mode. A period of 256 days can be obtained by adopting $R_c = 7.7$ km, which translates into $k = 8.16 \times 10^{-6}$ cm^{-1}.

We now consider the effects of the shear viscosity and the mutual friction on the propagation of the Tkachenko modes. It is convenient to use the drag-to-lift ratios ζ and ζ' instead of β and β' to describe mutual friction. These ratios are related by the following equations

$$\beta = \frac{\zeta}{[(1-\zeta')2 + \zeta 2]}, \quad \beta' = 1 - \frac{\beta(1-\zeta')}{\zeta}. \tag{4.26}$$

Microscopic calculations indicate that $\zeta' \simeq 0$. The limit $\zeta \to 0$ corresponds to a weak coupling between the vortices and normal fluid, while $\zeta \to \infty$ implies strong coupling.

Figure 4.2 shows the dependence of the eigenmodes derived from Eq. (4.22) on the drag-to-lift ratio ζ for several values of the shear viscosity and $d = 0$. The value of $\tilde{\eta}$ is determined assuming a constant density of 3×10^{14} g cm^{-3}. In the limit where ζ and η vanish we recover the results for the non-dissipative case discussed above. For $\eta = 0$ the real part of the Tkachenko mode, which is doubly degenerate, vanishes only in a narrow window of values of ζ. For larger values of ζ, which corresponds to the strongly coupled region, the real part reaches an asymptotic value that is about 25% smaller than its value in the undamped limit. Note that in our plots only the regions where the modes change significantly are shown.

Assuming that the normal fluid is inviscid, the results in Fig. 4.2 imply that there are oscillations with even longer periods in the strongly coupled limit. The Tkachenko modes are significantly damped by mutual friction in the region where the real part vanishes. There the number of imaginary roots of the characteristic equation increases by one. Moreover, one of the imaginary roots is given by Im $\omega = i\beta\Omega$, which continues beyond the figure's y scale.

This reflects the damping of the differential rotation between the superfluid and the normal fluid caused by mutual friction. This damping has no effect on the Tkachenko mode in strong coupling. For moderate values of viscosity, $\eta = 5 \times 10^{17}$ dyn s cm^{-2}, the real part of the Tkachenko mode is reduced in the strongly coupled region. Also note that the oscillations are weakly damped because of the contribution of the imaginary part. For large values of the shear viscosity ($\eta \sim 10^{19}$ dyn s cm^{-2}) the real part of the Tkachenko mode vanishes in the strongly coupled limit. There are no inertial modes when $d = 0$.

The modes when $d = 10^{-14}$ are shown in Fig. 4.3. As discussed above, in the non-dissipative limit the Tkachenko and inertial modes coincide for sufficiently large d. For $\eta = 0$ the modes can be distinguished in the strongly coupled limit because the Tkachenko mode vanishes for sufficiently large values of ζ. When larger shear viscosities are considered ($\eta = 10^{19}$ dyn s cm^{-2}) the difference between the real parts of the inertial and the Tkachenko modes can be clearly resolved. If we increase η even further we see that the real part of the inertial mode decreases and the imaginary part, which increases with η, becomes relevant. Finally, the real part of the inertial mode vanishes at $\eta \simeq 5 \times 10^{19}$ dyn s cm^{-2}.

The outer cores of neutron stars are mainly composed of light baryons, which pair in the isospin triplet states, and leptons. For densities of $2 - 3 \times 10^{14}$ g cm^{-3} and temperatures of $T \sim 10^8$ K the shear viscosity of the electron fluid was determined to be in the interval between $8 - 40 \times 10^{17}$ dyn s cm^{-2} [189]. This value of the temperature is a realistic upper bound on the temperature in the core of neutron stars except for very young objects like the Vela and Crab pulsars. For colder stars the viscosity could be a few orders of magnitude larger because $\eta \sim T^{-2}$.

Our results imply that type-I proton superconductivity is not the only solution for the precession puzzle by demonstrating that the long-term variation in the spin of PSR 1828-11 can be explained in terms of Tkachenko oscillations within superfluid shells. Our analysis indicates that Tkachenko modes are broadly consistent with weakly coupled theories between the superfluid and the normal fluid independent of the shear viscosity. Their subclass with $d = \cos^2\theta = 0$ has periods that are consistent with the lowest observed periodicity in PSR 1828-11 of 256 days.

The existence of Tkachenko modes in the strongly coupled limit depends on the shear viscosity of normal matter. For low viscosities the Tkachenko modes are (in strong coupling) renormalized to values that are a few times smaller than their corresponding non-dissipative limits. This implies that in strong coupling the Tkachenko oscillations have periods that are larger than their non-dissipative counterparts. In fact, the damping caused by mutual friction is not always strong enough to preclude an oscillatory behavior. Therefore, we claim that the long-term variation in the spin of PSR 1828-11 can in principle be explained in terms of Tkachenko oscillations within superfluid shells for certain values of the mutual friction and the normal fluid shear viscosity.

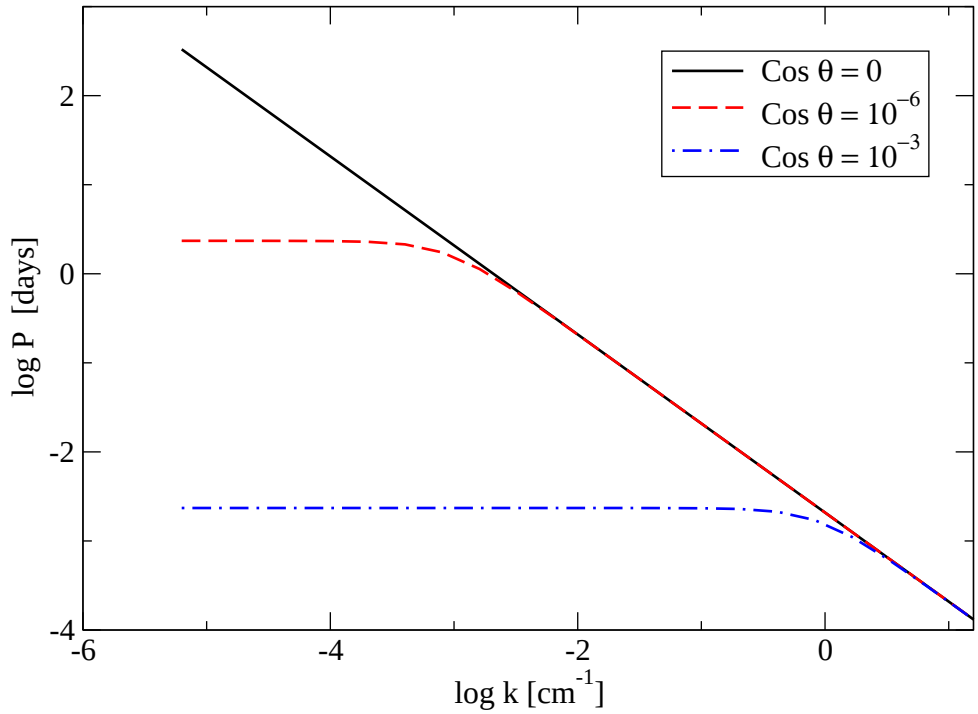

Figure 4.1: Dependence of the period $P = 2\pi/|p_T|$ of Tkachenko modes on the wave vector for $d = 0$ (solid black line), $d = 10^{-12}$ (dashed red line), and $d = 10^{-6}$ (dashed-dotted line). In the large wavelength limit the periods are on the order of 100 days. In particular, for $\Omega_\star = 15.51$ Hz we obtain that $P(k_{\rm min}, d = 0) = 331$ days if the core size is $R_c = 10$ km and $P(k_{\rm min}, d = 0) = 256$ days when $R_c = 7.7$ km.

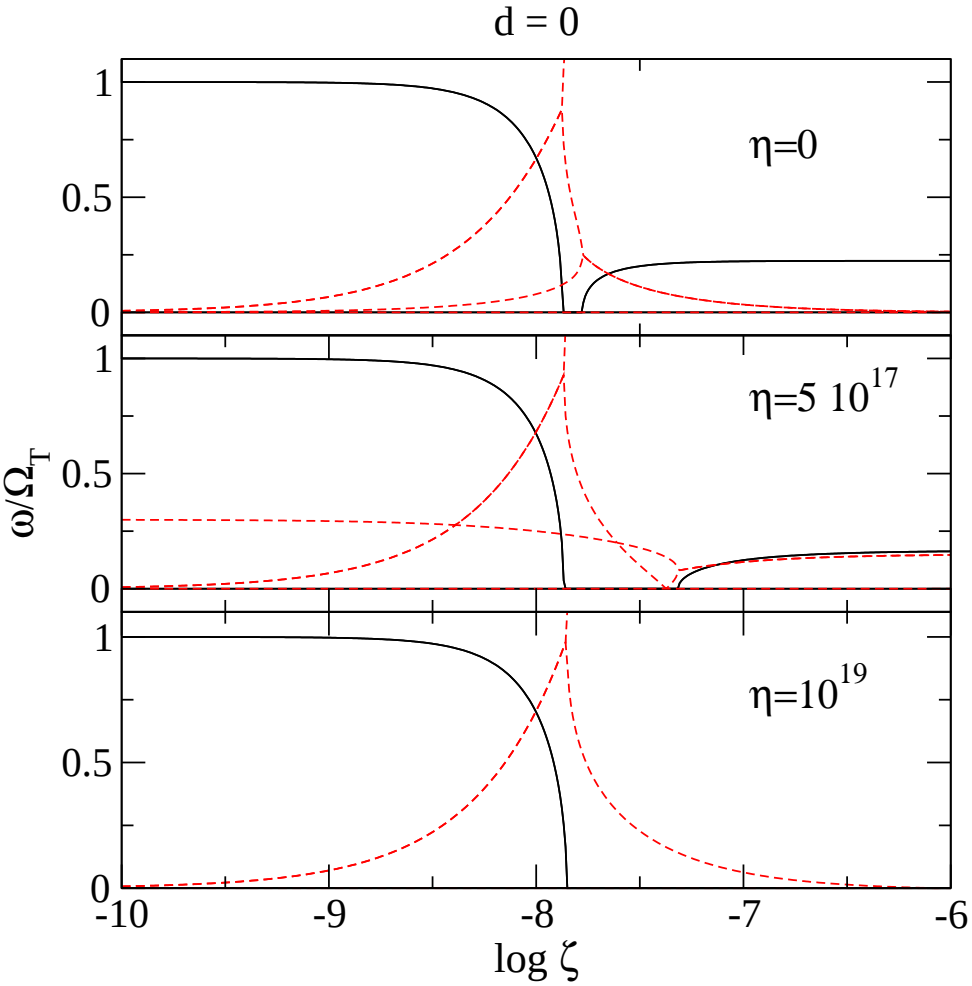

Figure 4.2: Dependence of the real (solid black line) and imaginary (dashed red line) parts of the Tkachenko modes ($\omega = ip$) on the drag-to-lift ratio ζ for $\eta = 0$ (upper panel), $\eta = 5 \times 10^{17}$ (middle panel), and $\eta = 10^{19}$ (lower panel) in dyn s cm^{-2} units. All modes are normalized by the non-dissipative value of the Tkachenko mode $\Omega_T = 2\pi/P$. The modes are computed taking $d = 0$, which means that there are no inertial modes.

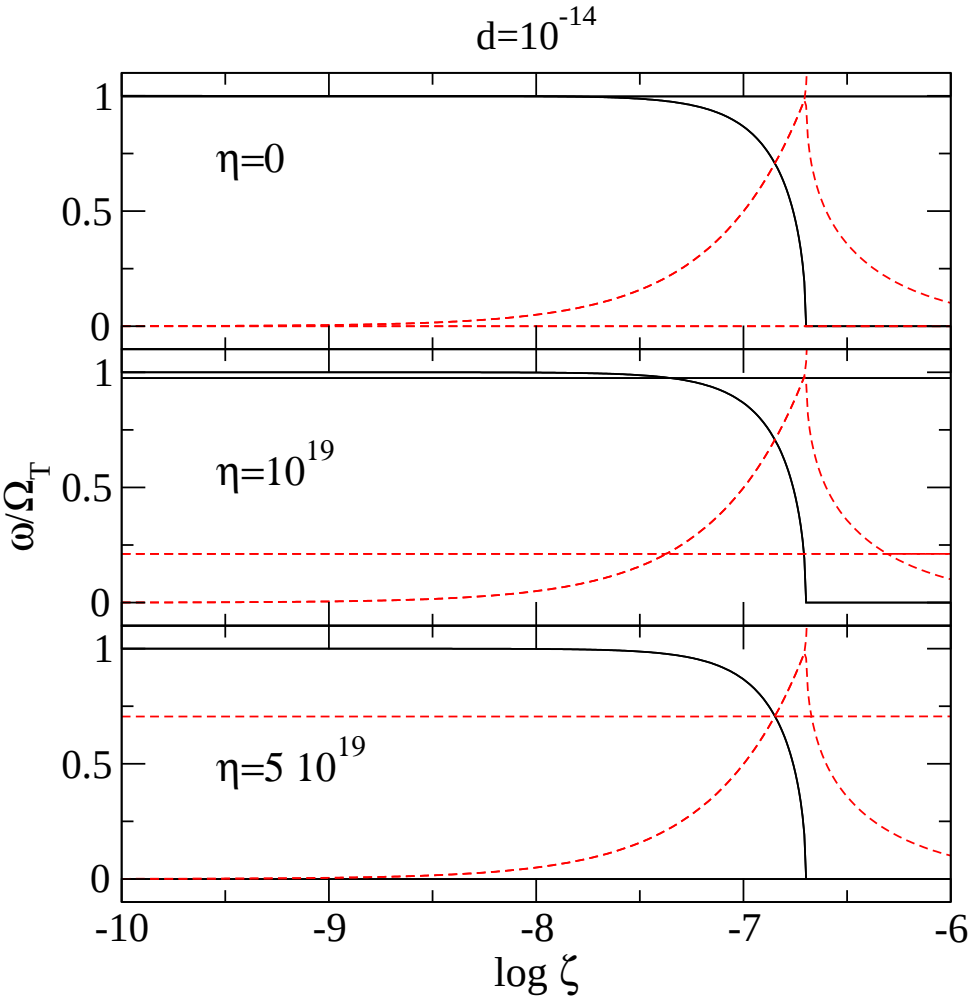

Figure 4.3: The same as in Fig. 4.2 in case of $d = 10^{-14}$ and $\eta = 0$ (upper panel), $\eta = 10^{19}$ (middle panel), and $\eta = 5 \times 10^{19}$ (lower panel) in dyn s cm^{-2} units. Note that both the Tkachenko and inertial modes are displayed here.

Chapter 5

Summary and Outlook

Color superconductivity has been extensively studied in the last years in spite of the fact that there are as of yet no experimental observations that can ultimately attest to its existence. Perhaps one of the main arguments that justifies these investigations is that the existence of color superconductivity in cold and dense quark matter can be shown to be a direct consequence of QCD's asymptotic freedom (see Sec. 1.5). Therefore, since QCD is known to be the correct theory of strong interactions, it was only a matter of finding the perfect conditions in which this new state of matter could be observed.

It turns out that inner cores of neutron stars, which are expected to have densities up to ten times the nuclear saturation density and temperatures $T < 1$ MeV, are probably the most likely places where deconfined quark matter can exist considering the very specific conditions needed for color superconductivity. In this thesis we explored the role played by gauge fields in obtaining new observable signatures that can attest to the existence of color superconductivity in the central regions of compact stars. Let us recapitulate how these new observable effects were obtained in our study.

The order parameter that defines the CFL phase simultaneously breaks color and flavor symmetries. The formation of the color-superconducting state then involves a complicated interplay between the gluons and the Cooper pairs because both of them carry non-Abelian color charge. In the CFL phase the gluons have a nonzero color Meissner mass, which plays an important role when their thermal fluctuations are taken into account. We have systematically calculated the effects of gauge-field fluctuations on the GL free energy density of a homogeneous CFL color superconductor in the two-loop approximation. Recall that in electronic superconductors a fluctuating electromagnetic field induces a weakly first-order phase transition (see Sec. 1.3.2). Similarly, adding thermal gluon fluctuations to the GL free energy density of a CFL superconductor changes the order of the phase transition.

We evaluated the temperature of the fluctuation-induced first-order phase transition both analytically and numerically and we also computed the latent heat and the maximum temperature of the superheated superphase. It was also shown that the London limit for color-magnetic interactions does not exist in CFL color superconductors. This comes about as a consequence of the weakness of electromagnetic interactions in comparison to strong interactions, i.e., $\alpha_e \ll \alpha_s$. Thus, once the thermal gluon fluctuations are taken into account, the local-coupling approxima-

tion between the color-superconductive order parameter and the gluons is not valid in the CFL phase.

The superconducting critical temperature obtained in the first-order phase transition is substantially larger than the critical temperature calculated without the gluon fluctuations. Also, the energy gap in the quasiparticle excitation spectrum changes discontinuously from zero (at high temperatures) to a nonzero value at the new critical temperature. It remains to be determined how much this would affect the cooling of a proto-neutron star with a CFL core.

By using an inhomogeneous GL theory, Iida and Baym [76] investigated the formation of vortices and supercurrents induced by external magnetic fields and rotation in pairing states near the critical temperature. Since they used a mean-field approximation, all gauge fields were regarded as averaged quantities and fluctuations around their mean values were not considered. In order to see how the inclusion of fluctuations would change their results one has to derive an effective action that depends only on the order parameter and the gauge fields. According to our results for the absence of the London limit in color superconductivity, this action would display non-local interactions between the gauge fields and the diquark condensate. Such an effective action could be obtained using the formalism developed in Ref. [104].

Recently, a GL free energy density that takes into account the effects of nonzero quark masses and charge neutrality has been derived within the mean-field approximation [77]. It would be interesting to see how the phase diagram obtained in Ref. [77] changes once the effects of gauge-field fluctuations are taken into account. Finally, note that we only considered the transition between the normal and the CFL phase. At intermediate densities, however, there is also the possibility of a transition to the 2SC phase. Moreover, a transition between the 2SC and the CFL phase, as studied in Ref. [155], could also occur.

We have seen in Sec. 1.5 that CFL superconductors are not electromagnetic superconductors because the initial local symmetry that corresponds to electromagnetism is not really broken in the medium but rotated. In Chapter 3 we studied the effects of a moderately strong magnetic field on the Cooper pairing dynamics in cold and dense massless three-flavor quark matter. We solved the corresponding gap equations numerically and calculated the magnetization for a wide range of magnetic fields ($eB/\mu^2 \lesssim 1$). We found that as the magnetic field increases the system undergoes a continuous crossover from the usual CFL phase to the mCFL phase. Notably, for $eB/\mu^2 \lesssim 0.1$, which corresponds to $B \lesssim 4.2 \times 10^{18}$ G (provided that $\mu = 500$ MeV), there is no large difference between the mCFL and CFL gaps. We would like to remark that the effects of color and charge neutrality on the gap equations have been recently computed by Fukushima and Warringa in Ref. [191].

Our numerical solutions for the gaps display magnetic oscillations, which is a direct consequence of the Landau quantization of the energy levels in a magnetic field. The fact that the mCFL gaps oscillate as functions of the magnetic field can also be shown analytically by performing a Lifshitz-Kosevich analysis of the gap equations. Similar magnetic oscillations were predicted and later observed in type-II electronic superconductors [192]. The effects of these oscillations on the transport properties of mCFL superconductors still remain to be understood.

In Fig. 5.1 we see how the diverse length scales that define the mCFL phase behave as a function of eB/μ^2. The coherence lengths are inversely proportional to the gaps. When the magnetic length is as large as the interquark distance, which occurs at $B \simeq 7 \times 10^{18}$ G if $\mu = 500$ MeV, a more careful analysis of the assumptions made about the electromagnetic

properties of color superconductors has to be performed. For larger fields the magnetic length becomes smaller than the interquark distance and in this limit the most important effect caused by the field may be the magnetic catalysis of chiral symmetry breaking [97, 98, 99].

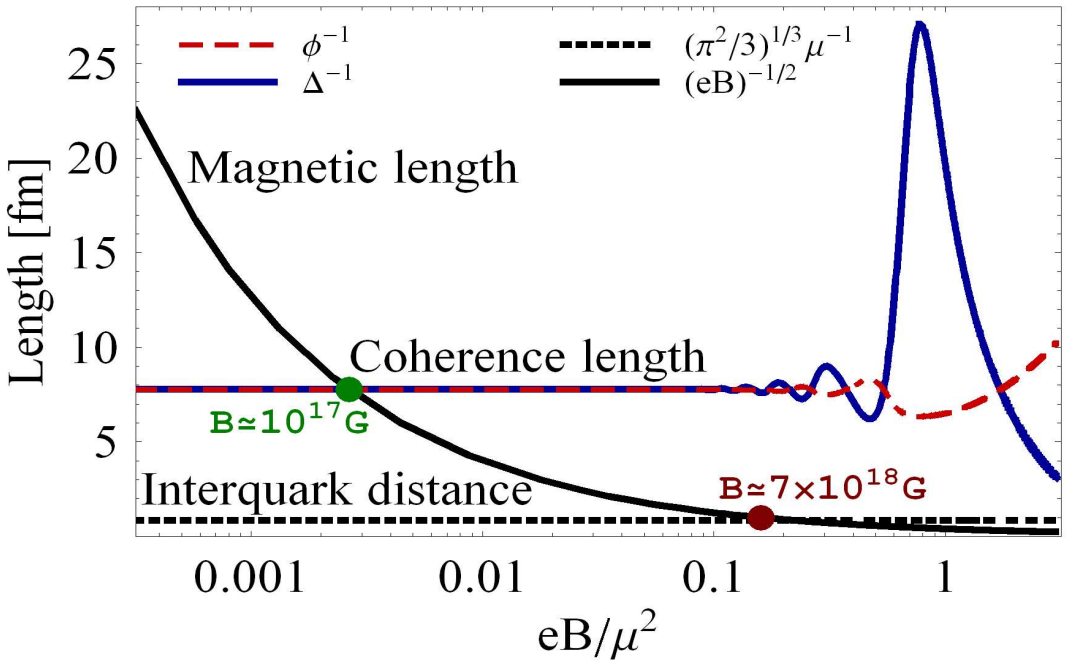

Figure 5.1: Dependence of the system's length scales on eB/μ^2.

The mCFL free energy density as well as the corresponding gap equations are in principle ultraviolet divergent and, consequently, they need to be regularized. In effective quark models, such as the NJL model used here, it is common to restrict the phase space by introducing a sharp finite cutoff in momentum space. However, because of the special properties of the system in a magnetic field, such a prescription is not very useful. Utilizing a sharp cutoff when the energy spectrum has discrete Landau levels introduces unphysical discontinuities in many thermodynamical quantities.

We performed an analytical study of the mCFL gap equations by using the proper time regularization [167]. We showed that within this approach it is possible to obtain analytical solutions for the gap equations when the magnetic field is very strong or zero (CFL limit). Moreover, our analytical results have the same physical properties as those found in Ref. [96, 164].

We showed that the magnetization of mCFL quark matter displays de Haas-van Alphen oscillations whose amplitude can be as large as the magnetic field for a wide range of parameters. Since the magnetization of dense hadronic matter is negligible, the nonzero magnetization of color-superconducting quark matter may provide new observable effects that can help to distinguish purely hadronic magnetars from magnetars with color-superconducting cores. Our results for the oscillations of the magnetization suggest that homogeneous quark matter may become unstable for the range of parameters that are phenomenologically relevant to magnetars (see

Fig. 5.2).

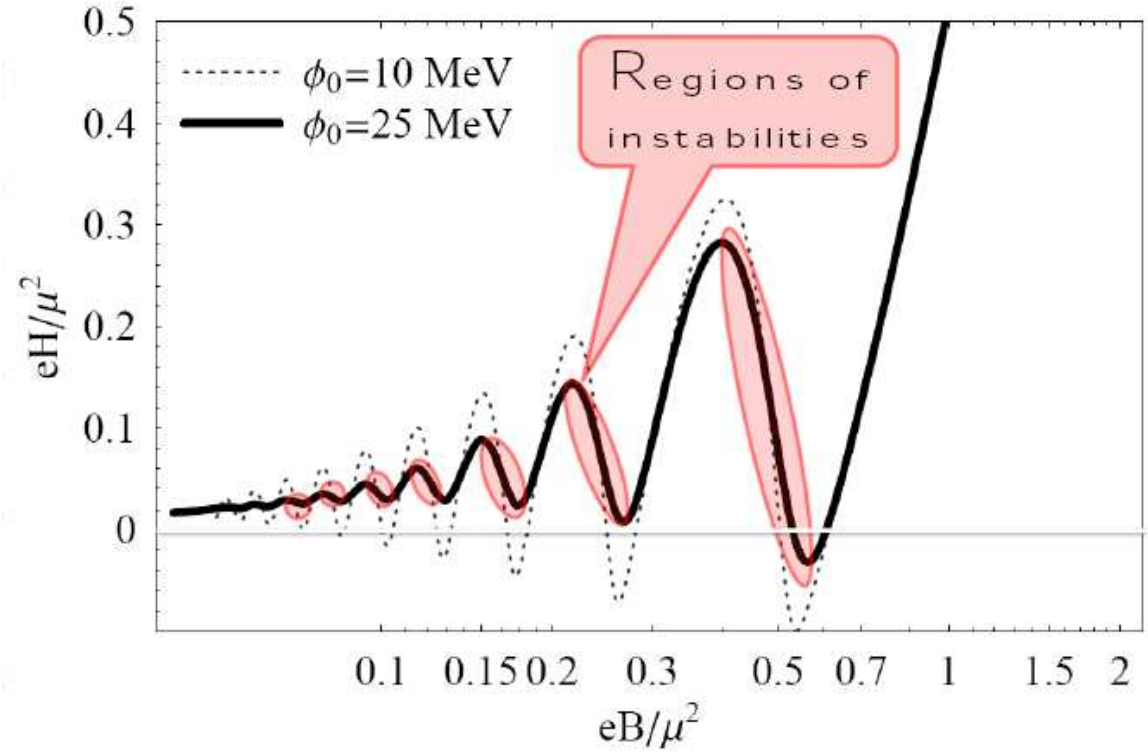

Figure 5.2: Unstable regions in the eH/μ^2 versus eB/μ^2 plot for the two sets of parameters used in Chapter 3. Homogeneous quark matter is unstable in the region below the $H = 0$ line and also in the pink shaded areas.

The type of instabilities obtained here indicates that the free energy density is not convex in these regions. This is usually fixed by allowing the formation of magnetic domains or other magnetic inhomogeneities in the system [41]. Therefore, we expect that magnetic inhomogeneities can be found in the quark cores of magnetars. We argued in Sec. 3.4.1 that the successive phase transitions coming from discontinuous changes of the induced magnetic field B during the star's evolution can release a vast amount of energy that would heat up the star, which would then cool down by, for example, the emission of neutrinos. Therefore, bursts of neutrinos coming from magnetars with color-superconducting cores could be expected even after the deleptonization period.

There are several questions regarding color-superconducting matter in strong fields and its consequent use in the study of superconducting magnetars that remain to be investigated. One could, for example, study the cooling of their ultramagnetized cores. Also, the effects of strong magnetic fields on the global structure of the star, such as its mass and radius, are also very important and will be discussed elsewhere [193]. A very important detail that has to be taken into account when computing the mass and radius of magnetars is that the magnetic field in these objects is so strong that the spacetime metric is not spherically symmetric anymore [194]. Therefore, the normal TOV equations cannot be used to determine the mass and radius of these

stars.

The low-energy effective theory for the Nambu-Goldstone bosons in the mCFL phase was recently derived by Ferrer and de la Incera in Ref. [168]. However, the pion decay constant and the meson maximum velocities still have to be determined using the microscopic theory. Using the zero-field values of these parameters calculated in Ref. [163] they obtained that the charged mesons decouple from the low-energy theory only when $eB \gtrsim 12\,\phi_0^2$. Incidently, this corresponds to the region where the oscillations of the magnetization and the gaps become noticeable. This brings up an interesting question: how do the magnetic oscillations affect the low-energy dynamics of the mCFL phase? This problem is left for future study. The effects of a nonzero strange quark mass on the low-energy description of mCFL color superconductors should also be considered in a future work.

At moderate densities neutral two-flavor color superconductivity displays a chromomagnetic instability [113, 114]. It has been recently pointed out in Ref. [195] that this chromomagnetic instability can be removed by the formation of an inhomogeneous condensate of charged gluons and the corresponding induction of a magnetic field. This may then be relevant to the explanation of strong magnetic fields and other unusual properties observed in magnetars. However, the field strengths used in their approach are comparable to those that cause the large-magnitude de Haas-van Alphen oscillations. This indicates that the effects from the strong magnetization of mCFL quark matter should also be included in their discussion. Therefore, we expect that the combined effects from the de Haas-van Alphen oscillations and the inhomogeneous gluon condensate may shed some light on the problem with the chromomagnetic instability present in color superconductors.

Obviously, our results only apply if the strong magnetic fields observed on the surface of magnetars can be transmitted into their inner cores. This can occur if the superconducting protons, which are expected to exist in the outer core, form a type-II superconductor so that the external magnetic field can penetrate in the form of vortices. However, it has been argued that the long periodic oscillations observed in isolated pulsars can only be explained if the outer core is a type-I superconductor rather than type-II [131]. This is because free precession, which is the standard explanation for these timing variations, cannot occur in strong coupling [180]. If type-I superconductivity is indeed realized in the outer core of neutron stars, the glitch models based on the interactions between the neutron vortices and the proton flux tubes, such as the model in Ref. [128], would no longer apply.

We showed in Chapter 4 that type-I proton superconductivity is not the only solution for the precession puzzle by demonstrating that the long-term variation in the spin of PSR 1828-11 can be explained in terms of Tkachenko oscillations within superfluid shells. Our analysis indicates that Tkachenko modes are broadly consistent with weakly coupled theories between the superfluid and the normal fluid independent of the shear viscosity. Their subclass with $d = \cos^2\theta = 0$ has periods that are consistent with the lowest observed periodicity in PSR 1828-11 of 256 days.

The existence of Tkachenko modes in the strongly coupled limit depends on the shear viscosity of normal matter. For low viscosities the Tkachenko modes are (in strong coupling) renormalized to values that are a few times smaller than their corresponding non-dissipative limits. This implies that in strong coupling the Tkachenko oscillations have periods that are larger than their non-dissipative counterparts. In fact, the damping caused by mutual friction

is not always strong enough to preclude an oscillatory behavior. Therefore, we conclude that the long-term variation in the spin of PSR 1828-11 can in principle be explained in terms of Tkachenko oscillations within superfluid shells for certain values of the mutual friction and the normal fluid shear viscosity.

Our model involves certain approximations. We have adopted the two-fluid superfluid hydrodynamics which should be modified in order to account for the multiple fluids in the neutron star's core [190]. Also, we did not consider the dissipative effects due to nonzero thermal conduction and bulk viscosities. Furthermore, the cylindrical symmetry of our setup and the assumption of uniform density need to be reconsidered in more realistic treatments of spherical superfluid shells with density gradients.

Tkachenko modes were observed in superfluid helium in 1982 [196]. Recently, Tkachenko waves have been observed in rapidly rotating Bose-Einstein condensates [197]. The frequencies of the modes were measured for rotation rates as high as 98% of the centrifugal limit for the harmonically trapped gas. The agreement between the observed frequency of the waves with hydrodynamic predictions worsens with increasing rotation rate because as the rotation velocity increases the volume displaced by the vortex cores becomes larger. Right after the publication of these results Baym was able to explain them in [198].

Ref. [199] reported a very interesting study involving ultracold gases that may have serious implications for the physics of color superconductivity. They considered a system composed of fermionic atoms of three different internal quantum states (colors) that displays attractive interactions on an optical lattice. Using a variational calculation for equal color densities, it was shown that a color superfluid state occurs in the system in weak coupling while triplets of atoms with different colors form singlet fermions (called trions) in the strongly coupled regime. These phases are very similar to the color-superconducting and hadronic phases of QCD, respectively. Their study indicates that one does not need to travel to the heavens in order to understand color superconductivity.

Appendix A

Ginzburg-Landau Free Energy Density

In this appendix, we sketch some important steps for the derivation of the generalized GL free energy density in the presence of gauge-field fluctuations, which is shown in Eq. (2.29), in terms of Feynman diagrams. We have

$$\left[S^{-1}(P)\right]^{c_1c_2}_{f_1f_2} = (i\gamma_\mu P_\mu - \mu\gamma_4\rho_3)\delta^{c_1c_2}\delta_{f_1f_2}\ , \tag{A.1a}$$

$$\left[\delta\mathcal{S}^{-1}(P)\right]^{c_1c_2}_{f_1f_2} = i\phi(P)\gamma_5\rho_2(\delta^{c_1}_{f_1}\delta^{c_2}_{f_2} - \delta^{c_1}_{f_2}\delta^{c_2}_{f_1})\ , \tag{A.1b}$$

$$\mathcal{D}^{ll'}_n(K)_{ij} \approx \frac{\delta^{ll'}}{k^2 + \frac{\pi}{4}m_D^2\frac{|\omega|}{k}}\left(\delta_{ij} - \frac{k_ik_j}{k^2}\right)\ , \tag{A.1c}$$

$$\mathcal{D}^{ll'}_n(K)_{j4} = 0\ , \tag{A.1d}$$

$$\mathcal{D}^{ll'}_n(K)_{44} \approx \frac{\delta^{ll'}}{k^2 + m_D^2}, \tag{A.1e}$$

where $P = (\nu, \vec{p})$, $K = (\omega, \vec{k})$, $m_D^2 = 3\,g^2\mu^2/(2\pi^2)$, ρ_i are Pauli matrices with respect to Nambu-Gorkov indices, c_i and l, l' stand for the fundamental and adjoint color indices, respectively, f_i are fundamental flavor indices, and ν, μ correspond to discrete Matsubara frequencies. The symbol "$\approx$" in the gluon propagator means that we used the approximation for the total HDL gluon propagator that is relevant for the CSC energy scale.

Diagrammatically, $\mathcal{D}_n$ is denoted by a wavy line, $\mathcal{S}_n$ is represented by a thick line, and the CSC correction to the inverse quark propagator (A1b) is associated with a two-point vertex bearing a cross. The corresponding diagrammatic expansions for $\delta\mathcal{S}$ and $\delta\Pi$ are

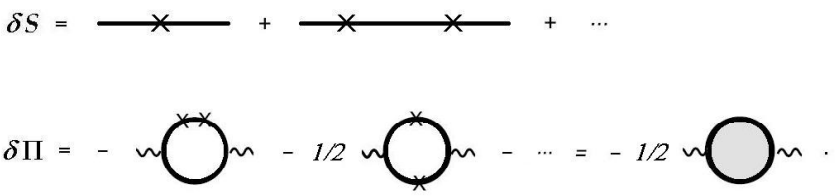

In weak coupling we expand $\mathcal{S}_n$ as

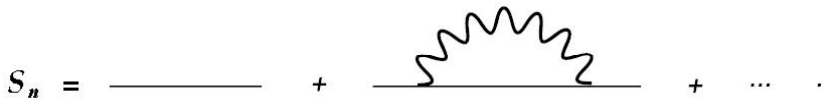

Expanding $\Gamma_{\rm cond}$ up to the fourth power in $\phi(P)$ we find

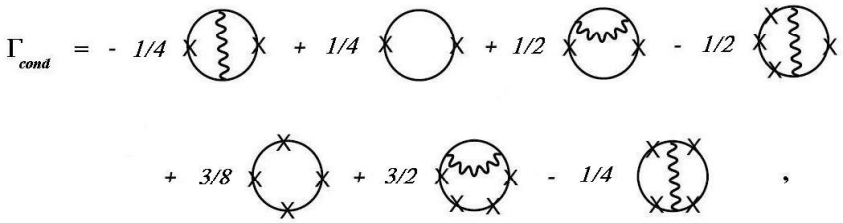

where the weak-coupling approximation has been employed in order to retain the diagrams with at most one HDL gluon line. The diagram bearing two crosses yields the expression $\sum_{PP'}\Phi(P)K(P|P')\Phi(P')$, where the kernel $K(P|P')$ is isomorphic to the kernel in the Dyson-Schwinger equation for the diquark scattering amplitude in the normal phase. Moreover, taking $\Phi(P)$ to be proportional to the pairing mode [the eigenmode of $K(P|P')$ with the minimum eigenvalue at a given T [72]], i.e.,

$$\phi(P) = \Delta \sin\Big[\frac{g}{3\sqrt{2}\pi}\ln\Big(\frac{1}{\hat{\nu}}\Big)\Big] \quad , \tag{A.2}$$

where Δ is the energy gap, $\hat{\nu} = (3/2)^{5/2}\, g^5\nu/(256\pi^4\mu)$, we have that

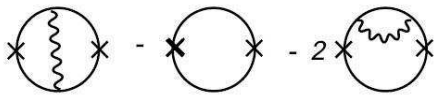

is proportional to $T - T_c$, with T_c determined up to subleading order in g [see Eq. (2.2)]. For the diagrams with four crosses the same mechanism yields

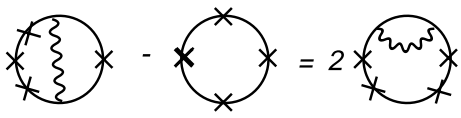

at $T = T_c$, which reduces the number of quartic terms in $\Gamma_{\rm cond}$. Moreover, it will be shown at the end of this appendix that the following two diagrams

(A.3)

are of higher order in weak coupling and can be dropped. For $\Gamma_{\rm cond}$ we end up with

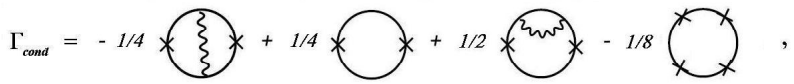

which produces the terms in Eq. (2.1). Now we consider the fluctuation terms $\Gamma_{\rm fluc} + \Gamma'_{\rm fluc}$. Expanding the logarithms in Eqs. (2.24c,2.24d), the diagrammatic representation of the first three terms is

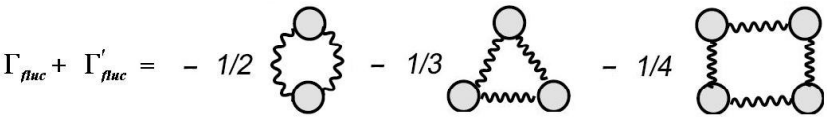

(A.4)

where $\Gamma_{\rm fluc}$ includes only the contribution from the static gluons and $\Gamma'_{\rm fluc}$ contains the remaining contributions. Due to the Meissner effect, the shaded bubble does not vanish when the spatial momentum of the gluon line goes to zero at zero Matsubara energy. A resummation of all ring diagrams in Eq. (A.4) is necessary for $\Gamma_{\rm fluc}$ and the result is the right-hand side of Eq. (2.25). Regarding $\Gamma'_{\rm fluc}$, where the Matsubara energy of the gluon line is nonzero, dynamical screening prevents an infrared divergence for the integral over gluon momentum. In weak coupling $\Gamma'_{\rm fluc}$ is dominated by the first diagram in Eq. (A.4), which is again of higher order. Therefore, the contribution of $\Gamma'_{\rm fluc}$ can be safely neglected.

Now we present the argument supporting our assertion that the two diagrams in Eq. (A.3) and the first diagram in $\Gamma'_{\rm fluc}$ can be neglected in weak coupling. Let us denote the contribution of the first diagram in Eq. (A.3) by $c_1\Delta^4$. It consists of five free quark propagators with four-momentum $(\nu,\vec{p})$ and a self-energy insertion $\Sigma(P)\sim g^2\nu\ln(\mu/|\nu|)\sim g\nu$. The main contribution to the $\vec{p}$-integration comes from a shell of thickness $\sim|\nu|$ around the Fermi surface and then we have

$$c_1\sim\mu^2T\sum_\nu\frac{1}{|\nu|^4}\,\Sigma(\nu)\sim g\,\frac{\mu^2}{T_c^2}, \tag{A.5}$$

which is of $\mathcal{O}(g)$ in comparison to the quartic term in Eq. (2.1). The contribution of the second diagram in Eq. (A.3), denoted by $c_2\Delta^4$, can be estimated similarly. As is the case with the gap equation, the dominating contribution comes from the magnetic gluons with nonzero Matsubara energy. The integration for the quark propagators over the magnitude of their momenta $\vec{p}$, $\vec{p}\,'$, on each side of the gluon line can be approximately decoupled from the integration for the gluon propagator over the angle between $\vec{p}$ and $\vec{p}\,'$, where the latter produces the forward logarithm. We then find

$$c_2\sim g^2T^2\mu^4\sum_{\nu\neq\nu'}\frac{1}{\nu^2\nu'^2}\,\frac{1}{\mu^2}\ln\left(\frac{\mu}{\nu-\nu'}\right)\sim g\,\frac{\mu^2}{T_c^2}, \tag{A.6}$$

which is again of higher order. Now we consider the first diagram in $\Gamma'_{\rm fluc}$ and denote its contribution as $c_3\Delta^4$. Since the typical momentum for the gluon line is $k\sim m_D^{2/3}|\omega|^{1/3}\gg\omega$ and $\omega\sim T_c$, each bubble can be approximated by the static magnetic self-energy of gluons at the Pippard limit, i.e.,

$$c_3\sim g^4T\sum_{\omega\neq0}\int\frac{d^3\vec{k}}{(2\pi)^3}\,\frac{1}{(k^2+\frac{\pi}{4}m_D^2\frac{|\omega|}{k})^2}\left(\frac{\mu^2}{T_c^2}\,\frac{T_c}{k}\right)^2\sim\frac{g^4\mu^4}{T_c^2m_D^2}\sum_{\omega\neq0}\frac{1}{|\omega|}\,. \tag{A.7}$$

The sum over ω has a cutoff when $\omega\sim m_D$ and then we end up with $\sum_{\omega\neq0}|\omega|^{-1}\sim\ln(\mu/T_c)\sim 1/g$. Consequently, we have $c_3\sim g\,\mu^2/T_c^2$, which is also negligible.

Appendix B

Evaluation of the Determinant in the mCFL Phase

In this appendix we present the details of the computation of $\Gamma(T,\mu,\Delta,\phi,B)$. The usual way to compute these determinants is to use the identity

$$\det\begin{pmatrix} A & B \\ C & D \end{pmatrix} = \det\left(AD - ACA^{-1}B\right) \tag{B.1}$$

for the determinant of a block matrix. Using this identity we can rewrite Eq. (3.9) as

$$\begin{aligned}\Gamma &= \frac{1}{2}\ln\det\Big\{[G^{+}_{0(\widetilde{Q})}]^{-1}[G^{-}_{0(-\widetilde{Q})}]^{-1} \\ &\quad -[G^{+}_{0(\widetilde{Q})}]^{-1}\Phi^{+}[G^{+}_{0(\widetilde{Q})}]\Phi^{-}\Big\},\end{aligned} \tag{B.2}$$

where $[G^{\pm}_{0(\widetilde{Q})}]^{-1} = [i\partial\!\!\!/ + e\widetilde{Q}A\!\!\!/(X) \pm \mu\gamma_0]$. However, the nontrivial color-flavor structure of $[G^{\pm}_{0(\pm\widetilde{Q})}]^{-1}$ complicates the calculations.

B.1 Introducing the Charge Projectors

The easiest way to calculate Eq. (B.2) is to go back to the Lagrangian density and introduce the charge projectors in color-flavor space [96, 164]

$$\Omega_{(0)} = \mathrm{diag}(1,1,0,1,1,0,0,0,1), \tag{B.3a}$$
$$\Omega_{(+)} = \mathrm{diag}(0,0,0,0,0,0,1,1,0), \tag{B.3b}$$
$$\Omega_{(-)} = \mathrm{diag}(0,0,1,0,0,1,0,0,0), \tag{B.3c}$$

which satify

$$\Omega_{(a)}\Omega_{(b)} = \delta_{ab}\Omega_{(b)}, \quad a,b = 0,+,-, \quad \sum_{a=0,\pm}\Omega_{(a)} = 1. \tag{B.4}$$

In terms of these projectors the charge operator in color-flavor space is $\widetilde{Q} = \Omega_{(+)} - \Omega_{(-)}$. However, it is convenient to define the following charge operator in Nambu-Gorkov space $\widetilde{Q}_{NG} = \mathrm{diag}_{NG}(\widetilde{Q}, -\widetilde{Q})$, with eigenstates

$$\widetilde{Q}_{NG}\,\Psi_{(a)} = a\,\Psi_{(a)}, \tag{B.5}$$

where

$$\Psi_{(a)} = \begin{pmatrix} \psi_{(a)} \\ \psi_{c\,(-a)} \end{pmatrix}, \quad \psi_{(a)} = \Omega_{(a)}\psi. \tag{B.6}$$

The charge operators can also be generalized to include the Nambu-Gorkov structure present throughout this derivation. In fact, one has

$$\Omega^{NG}_{(a)} = \begin{pmatrix} \Omega_{(a)} & 0 \\ 0 & \Omega_{(-a)} \end{pmatrix}, \tag{B.7}$$

which then satifies

$$\Omega^{NG}_{(a)}\,\Omega^{NG}_{(b)} = \delta_{ab}\,\Omega^{NG}_{(b)}, \quad a,b = 0,+,-, \quad \sum_{a=0,\pm}\Omega^{NG}_{(a)} = 1, \tag{B.8}$$

where $\Psi_{(a)} = \Omega^{NG}_{(a)}\,\Psi$. Using these projectors Eq. (3.5) can be expressed as

$$\mathcal{L} = -\sum_{\eta=1}^{3}\frac{|\Delta_\eta|^2}{G} + \sum_{a,b=0,\pm}\frac{1}{2}\bar{\Psi}_{(a)}\Omega^{NG}_{(a)}\mathcal{S}^{-1}\Omega^{NG}_{(b)}\,\Psi_{(b)}. \tag{B.9}$$

However, it can be shown that

$$\Omega^{NG}_{(a)}\,\mathcal{S}^{-1}\Omega^{NG}_{(b)} = \delta_{ab}\,\Omega^{NG}_{(a)}\,\mathcal{S}^{-1}\Omega^{NG}_{(a)}, \tag{B.10}$$

where we used that $\Omega_a\Phi^+\Omega_{-a}$ is the only combination that is not identically zero. We define $\mathcal{S}^{-1}_{(a)} \equiv \Omega^{NG}_{(a)}\,\mathcal{S}^{-1}(X)$, which then implies that

$$\mathcal{S}^{-1} = \sum_{a=0,\pm}\Omega^{NG}_{(a)}\,\mathcal{S}^{-1}_{(a)}. \tag{B.11}$$

It is possible to show that $[\Omega^{NG}_{(a)}, \mathcal{S}^{-1}_{(b)}] = 0$.

The term involving the full inverse propagator in the Lagrangian density can be written as

$$\begin{aligned} \frac{1}{2}\bar{\Psi}\,\mathcal{S}^{-1}\,\Psi &= \frac{1}{2}\sum_{a=0,\pm}\bar{\Psi}_{(a)}\,\mathcal{S}^{-1}\,\Psi_{(a)} \\ &= \frac{1}{2}\sum_{a=0,\pm}\bar{\Psi}_{(a)}\,\mathcal{S}^{-1}_{(a)}\,\Psi_{(a)}. \end{aligned} \tag{B.12}$$

Therefore, the Lagrangian density in Eq. (3.5) can be rewritten as

$$\mathcal{L} = -\sum_{\eta=1}^{3}\frac{|\Delta_\eta|^2}{G} + \sum_{a=0,\pm}\frac{1}{2}\bar{\Psi}_{(a)}\mathcal{S}^{-1}_{(a)}\Psi_{(a)} \tag{B.13}$$

where

$$\mathcal{S}^{-1}_{(a)} = \begin{pmatrix} [G^{+}_{0(a)}]^{-1} & \Phi^{-}_{(a)} \\ \Phi^{+}_{(a)} & [G^{-}_{0(a)}]^{-1} \end{pmatrix} \tag{B.14}$$

$[G^{\pm}_{0(a)}]^{-1} = \not{\Pi}_{(a)} \pm \mu\gamma_0$, and $\not{\Pi}_{(a)} = i\not{\partial} + a\, e\not{A}$. The new gap matrices in the equation above are given by $\Phi^{+}_{(a)} = \Phi^{+}\Omega_{(a)}$ whereas $\Phi^{-}_{(a)} = \gamma_0(\Phi^{+}_{(a)})^{\dagger}\gamma_0$.

B.2 Lagrangian Density in Momentum Space

It is very convenient to express the Lagrangian density in Eq. (B.9) in momentum space because it simplifies the computation of the determinants. Here we follow Ref. [164] and use the method originally developed for charged fermions by Ritus in Ref. [172]. In Ref. [173], the method was also extended to include charged vector fields. In this approach the diagonalization of the Green's functions of charged fermions in a uniform magnetic field in momentum space is obtained using the eigenfunction matrices $E_p(X)$. These functions are the wave functions corresponding to asymptotic states of charged fermions in a uniform background magnetic field.

The $E_p(X)$ functions were described in detail in Refs. [164, 173] and some of their main properties are presented in Appendix C. Using these eigenfunctions it is possible to express the charged fields $\psi_{(\pm)}$ as

$$\psi_{(\pm)}(X) = \sum_{\bar{P}_{(\pm)}} E^{(\pm)}_{p}(X)\psi_{(\pm)}(\bar{P}_{(\pm)}), \tag{B.15a}$$

$$\bar{\psi}_{(\pm)}(X) = \sum_{\bar{P}_{(\pm)}} \bar{\psi}_{(\pm)}(\bar{P}_{(\pm)})\bar{E}^{(\pm)}_{p}(X), \tag{B.15b}$$

where, by definition, $\bar{E}^{(\pm)}_{p}(X) = \gamma_0\,(E^{(\pm)}_{p}(X))^{\dagger}\,\gamma_0$, $\bar{P}_{(\pm)} = (p_0, 0, \pm\sqrt{2eBn}, p_3)$, and $n = 0, 1, 2, \ldots$, denotes the Landau levels. The 4-vector potential is in the Landau gauge, i.e., $A^{\mu} = (0, 0, Bx, 0)$. Moreover, one can show that

$$[G^{\pm}_{0(\pm)}]^{-1}(X)E^{(\pm)}_{p}(X) = E^{(\pm)}_{p}(X)[\not{\bar{P}}_{(\pm)} \pm \mu\gamma_0]. \tag{B.16}$$

This implies that

$$\int d^4X\, \bar{\Psi}_{(a)}(X)\, \mathcal{S}^{-1}_{(a)}(X)\Psi_{(a)}(X) = \sum_{\bar{P}_{(a)}} \bar{\Psi}_{(a)}(\bar{P}_{(a)}) \begin{pmatrix} [G^{+}_{0(a)}]^{-1}(\bar{P}_{(a)}) & \Phi^{-}_{(a)} \\ \Phi^{+}_{(a)} & [G^{-}_{0(a)}]^{-1}(\bar{P}_{(a)}) \end{pmatrix} \Psi_{(a)}(\bar{P}_{(a)}), \tag{B.17}$$

for $a = 0, \pm$. Also, we have defined $\bar{P}_{(0)} = (p_0, \vec{p})$ and $[G^{+}_{0(0)}]^{-1}(\bar{P}_{(0)}) = [\not{\bar{P}}_{(0)} \pm \mu\gamma_0]$. In the following section we will compute the determinants using the momentum representation of the inverse propagators.

B.3 Calculating the Determinants

The operators $\mathcal{S}^{-1}$ and $\mathcal{S}_{(a)}^{-1}$ are defined in a 72-dimensional vector space $\Sigma = \mathcal{C}_{c,f} \otimes \mathcal{D}_{Dirac} \otimes \mathcal{N}_{NG}$. However, the charge projectors express Σ as the direct sum of three different spaces, i.e., $\Sigma = \Sigma_{(0)} \oplus \Sigma_{(+)} \oplus \Sigma_{(-)}$, with vector bases given by

$$\Sigma_{(0)} \Rightarrow \{|s_1, \pm\rangle, |s_2, \pm\rangle, |d_1, \pm\rangle, |d_2, \pm\rangle, |u_3, \pm\rangle\}, \tag{B.18}$$

$$\Sigma_{+} \Rightarrow \{|u_1, +\rangle, |u_2, +\rangle, |s_3, -\rangle, |d_3, -\rangle\}, \tag{B.19}$$

$$\Sigma_{-} \Rightarrow \{|u_1, -\rangle, |u_2, -\rangle, |s_3, +\rangle, |d_3, +\rangle\}, \tag{B.20}$$

where $\{|+\rangle, |-\rangle\}$ is the basis of Nambu-Gorkov space. The color, flavor, and Dirac structures are automatically taken into account by describing a quark spinor ψ as

$$\psi = \{s_1, s_2, s_3, d_1, d_2, d_3, u_1, u_2, u_3\}, \tag{B.21}$$

where $(1, 2, 3) = (b, g, r)$ denotes the color indices. Thus, $\Sigma_{(0)}$, $\Sigma_{(+)}$, and $\Sigma_{(-)}$ are vector spaces with dimensions 40, 16, and 16, respectively.

We can now compute the determinant of the inverse propagator in Eq. (3.9) in terms of its corresponding charge projections. In fact, one sees that the determinant splits into three separate pieces

$$\Gamma(T, \mu, \Delta, \phi, B) = \sum_{a=0,\pm} \Gamma_{(a)} = \sum_{a=0,\pm} \frac{1}{2} \ln \det \widetilde{\mathcal{S}}_{(a)}^{-1}. \tag{B.22}$$

Note that in the evaluation of the determinants only the projection of $\mathcal{S}_{(a)}^{-1}$ on the corresponding lower dimensional subspaces $\Sigma_{(a)}$, which we call $\widetilde{\mathcal{S}}_{(a)}^{-1}$, is relevant. The inverse propagator $\widetilde{\mathcal{S}}_{(0)}^{-1}$ that appears in the evaluation of the determinant is defined as

$$\widetilde{\mathcal{S}}_{(0)}^{-1} = \begin{pmatrix} [G_{0(0)}^{+}]^{-1} \otimes 1_{5\times5} & \widetilde{\Phi}_{(0)}^{*} \\ \widetilde{\Phi}_{(0)} & [G_{0(0)}^{-}]^{-1} \otimes 1_{5\times5} \end{pmatrix}, \tag{B.23}$$

whereas

$$\widetilde{\Phi}_{(0)} = i\gamma_5 \begin{pmatrix} 0 & 0 & 0 & \phi & \Delta \\ 0 & 0 & -\phi & 0 & 0 \\ 0 & -\phi & 0 & 0 & 0 \\ \phi & 0 & 0 & 0 & \Delta \\ \Delta & 0 & 0 & \Delta & 0 \end{pmatrix}. \tag{B.24}$$

This matrix can be easily diagonalized and its eigenvalues are $|\phi|^2, |\phi|^2, |\phi|^2, \Delta_1^2, \Delta_2^2$, where $\Delta_{1,2}^2 = \frac{1}{4}(\sqrt{|\phi|^2 + 8|\Delta|^2} \pm |\phi|)^2$. Moreover, the other inverse propagators are given by

$$\widetilde{\mathcal{S}}_{(\pm)}^{-1} = \begin{pmatrix} [G_{0(\pm)}^{+}]^{-1} \otimes 1_{2\times2} & \widetilde{\Phi}_{(\pm)}^{*} \\ \widetilde{\Phi}_{(\pm)} & [G_{0(\pm)}^{-}]^{-1} \otimes 1_{2\times2} \end{pmatrix}, \tag{B.25}$$

where

$$\widetilde{\Phi}_{(\pm)} = -i\gamma_5 \Delta \, 1_{2\times2}. \tag{B.26}$$

Now, each term in Eq. (B.22) can be simplified using the identity in Eq. (B.1), which then gives

$$\Gamma_{(a)} = \frac{1}{2}\ln\det\left[[G^{+}_{0(a)}]^{-1}[G^{-}_{0(a)}]^{-1} + \widetilde{\Phi}_{(a)}\widetilde{\Phi}^{*}_{(a)}\right], \tag{B.27}$$

where we used that $[G^{\pm}_{0(a)}]^{-1}\widetilde{\Phi}^{+}_{(a)} = -\widetilde{\Phi}^{+}_{(a)}[G^{\pm}_{0(a)}]^{-1}$. Since only the absolute square of the gaps appears in the expressions, from now on we take $\Delta,\, \phi > 0$.

In order to compute the determinants it is convenient to use the chiral and energy projectors defined in Eqs. (C.9) and (C.10). First, it can be shown that

$$[G^{\pm}_{0(a)}]^{-1}[G^{\mp}_{0(a)}]^{-1} = \sum_{c=\pm}[\,p_0^2 - (c|\bar{\mathbf{p}}_{(a)}| \pm \mu)^2]\Lambda^{c}_{(a)}, \tag{B.28}$$

which then gives

$$\Gamma_{(a)} = \frac{1}{2}\mathrm{tr}_{c,f,\chi}\sum_{p_0,\bar{\mathbf{p}}_{(a)}}\ln\left(\frac{p_0^2 - (|\bar{\mathbf{p}}_{(a)}| - \mu)^2 - \lambda^2_{(a)}}{T^2}\right) + \frac{1}{2}\mathrm{tr}_{\mathrm{c,f},\chi}\sum_{\mathrm{p_0},\bar{\mathbf{p}}_{\mathrm{a}}}\ln\left(\frac{\mathrm{p}_0^2 - (|\bar{\mathbf{p}}_{(\mathrm{a})}| + \mu)^2 - \lambda^2_{(\mathrm{a})}}{\mathrm{T}^2}\right), \tag{B.29}$$

where $-\lambda^2_{(a)}$ are the eigenvalues of the matrices $\widetilde{\Phi}_{(a)}\widetilde{\Phi}^{*}_{(a)}$. Also, $\mathrm{tr}_{c,f,\chi}$ is the remaining trace over the color, flavor, and chiral indices. Moreover, $|\bar{\mathbf{p}}_{(0)}| = \sqrt{p_3^2 + \vec{p}_{\perp}^{\,2}}$ and $|\bar{\mathbf{p}}_{(\pm)}| = \sqrt{p_3^2 + 2eBn}$, where $n \geq 0$ is an integer that labels the Landau levels, and $\vec{p}_{\perp}$ is the momentum perpendicular to the field. Also, it is clear now that $\Gamma_{(+)} = \Gamma_{(-)}$. The sums in the equation above are defined as follows

$$\sum_{p_0,\bar{p}_{(0)}} f(p_0,\bar{\mathbf{p}}_{(0)}) = T\sum_k \int \frac{d^3\vec{p}}{(2\pi)^3} f(i\omega_k,\vec{p}), \tag{B.30}$$

and

$$\sum_{p_0,\bar{\mathbf{p}}_{(\pm)}} f(p_0,\bar{\mathbf{p}}_{(\pm)}) = T\sum_k \frac{eB}{8\pi^2}\sum_{n=0}^{\infty}\alpha_n\int_{-\infty}^{\infty} dp_3 f(i\omega_k,n,p_3), \tag{B.31}$$

where f is an arbitrary function, and $\alpha = 2 - \delta_{n0}$ stands for the fact that Landau levels with $n > 0$ are doubly degenerate. Since these sums do not converge, some sort of cutoff procedure has to be used. The Matsubara sum can be evaluated using the identity

$$T\sum_k \ln\left(\frac{\omega_k^2 + z^2}{T^2}\right) = |z| + 2T\,\ln(1 + e^{-|z|/T}). \tag{B.32}$$

Therefore, we can now write the one-loop quark contribution to the pressure of the mCFL phase as

$$\Gamma = 3P_T(\phi) + P_T(\Delta_1) + P_T(\Delta_2) + 4F_T(\Delta). \tag{B.33}$$

The function $P_T(\phi)$ is defined as follows

$$\begin{aligned} P_T(\phi) &= \mathrm{tr}_{B=0}\left[E_0^{+}(\phi) + E_0^{-}(\phi)\right] \\ &\quad + 2T\,\mathrm{tr}_{B=0}\left[\ln(1 + e^{-E_0^{+}/T}) + \ln(1 + e^{-E_0^{-}/T})\right], \end{aligned} \tag{B.34}$$

where $\mathrm{tr}_{B=0}[\ldots] = \int \frac{d^3\vec{p}}{(2\pi)^3}[\ldots]$, $E_0^{\pm}[\phi] = \sqrt{(p \mp \mu)^2 + \phi^2}$, with $p = \sqrt{p_3^2 + \vec{p}_\perp^{\,2}} = |\vec{p}|$. The zero-temperature terms are divergent and they are regularized in Sec. 3.2.1. The other function in Eq. (B.33) reads

$$\begin{aligned} F_T(\Delta) &= \mathrm{tr}_B\left[E_B^+(\Delta) + E_B^-(\Delta)\right] \\ &\quad + 2T\,\mathrm{tr}_B\left[\ln(1 + e^{-E_B^+/T}) + \ln(1 + e^{-E_B^-/T})\right] \end{aligned} \tag{B.35}$$

where $\mathrm{tr}_B[\ldots] = \frac{eB}{8\pi^2}\sum_{n=0}^{\infty}\alpha_n \int_{-\infty}^{\infty} dp_3[\ldots]$, $E_B^{\pm}[\Delta] = \sqrt{(\varepsilon_B \mp \mu)^2 + \Delta^2}$, with $\varepsilon_B = \sqrt{p_3^2 + 2eBn}$. Note that $\lim_{B\to 0} F_T(x) = P_T(x)$ and, once the limit $\Delta = \phi$ and $B = H = 0$ is taken, we recover the free energy of the CFL phase in the absence of an external field.

Appendix C

Properties of Ritus' Eigenfunctions

The transformation functions $E_P^{\pm}$ for positively (+) and negatively (-) charged fermions are obtained as solutions of the field-dependent eigenvalue equation

$$(\Pi_{(\pm)} \cdot \gamma) E_P^{\pm}(X) = E_P^{\pm}(X)(\bar{P}_{(\pm)} \cdot \gamma), \tag{C.1}$$

where $\bar{P}_{(\pm)} = (p_0, 0, \pm\sqrt{2eBn}, p_3)$ and

$$E_P^{\pm}(X) = \sum_{\sigma} E_{P\sigma}^{\pm}(X)\Delta[\sigma], \tag{C.2}$$

with eigenfunctions

$$E_{P\sigma}^{\pm}(X) = \mathcal{C}_{l\,(\pm)}\, e^{-i(p_0x^0+p_2x^2+p_3x^3)}\, D_{l\,(\pm)}[\rho_{(\pm)}], \tag{C.3}$$

where $D_{l\,(\pm)}[\rho_{(\pm)}]$ are parabolic cylinder functions with argument $\rho_{(\pm)}$ defined as

$$\rho_{(\pm)} = \sqrt{2eB}(x_1 + p_2/eB), \tag{C.4}$$

and index $l\,(\pm)$ given by

$$l\,(\pm) = n \pm \frac{\sigma}{2} - \frac{1}{2}, \qquad l(\pm) = 0, 1, 2, \ldots, \tag{C.5}$$

whereas $n = 0, 1, 2, \ldots$, denotes the Landau levels and σ is the spin projection that can take values ± 1. Moreover, the normalization constant is

$$\mathcal{C}_{l\,(\pm)} = (4\pi\, eB)^{1/4}/\sqrt{l\,(\pm)\,!}\,. \tag{C.6}$$

The spin matrices $\Delta[\sigma]$ in Eq. (C.2) are spin projectors. They are defined as

$$\Delta[\sigma] = \mathrm{diag}(\delta_{\sigma 1}, \delta_{\sigma -1}, \delta_{\sigma 1}, \delta_{\sigma -1}), \qquad \sigma = \pm 1, \tag{C.7}$$

and satisfy the following relations

$$\Delta[\pm]^{\dagger} = \Delta[\pm], \qquad \Delta[+] + \Delta[-] = 1, \tag{C.8a}$$

$$\Delta[\pm]\Delta[\pm] = \Delta[\pm], \qquad \Delta[\mp]\Delta[\pm] = 0, \tag{C.8b}$$

$$\gamma_{\parallel}\Delta[\pm] = \Delta[\pm]\gamma_{\parallel}, \qquad \gamma_{\perp}\Delta[\pm] = \Delta[\mp]\gamma_{\perp}. \tag{C.8c}$$

In the equations above we used that $\gamma_{\parallel} = (\gamma^0, \gamma^3)$ and $\gamma_{\perp} = (\gamma^1, \gamma^2)$.

Massless quarks can be fully characterized by the chiral and energy projection operators,

$$P_{R,L} = \frac{1 \pm \gamma_5}{2}, \tag{C.9}$$

$$\Lambda^{\pm}_{(a)} = \frac{1 \pm \gamma_0 \, \vec{\gamma} \cdot \hat{\vec{\mathbf{p}}}_{(a)}}{2}, \quad \text{with} \quad a = 0, \pm. \tag{C.10}$$

respectively. Similarly to the free case, in the presence of a uniform magnetic field these two operators commute.

In Ref. [83] it was shown that only massless quarks with the same chirality pair in the spin-zero channel. One can show that there are four different gap functions that describe the possible pairings. However, in an NJL theory with the gap functions independent of the 3-momentum, the total number of independent gaps is reduced to one. This means that the gap for quasi-particles and quasi-antiparticles are the same, in spite of the chirality of the particles. Moreover, the Dirac structure of the gap matrix is simply given by $C\gamma_5$, where $C = i\gamma^2\gamma^0$ is the charge conjugation matrix.

Bibliography

[1] M.E. Peskin and D.V. Schroeder, *An Introduction to Quantum Field Theory* (Westview Press, 1995); S. Weinberg, *The Quantum Theory of Fields* (Cambridge University Press, 1995), Vol. 1 and 2.

[2] A. Zee, *Quantum field theory in a nutshell* (Princeton University Press, 2003).

[3] D. Clowe, M. Bradac, A.H. Gonzalez, M. Markevitch, S.W. Randall, C. Jones, and D. Zaritsky, Astrophys. J. **648**, L109-L113 (2006).

[4] D. Feldman, B. Kors, and P. Nath, Phys. Rev. D **75**, 023503 (2007); M. E. Peskin, arXiv:0707.1536 [hep-ph]; T. Boeckel and J. Schaffner-Bielich, Phys. Rev. D **76**, 103509 (2007) [arXiv:0707.3260 [astro-ph]].

[5] C. Kuhn [ALICE Collaboration], Nucl. Phys. A **787**, 19 (2007); N. E. Mavromatos, arXiv:0708.0134 [hep-ph]; D. d'Enterria, arXiv:0708.0551 [hep-ex]; P. Meade and L. Randall, arXiv:0708.3017 [hep-ph].

[6] For a general reference check the web site http://www-bdnew.fnal.gov/tevatron/ .

[7] J. Polchinski, *String Theory* (Cambridge University Press, 1998), Vol. 1 and 2.

[8] N. Arkani-Hamed, S. Dimopoulos, and G. R. Dvali, Phys. Lett. B **429**, 263 (1998); I. Antoniadis, N. Arkani-Hamed, S. Dimopoulos, and G. R. Dvali, Phys. Lett. B **436**, 257 (1998); N. Arkani-Hamed, S. Dimopoulos, and G. R. Dvali, Phys. Rev. D **59**, 086004 (1999); L. Randall and R. Sundrum, Phys. Rev. Lett. **83**, 3370 (1999); L. Randall and R. Sundrum, Phys. Rev. Lett. **83**, 4690 (1999).

[9] D.H. Rischke, Prog. Part. Nucl. Phys. **52**, 197 (2004).

[10] E. Hubble, Proceedings of the National Academy of Sciences of the United States of America, Volume 15, Issue 3, pp. 168-173 (1929).

[11] S. Weinberg, *Gravitation and Cosmology: Principles and Applications of the General Theory of Relativity* (John Wiley & Sons, 1972).

[12] H.D. Politzer, Phys. Rev. Lett. **30**, 1346 (1973); D.J. Gross and F. Wilczek, Phys. Rev. D **8**, 3633 (1973); Phys. Rev. D **9**, 980 (1974).

[13] See for instance: Proc. of the 15th Int. Conf. on Ultra-relativistic Nucleus-Nucleus Collisions, *Quark Matter 2001* (eds. T.J. Hallman, D.E. Kharzeev, J.T. Mitchell, and T.S. Ullrich), Nucl. Phys. A **698**, 1 (2002); and U. W. Heinz, arXiv:hep-ph/0407360, for an excellent introduction to the physics of heavy-ion collisions.

[14] M. Gyulassy and L. McLerran, Nucl. Phys. A **750**, 30 (2005); J. Adams *et al.* [STAR Collaboration], Nucl. Phys. A **757**, 102 (2005); B. B. Back *et al.*, Nucl. Phys. A **757**, 28 (2005); I. Arsene *et al.* [BRAHMS Collaboration], Nucl. Phys. A **757**, 1 (2005); K. Adcox *et al.* [PHENIX Collaboration], Nucl. Phys. A **757**, 184 (2005).

[15] C. Kuhn [ALICE Collaboration], Nucl. Phys. A **787**, 19 (2007), and references therein.

[16] See for instance: EOS collaboration, Phys. Rev. Lett. **85**, 1194 (2000); Phys. Rev. C **64**, 054602 (2001); Phys. Rev. C **65**, 054617 (2002); INDRA Collaboration (J.D. Frankland et al.), Nucl. Phys. A **689**, 905 (2001); 940 (2001).

[17] For a general reference check the web site http://www.gsi.de/fair/experiments/CBM/index.html.

[18] M. Kitazawa, T. Koide, T. Kunihiro, and Y. Nemoto, Phys. Rev. D **65**, 091504 (2002); Prog. Theor. Phys. **114**, 117 (2005).

[19] G. 't Hooft, Phys. Rept. **142**, 357 (1986).

[20] D. J. Gross, R. D. Pisarski, and L. G. Yaffe, Rev. Mod. Phys. **53**, 42 (1981).

[21] J. I. Kapusta, *Finite Temperature Field Theory* (Cambridge University Press, Cambridge, 1983).

[22] M. Le Bellac, *Thermal Field Theory* (Cambridge University Press, Cambridge, 1996).

[23] Review of Particle Physics by Particle Data Group, Phys. Rev. D **66**, 010001 (2002).

[24] B. Freedman and L. McLerran, Phys. Rev. D **16**, 1169 (1977).

[25] R. D. Pisarski and D. H. Rischke, Phys. Rev. Lett. **83**, 37 (1999).

[26] A. D. Linde, Phys. Lett. B **96**, 289 (1980).

[27] K. Kajantie, M. Laine, K. Rummukainen, and Y. Schröder, Phys. Rev. Lett. **86**, 10 (2001); Phys. Rev. D **65**, 045008 (2002); Phys. Rev. D **67**, 105008 (2003); JHEP **0304**, 036 (2003).

[28] M. Creutz, *Quarks, Gluons, and Lattices* (Cambridge University Press, Cambridge, 1983).

[29] E. Laermann and O. Philipsen, Ann. Rev. Nucl. Part. Sci. **53**, 163 (2003).

[30] Z. Fodor and S. D. Katz, JHEP **0404**, 050 (2004); Y. Aoki, G. Endrodi, Z. Fodor, S. D. Katz, and K. K. Szabo, Nature **443**, 675 (2006).

[31] S. Ejiri, C. R. Allton, S. J. Hands, O. Kaczmarek, F. Karsch, E. Laermann, and C. Schmidt, Prog. Theor. Phys. Suppl. **153**, 118 (2004).

[32] M. Buballa, Phys. Rept. **407**, 205 (2005).

[33] T. Schafer, arXiv:nucl-th/0609075.

[34] H. K. Onnes, Comm. Leiden **120b** (1911).

[35] J. Bardeen, L. N. Cooper, and J. R. Schrieffer, Phys. Rev. **106**, 162 (1957); **108**, 1175 (1957).

[36] A. A. Abrikosov, L. P. Gorkov, and I. E. Dzyaloshinski, *Methods of Quantum Field Theory in Statistical Physics* (Dover Publications, New York, 1963).

[37] H. Fröhlich, Phys. Rev. **79**, 845 (1950).

[38] L. N. Cooper, Phys. Rev. **104**, 1189 (1956).

[39] J. G. Bednorz and K. A. Müller, Z. Physik B **64**, 189 (1986).

[40] V. L. Ginzburg and L. D. Landau, Zh. Eksp. Teor. Fiz. **20**, 1044 (1950).

[41] N. Goldenfeld, *Lectures on Phase Transitions and the Renormalization Group* (Addison-Wesley Publishing Company, 1992).

[42] A. A. Abrikosov, Zh. Eksp. Teor. Fiz. **32**, 1442 (1957); Sov. Phys. JETP **5**, 1174 (1957).

[43] M. Tinkham, *Introduction to Superconductivity* (McGraw-Hill, New York, 1975).

[44] B. I. Halperin, T. C. Lubensky, and S. Ma, Phys. Rev. Lett. **32**, 292 (1974).

[45] P. G. de Gennes, Solid State Commun. **10**, 753 (1972); T. C. Lubensky and J.-H. Chen, Phys. Rev. B **17**, 366 (1978).

[46] A. Vilenkin and E. P. S. Shellard, *Cosmic Strings and Other Topological Defects* (Cambridge University Press, Cambridge, England, 1994).

[47] X. G. Wen and Y. S. Wu, Phys. Rev. Lett. **70**, 1501 (1993); L. Pryadko and S. C. Zhang, Phys. Rev. Lett. **73**, 3282 (1994).

[48] S. Mo, J. Hove, and A. Sudbo, Phys. Rev. B **65**, 104501 (2002).

[49] A. L. Fetter and J. D. Walecka, *Quantum Theory of Many-Particle Systems* (McGraw Hill, New York, 1971).

[50] P. L. Kapitza, Nature **141**, 47 (1938).

[51] For a short review see A. J. Leggett, Rev. Mod. Phys. **71**, S318 - S323 (1999).

[52] L. Tisza, Nature **141**, 913 (1938).

[53] L. D. Landau, J. Phys. (USSR) **5**, 71 (1941); **11**, 91 (1947).

[54] L. D. Landau, E. M. Lifshitz, *Statistical Physics* (Pergamon Press, New York, 1980), Vol. 5, Part I; Vol. 9, Part II.

[55] D. D. Osheroff, R. C. Richardson, and D. M. Lee, Phys. Rev. Lett. **28**, 885 (1972).

[56] A. J. Leggett, Rev. Mod. Phys. **47**, 331 (1975).

[57] A. Schmitt, *Spin-one color superconductivity in cold and dense quark matter*, Ph.D. dissertation, arXiv:nucl-th/0405076; Phys. Rev. D **71**, 054016 (2005).

[58] D. V. Osborne, Proc. Phys. Soc. A **63**, 909 (1950).

[59] L. Onsager, Nuovo Cimento **6**, Suppl. 2, 249 (1949).

[60] R. P. Feynman, Phys. Rev. **91**, 1301 (1953); **94**, 262 (1954); *Statistical Mechanics: A Set of Lectures* (Perseus Books Group, 1998).

[61] W. F. Vinen, Proc. Roy. Soc. A **260**, 218 (1961); G. W. Rayfield and F. Reif, Phys. Rev. **136**, 1194 (1964).

[62] D. Ivanenko and D. F. Kurdgelaidze, Astrofiz. **1**, 479 (1965); Lett. Nuovo Cim. **2**, 13 (1969); N. Itoh, Prog. Theor. Phys. **44**, 291 (1970); F. Iachello, W. D. Langer, and A. Lande, Nucl. Phys. A **219**, 612 (1974). J. C. Collins and M. J. Perry, Phys. Rev. Lett. **34**, 1353 (1975).

[63] M. Alford, K. Rajagopal, and F. Wilczek, Phys. Lett. B **422**, 247 (1998); R. Rapp, T. Schäfer, E. V. Shuryak, and M. Velkovsky, Phys. Rev. Lett. **81**, 53 (1998).

[64] G. W. Carter and D. Diakonov, Phys. Rev. D **60**, 016004 (1999); J. Berges and K. Rajagopal, Nucl. Phys. B **538**, 215 (1999); M. Buballa and M. Oertel, Nucl. Phys. A **703**, 770 (2002); F. Gastineau, R. Nebauer, and J. Aichelin, Phys. Rev. C **65**, 045204 (2002); M. Huang, P. F. Zhuang, and W. Q. Chao, Phys. Rev. D **65**, 076012 (2002); M. Huang, P. F. Zhuang, and W. Q. Chao, Phys. Rev. D **67**, 065015 (2003).

[65] D. T. Son, Phys. Rev. D **59**, 094019 (1999).

[66] T. Schäfer and F. Wilczek, Phys. Rev. D **60**, 114033 (1999).

[67] D. K. Hong, V. A. Miransky, I. A. Shovkovy, and L. C. R. Wijewardhana, Phys. Rev. D **61**, 056001 (2000) [Erratum-ibid. D **62**, 059903 (2000)].

[68] S. D. H. Hsu and M. Schwetz, Nucl. Phys. B **572**, 211 (2000).

[69] R. D. Pisarski and D. H. Rischke, Phys. Rev. D **61**, 051501 (2000); 074017 (2000).

[70] I. A. Shovkovy and L. C. R. Wijewardhana, Phys. Lett. B **470**, 189 (1999); T. Schäfer, Nucl. Phys. B **575**, 269 (2000); T. Schäfer, Nucl. Phys. A **728**, 251 (2003).

[71] K. Iida and G. Baym, Phys. Rev. D **63**, 074018 (2001).

[72] I. Giannakis and H.C. Ren, Phys. Rev. D **65**, 054017 (2002).

[73] T. Matsuura, K. Iida, T. Hatsuda, and G. Baym, Phys. Rev. D **69**, 074012 (2004).

[74] I. Giannakis, D. Hou, H.C. Ren, and D.H. Rischke, Phys. Rev. Lett. **93**, 232301 (2004).

[75] J.L. Noronha, I. Giannakis, D. Hou, H.C. Ren, and D.H. Rischke, Phys. Rev. D **73**, 094009 (2006); Acta Phys. Hung. A **27**, 311 (2006).

[76] K. Iida and G. Baym, Phys. Rev. D **66**, 014015 (2002), [Erratum-ibid., Phys. Rev. D **66**, 059903(E) (2002)].

[77] K. Iida, T. Matsuura, M. Tachibana, and T. Hatsuda, Phys. Rev. D **71**, 054003 (2005).

[78] B. C. Barrois, Nucl. Phys. B **129**, 390 (1977); S. C. Frautschi, in *Hadronic matter at extreme energy density*, edited by N. Cabibbo and L. Sertorio (Plenum Press, 1980); D. Bailin and A. Love, Nucl. Phys. B **190**, 175 (1981); Nucl. Phys. B **205**, 119 (1982); Phys. Rep. **107**, 325 (1984).

[79] K. Rajagopal and F. Wilczek, in *At the Frontier of Particle Physics/Handbook of QCD*, edited by M. Shifman (World Scientific, Singapole, 2001); M. G. Alford, Annu. Rev. Nucl. Part. Sci. **51**, 131 (2001); D. K. Hong, Acta. Phys. Pol. B **32**, 1253 (2001); S. Reddy, Acta. Phys. Pol. B **33**, 4101 (2002); M. Buballa, Phys. Rept. **407**, 205 (2005); T. Schäfer, hep-ph/0304281; M. Huang, Int. J. Mod. Phys. E **14**, 675 (2005); I. A. Shovkovy, Found. Phys. **35**, 1309 (2005).

[80] T. Schäfer and K. Schwenzer, Phys. Rev. D **70**, 114037 (2004); H. Grigorian, D. Blaschke, and D. Voskresensky, Phys. Rev. C **71**, 045801 (2005); D. N. Aguilera, D. Blaschke, M. Buballa, and V.L. Yudichev, Phys. Rev. D **72**, 034008 (2005); P. Jaikumar, C. D. Roberts, and A. Sedrakian, Phys. Rev. C **73**, 042801 (2006); A. Schmitt, I. A. Shovkovy, and Q. Wang, Phys. Rev. D **73**, 034012 (2006).

[81] J. Madsen, Phys. Rev. Lett. **85**, 10 (2000); C. Manuel, A. Dobado, and F.J. Llanes-Estrada, JHEP **0509**, 076 (2005).

[82] A. Drago, A. Lavagno, and G. Pagliara, Phys. Rev. D **69**, 057505 (2004).

[83] R. D. Pisarski and D. H. Rischke, Phys. Rev. D **60**, 094013 (1999).

[84] M. G. Alford, K. Rajagopal, and F. Wilczek, Nucl. Phys. B **537**, 443 (1999).

[85] T. Schafer and F. Wilczek, Phys. Rev. Lett. **82**, 3956 (1999).

[86] S. Elitzur, Phys. Rev. D **12**, 3978 (1975).

[87] D. Vollhardt and P. Wölfle, *The Superfluid Phases of Helium 3* (Taylor & Francis, London, 1990).

[88] I. A. Shovkovy and P. J. Ellis, Phys. Rev. C **67**, 048801 (2003).

[89] J. L. Noronha and I. A. Shovkovy, Phys. Rev. D **76**, 105030 (2007), arXiv:0708.0307 [hep-ph].

[90] D. F. Litim and C. Manuel, Phys. Rev. D **64**, 094013 (2001).

[91] M. G. Alford, J. A. Bowers, J. M. Cheyne, and G. A. Cowan, Phys. Rev. D **67**, 054018 (2003).

[92] T. Schäfer, Phys. Rev. D **62**, 094007 (2000).

[93] A. Schmitt, Q. Wang, and D. H. Rischke, Phys. Rev. D **66**, 114010 (2002).

[94] A. Schmitt, Q. Wang, and D. H. Rischke, Phys. Rev. Lett. **91**, 242301 (2003).

[95] S. L. Shapiro and S. A. Teukolsky, *Black Holes, White Dwarfs, and Neutron Stars* (John Wiley & Sons, 1983).

[96] E. J. Ferrer, V. de la Incera, and C. Manuel, Phys. Rev. Lett. **95**, 152002 (2005).

[97] V. A. Miransky and I. A. Shovkovy, Phys. Rev. D **66**, 045006 (2002).

[98] V. P. Gusynin, V. A. Miransky, and I. A. Shovkovy, Phys. Rev. Lett. **73**, 3499 (1994); Phys. Lett. B **349**, 477 (1995); Phys. Rev. D **52**, 4747 (1995); Phys. Rev. Lett. **83**, 1291 (1999); Nucl. Phys. B **563**, 361 (1999).

[99] C.N. Leung, Y.J. Ng, and A.W. Ackley, Phys. Rev. D **54**, 4181 (1996); D.S. Lee, C.N. Leung, and Y.J. Ng, Phys. Rev. D **55**, 6504 (1997); I.A. Shushpanov and A.V. Smilga, Phys. Lett. B **402**, 351 (1997); D.K. Hong, Phys. Rev. D **57**, 3759 (1998); E.J. Ferrer and V. de la Incera, Phys. Lett. B **481**, 287 (2000); J. Alexandre, K. Farakos, and G. Koutsoumbas, Phys. Rev. D **62**, 105017 (2000); D. Ebert, K.G. Klimenko, M.A. Vdovichenko, and A.S. Vshivtsev, Phys. Rev. D **61**, 025005 (2000); D. Kabat, K.M. Lee, and E. Weinberg, Phys. Rev. D **66**, 014004 (2002).

[100] E. Braaten and R. D. Pisarski, Nucl. Phys. B **337**, 569 (1990); **339**, 310 (1990); J. Frenkel and J. C. Taylor, Nucl. Phys. B **334**, 199 (1990); **374**, 156 (1992).

[101] T. Altherr and U. Kraemmer, Astropart. Phys. **1**, 133 (1992); J. -P. Blaizot and J. -Y. Ollitrault, Phys. Rev. D **48**, 1390 (1993); H. Vija and M. H. Thoma, Phys. Lett. B **342**, 212 (1995); C. Manuel, Phys. Rev. D **53**, 5866 (1996).

[102] W. E. Brown, J. T. Liu, and H. c. Ren, Phys. Rev. D **61**, 114012 (2000); ibid. **62**, 054013, 054016 (2000).

[103] Q. Wang and D. H. Rischke, Phys. Rev. D **65**, 054005 (2002).

[104] P. T. Reuter, Q. Wang, and D. H. Rischke, Phys. Rev. D **70**, 114029 (2004); Erratum-ibid. D **71**, 099901 (2005); *A general effective action for quark matter and its application to color superconductivity*, Ph.D. dissertation, arXiv:nucl-th/0602043.

[105] M. Alford and K. Rajagopal, JHEP **0206**, 031 (2002).

[106] S. B. Ruester, V. Werth, M. Buballa, I. A. Shovkovy and D. H. Rischke, Phys. Rev. D **72**, 034004 (2005); S. B. Ruester, *The phase diagram of neutral quark matter*, Ph.D. dissertation, arXiv:nucl-th/0612090.

[107] P. Bedaque, Nucl. Phys. A **697**, 569 (2002).

[108] K. Rajagopal and A. Schmitt, Phys. Rev. D **73**, 045003 (2006).

[109] H. Müther and A. Sedrakian, Phys. Rev. D **67**, 085024 (2003).

[110] W. V. Liu and F. Wilczek, Phys. Rev. Lett. **90**, 047002 (2003); M. M. Forbes, E. Gubankova, W. V. Liu, and F. Wilczek, Phys. Rev. Lett. **94**, 017001 (2005).

[111] A. I. Larkin and Y. N. Ovchinnikov, Zh. Eksp. Teor. Fiz. **47**, 1136 (1964) [Sov. Phys. JETP **20**, 762 (1965)]; P. Fulde and R. A. Ferrell, Phys. Rev. **135**, A550 (1964).

[112] M. Alford, J. A. Bowers, and K. Rajagopal, Phys. Rev. D 63, 074016 (2001); for a review see R. Casalbuoni and G. Nardulli, Rev. Mod. Phys. **76**, 263 (2004).

[113] I. Shovkovy and M. Huang, Phys. Lett. B **564**, 205 (2003); M. Huang and I. Shovkovy, Nucl. Phys. A **729**, 835 (2003); see also E. Gubankova, W. V. Liu and F. Wilczek, Phys. Rev. Lett. **91**, 032001 (2003).

[114] M. Huang and I. A. Shovkovy, Phys. Rev. D **70**, 051501 (R) (2004); Phys. Rev. D **70**, 094030 (2004).

[115] M. Alford, C. Kouvaris, and K. Rajagopal, Phys. Rev. Lett. **92**, 222001 (2004); Phys. Rev. D **71**, 054009 (2005); K. Fukushima, C. Kouvaris, and K. Rajagopal, Phys. Rev. D **71**, 034002 (2005); M. Alford, P. Jotwani, C. Kouvaris, J. Kundu, and K. Rajagopal, Phys. Rev. D **71**, 114011 (2005); K. Fukushima, Phys. Rev. D 72, 074002 (2005); R. Casalbuoni, R. Gatto, M. Mannarelli, G. Nardulli, and M. Ruggieri, Phys. Lett. B 605, 362 (2005); 615, 297(E) (2005); M. Alford and Q. h. Wang, J. Phys. G **31**, 719 (2005).

[116] I. Giannakis and H. C. Ren, Phys. Lett. B **611**, 137 (2005); Nucl. Phys. **B723**, 255 (2005);

[117] I. Giannakis, D. f. Hou, and H. C. Ren, Phys. Lett. B **631**, 16 (2005).

[118] M. Huang, Phys. Rev. D **73**, 045007 (2006).

[119] D. K. Hong, arXiv:hep-ph/0506097.

[120] E. V. Gorbar, M. Hashimoto, and V. A. Miransky, Phys. Lett. B **632**, 305 (2006).

[121] K. Iida and K. Fukushima, Phys. Rev. D **74**, 074020 (2006).

[122] K. Fukushima, Phys. Rev. D **73**, 094016 (2006).

[123] E. V. Gorbar, M. Hashimoto, and V. A. Miransky, Phys. Rev. Lett. **96**, 022005 (2006).

[124] O. Kiriyama, D. H. Rischke, and I. A. Shovkovy, Phys. Lett. B **643**, 331 (2006).

[125] S. Reddy and G. Rupak, Phys. Rev. C **71**, 025201 (2005); F. Neumann, M. Buballa, and M. Oertel, Nucl. Phys. **A714**, 481 (2003); I. Shovkovy, M. Hanauske, and M. Huang, Phys. Rev. D **67**, 103004 (2003).

[126] A. Kryjevski, hep-ph/0508180; T. Schäfer, Phys. Rev. Lett. **96**, 012305 (2006).

[127] D. Page and S. Reddy, Ann. Rev. Nucl. Part. Sci. **56**, 327 (2006).

[128] M. Ruderman, T. Zhu, and K. Chen, Astrophys. J. **492**, 267 (1998).

[129] A. A. Svidzinsky, Astrophys. J. **590**, 386 (2003).

[130] D. M. Sedrakian, A. D. Sedrakian, and G. F. Zharkov, Mon. Not. Roy. Astron. Soc. **290**, 203 (1997).

[131] B. Link, Phys. Rev. Lett. **91**, 101101 (2003).

[132] K. B. W. Buckley, M. A. Metlitski, and A. R. Zhitnitsky, Phys. Rev. Lett. **92**, 151102 (2004).

[133] J. Noronha and A. Sedrakian, arXiv:0708.2876 [astro-ph].

[134] F. Weber, *Pulsars as Astrophysical Laboratories for Nuclear and Particle Physics* (IOP Publishing Ltd., Bristol, 1999).

[135] M. Prakash, J. M. Lattimer, J. A. Pons, A. W. Steiner, and S. Reddy, Lect. Notes Phys. **578**, 364 (2001).

[136] R. C. Tolman, *Relativity, Thermodynamics and Cosmology* (Oxford, 1934); J. R. Oppenheimer and G. M. Volkoff, Phys. Rev. **55**, 374 (1939).

[137] M. Alford and S. Reddy, Phys. Rev. D **67**, 074024 (2003); I. Shovkovy, M. Hanauske, and M. Huang, Phys. Rev. D **67**, 103004 (2003); S. B. Ruester and D. H. Rischke, Phys. Rev. D **69**, 045011 (2004); D. B. Blaschke, D. Gomez Dumm, A. G. Grunfeld, T. Klahn, and N. N. Scoccola, Phys. Rev. C **75**, 065804 (2007); M. Alford, D. Blaschke, A. Drago, T. Klahn, G. Pagliara, and J. Schaffner-Bielich, Nature **445**, E7 (2007);

[138] M. Alford, M. Braby, M. W. Paris, and S. Reddy, Astrophys. J. **629**, 969 (2005).

[139] N. K. Glendenning, *Compact Stars* (Springer-Verlag, New York, 1997).

[140] P. M. Woods and C. Thompson, arXiv:astro-ph/0406133.

[141] R.C. Duncan and C. Thompson, Astrophys. J. **392**, L9 (1992); C. Thompson and R.C. Duncan, Astrophys. J. **408**, 194 (1993); C. Thompson and R. C. Duncan, Mon. Not. Roy. Astron. Soc. **275**, 255 (1995).

[142] B. Zhang, R. X. Xu, and G. J. Qiao, Astrophys. J. **545**, L127 (2000); I. S. Suh and G. J. Mathews, Astrophys. J. **546**, 1126 (2001); V. N. Kondratyev, Phys. Rev. Lett. **88**, 221101 (2002).

[143] J. S. Heyl and S. R. Kulkarni, Astrophys. J. **506**, L61 (1998).

[144] J. A. Pons, B. Link, J. A. Miralles, and U. Geppert, Phys. Rev. Lett. **98**, 071101 (2007).

[145] P. Haensel, J. L. Zdunik, and R. Schaefer, Astron. Astrophys. **160**, 121 (1986); C. Alcock, E. Farhi, and A. V. Olinto, Astrophys. J. **310**, 261 (1986).

[146] S. Chandrasekhar, Phys. Rev. Lett. **24**, 611 (1970); Astrophys. J. **161**, 561 (1970); J. Friedman and B. Schutz, Astrophys. J. **222**, 281 (1978); N. Andersson, Astrophys. J. **502**, 708 (1998); J. L. Friedman and S. M. Morsink, Astrophys. J. **502**, 714 (1998); L. Lindblom, B. J. Owen, and S. M. Morsink, Phys. Rev. Lett. **80**, 4843 (1998); for reviews see N. Andersson and K. D. Kokkotas, Int. J. Mod. Phys. D **10**, 381 (2001) and L. Lindblom, arXiv:astro-ph/0101136.

[147] R. F. Sawyer, Phys. Rev. D **39**, 3804 (1989); P. B. Jones, Phys. Rev. D **64**, 084003 (2001); L. Lindblom and B. J. Owen, Phys. Rev. D **65**, 063006 (2002); L. Lindblom and B. J. Owen, Phys. Rev. D **65**, 063006 (2002); A. Drago, A. Lavagno, and G. Pagliara, Phys. Rev. D **71**, 103004 (2005); P. Haensel, K. P. Levenfish, and D. G. Yakovlev, Astron. Astrophys. **357**, 1157 (2000); P. Haensel, K. P. Levenfish, and D. G. Yakovlev, Astron. Astrophys. **372**, 130 (2001); D. Chatterjee and D. Bandyopadhyay, Phys. Rev. D **74**, 023003 (2006).

[148] R. F. Sawyer, Phys. Lett. B **233**, 412 (1989); J. Madsen, Phys. Rev. D **46**, 3290 (1992); M. G. Alford, M. Braby, S. Reddy, and T. Schafer, Phys. Rev. C **75**, 055209 (2007); B. A. Sa'd, I. A. Shovkovy, and D. H. Rischke, Phys. Rev. D **75**, 065016 (2007); M. G. Alford and A. Schmitt, J. Phys. G **34**, 67 (2007); H. Dong, N. Su, and Q. Wang, Phys. Rev. D **75**, 074016 (2007); B. A. Sa'd, I. A. Shovkovy, and D. H. Rischke, Phys. Rev. D **75**, 125004 (2007); A. Drago, G. Pagliara, and I. Parenti, arXiv:0704.1510 [astro-ph]; C. Manuel and F. Llanes-Estrada, arXiv:0705.3909 [hep-ph]; M. G. Alford, M. Braby, and A. Schmitt, arXiv:0707.2389 [nucl-th].

[149] D.H. Rischke, Phys. Rev. D **62**, 054017 (2000).

[150] A. J. Paterson, Nucl. Phys. B **190**, 188 (1981).

[151] I. Giannakis and H.C. Ren, Nucl. Phys. B **669**, 462 (2003).

[152] I. Bonalde, B.D. Yanoff, M.B. Salamon, and E.E.M. Chia, Phys. Rev. B **67**, 012506 (2003).

[153] J.M. Cornwall, R. Jackiw, and E. Tomboulis, Phys. Rev. D **10**, 2428 (1974).

[154] See Ref. [54] and also V.P. Gusynin and I.A. Shovkovy, Nucl. Phys. A **700**, 577 (2002) for the case of a color superconductor.

[155] S. Digal, T. Hatsuda, and M. Ohtani, arXiv:hep-lat/0511018.

[156] I. Fushiki, E. H. Gudmundsson, and C. J. Pethick, Astrophys. J. **342**, 958 (1989); G. Chanmugam, Annu. Rev. Astron. Astrophys. **30**, 143 (1992); D. Lai, Rev. Mod. Phys. 73, 629 (2001).

[157] C. Thompson and R.C. Duncan, Astrophys. J. **473**, 322 (1996).

[158] M. G. Alford, J. Berges, and K. Rajagopal, Nucl. Phys. B **571**, 269 (2000); E. V. Gorbar, Phys. Rev. D **62**, 014007 (2000); D. H. Rischke, Phys. Rev. D **62**, 054017 (2000).

[159] K. Rajagopal and F. Wilczek, Phys. Rev. Lett. **86**, 3492 (2001).

[160] M. Buballa and I. A. Shovkovy, Phys. Rev. D **72**, 097501 (2005).

[161] A. Broderick, M. Prakash, and J. M. Lattimer, Astrophys. J. **537**, 351 (2000).

[162] R. Casalbuoni and R. Gatto, Phys. Lett. B **464**, 111 (1999).

[163] D. T. Son and M. A. Stephanov, Phys. Rev. D **61**, 074012 (2000).

[164] E. J. Ferrer, V. de la Incera, and C. Manuel, Nucl. Phys. B **747**, 88 (2006).

[165] I. M. Lifshitz and A. M. Kosevich, Zh. Éksp. Teor. Fiz. **29**, 730 (1955) [Sov. Phys. JETP **2**, 636 (1956)].

[166] M. Abramovitz, I. Stegun, *Handbook of Mathematical Functions* (Dover, New York, 1970).

[167] J. Schwinger, Phys. Rev. **82**, 664 (1951).

[168] E. J. Ferrer and V. de la Incera, nucl-th/0703034.

[169] I. Lerche and D. N. Schramm, Astrophys. J. **216**, 881 (1977).

[170] R. D. Blandford and L. Hernquist, J. Phys. C **15**, 6233 (1982).

[171] D. Ebert, K. G. Klimenko, M. A. Vdovichenko, and A. S. Vshivtsev, Phys. Rev. D **61**, 025005 (2000).

[172] V. I. Ritus, Annals Phys. **69**, 555 (1972); Sov. Phys. JETP **48**, 788 (1978) [Zh. Eksp. Teor. Fiz. **75**, 1560 (1978)].

[173] E. Elizalde, E. J. Ferrer, and V. de la Incera, Annals Phys. **295**, 33 (2002); E. Elizalde, E. J. Ferrer, and V. de la Incera, Phys. Rev. D **70**, 043012 (2004).

[174] A. G. Lyne and F. Graham-Smith, *Pulsar Astronomy* (Cambridge University Press, 1998).

[175] B. Carter, *Lecture Notes in Physics* (Springer, Berlin, 2000) vol. 578, p. 54, edited by D. Blaschke, N. K. Glendennig, and A. Sedrakian.

[176] D. J. Dean and M. Hjorth-Jensen, Rev. Mod. Phys. **75**, 607 (2003).

[177] For a discussion of timing irregularities and long-term variabilities in pulsars see J. M. Cordes, in Planets around Pulsars, ed. J. A. Phillips, S. E. Thorsett, and S. R. Kulkarni, (ASP, San Francisco, 1993), pg. 43 and references therein.

[178] I. H. Stairs, A. G. Lyne, and S. L. Shemar, Nature **406**, 484 (2000).

[179] T. Akgun, B. Link and I. Wasserman, Mon. Not. Roy. Astron. Soc. **365**, 653 (2006) I. Wasserman, Mon. Not. Roy. Astron. Soc. **341**, 1020 (2003); B. Link and R. I. Epstein, Astrophys. J. **556**, 392L (2001); D. I. Jones and N. Andersson, Mon. Not. Roy. Astron. Soc. **324**, 811 (2001).

[180] J. Shaham, Astrophys. J. **214**, 251 (1977); A. Sedrakian, I. Wasserman, and J. M. Cordes, Astrophys. J. **524**, 341 (1999); see [131] and also B. Link, Astron. and Astrophys. **458**, 881L (2006).

[181] A. Sedrakian, Phys. Rev. D **71**, 083003 (2005).

[182] V. K. Tkachenko, Sov. Phys. JETP **22**, 1282 (1966) [Zh. Eksp. Teor. Fiz. **49**, 1875]; V. K. Tkachenko, Sov. Phys. JETP **23**, 1049 (1966) [Zh. Eksp. Teor. Fiz. **50**, 1573]; V. K. Tkachenko, Sov. Phys. JETP **29**, 945 (1969) [Zh. Eksp. Teor. Fiz. **56**, 1763]; V. K. Tkachenko, 1973, Zh. Eksp. Teor. Fiz. Pis'ma Red., 17, 617.

[183] I. M. Khalatnikov, *An Introduction to the Theory of Superfluidity*, (Westview Press, New York, 2000).

[184] M. Ruderman, Nature **225**, 619 (1970).

[185] G. E. Volovik and V. S. Dotsenko 1980, Sov. Phys. JETP 51, 65 [Zh. Eksp. Teor. Fiz. 78, 132].

[186] G. Baym and E. Chandler 1983, J. Low Temp. Phys. 50, 57.

[187] E. Chandler and G. Baym, J. Low Temp. Phys 62, 119 (1985).

[188] L. D. Landau and E. M. Lifshitz, *Fluid Mechanics* (Pergamon Press, New York, 1987).

[189] E. Flowers and N. Itoh, Astrophys. J. **230**, 847 (1979).

[190] G. A. Vardanyan and D. M. Sedrakyan, Sov. Phys. JETP **54**, 919 (1981); G. Mendell, Astrophys. J. **380**, 515 (1991); ibid., pg. 530; G. Mendell and L. Lindblom, Ann. Phys. **205**, 110 (1991).

[191] K. Fukushima and H. J. Warringa, arXiv:0707.3785 [hep-ph].

[192] K. Yasui and T. Kita, Phys. Rev. B **66**, 184516 (2002), and references therein.

[193] J. L. Noronha and I. A. Shovkovy, in preparation.

[194] C.Y. Cardall, M. Prakash, and J.M. Lattimer, Astrophys. J. **554**, 322 (2001).

[195] E. J. Ferrer and V. de la Incera, arXiv:0705.2403 [hep-ph].

[196] C. D. Andereck and W. I. Glaberson, J. Low. Temp. Phys. **48**, 257 (1982).

[197] I. Coddington, P. Engels, V. Schweikhard, and E. A. Cornell, Phys. Rev. Lett. **91**, 100402 (2003).

[198] G. Baym, Phys. Rev. Lett. **91**, 110402 (2003); see also J. Low. Temp. Phys. **138**, 601 (2005).

[199] A. Rapp, G. Zarand, C. Honerkamp, and W. Hofstetter, Phys. Rev. Lett. **98**, 160405 (2007).

Acknowledgements

Let me start off by giving thanks to Dirk Rischke for supporting my studies in Frankfurt. He has always been a very supportive advisor and I have thoroughly enjoyed all the discussions I have had with him in the last three years. Special thanks also goes out to my unofficial advisor Igor Shovkovy. It has always been a lot of fun talking to him about physics and anything else under the sun even though he never really believes what I say ... For that matter, I want to thank the creators of Skype for allowing me to continue having discussions with Igor after he moved to the US. I would also like to thank Professor Kodama for making my Ph.D. here in Frankfurt possible as well as my previous advisors in Brazil, Monica Bahiana and Clovis Wotzasek, for providing me with a good and diverse background in physics.

I am very thankful for the financial support provided by FIGSS. I would also like to thank all the professors at ITP and FIAS for useful discussions. Especially, a heartfelt thanks goes out to Adrian Dumitru for his awesome classes and his ceaseless patience for my never ending questions that pretty much handled every area of physics (but mainly heavy-ion collisions). In the last months Armen Sedrakian has taken me under his wing and we have had very fruitful discussions about astrophysics, of which I am very thankful for. I also really enjoyed working with Haicang Ren, Ioannis Giannakis, and Defu Hou. Jürgen Schaffner-Bielich and Igor Mishustin have also provided a wealth of knowledge about astrophysics. Moreover, I have really appreciated time spent with Marcus Bleicher and Carsten Greiner. I also thank Prof. Walter Greiner for his insightful lectures. Horst Stöcker, last but not least, has been my extremely audible muse in physics for the past three years.

Over the last three years, I have really appreciated talking with the students and postdocs and I especially enjoyed our discussions about string theory and whatever else dared to enter our minds at that time. More specifically, Giorgio Torrieri has been a very loud friend with whom I could talk to about anything and everything involving physics. Hajo Drescher has helped me out a lot being the computer wiz that he is. Herr Ankerbrauerei, also known as Ben Koch, has been a great sounding board for my crazy physics ideas. Ulrich Harbach and Nan Su also contributed a lot to make our physics discussions more interesting. I also want to acknowledge Osamu Kiriyama for putting up with my antics when we were office mates. Dr. Reinhardt, Frau Bergmann, and Frau Palade have lead me through the murky administrative waters and I would like to thank them because of this.

I was able to meet some very cool (and crazy) people in the last years. Hossein Malekzadeh was the first person I tried to talk to during my first days in Germany. We have been very good friends since then. I have also been fortunate enough to meet such a great group of friends: Stefan Häussler, Sophie Nahrwold, Veronica Dexheimer, Alexandra Martin, Allan Sandlin, Haasna

Fatehi, Mariano Pereira, Graziela Grise, Xianglei Zhu, Wei Wu, Khin Linn, Irina Sagert, Mauricio Martinez, Joan Cerda, Elsa Henriques, Philipp Reuter, Barbara Betz, Hanna Petersen, and Sascha Vogel. Last year our group of friends increased by three guys from Columbia University: the good, the bad, and the ugly. Otherwise known as Azfar Adil, William Horowitz, and Simon Wicks; not in any particular order. Their owner, Miklos Gyulassy, was also here to make sure they behaved. While here, Miklos and I had many interesting and thought provoking discussions. Last but least, my dear friend, Basil Sa'd, suffered through all my jokes most of which were about him, and he was still such a good friend that he helped us move (thanks to Sophie too).

Finally, I would like to thank my family, which is more appropriate in Portuguese.

Agradeco a toda a minha familia e amigos por terem sempre acreditado em mim. Meus irmaos de coracao: Serginho, Rodrigo, e Andre da Silva. Quanta saudade, hein? Eu agradeco tambem aos meus grandes amigos na fisica, Kazu e Kamiza. Minhas queridas avos, meu avo, tios, tias, e primos que, embora morando muito longe nao foram nunca esquecidos. Pai e mae: sem voces eu nunca teria chegado aqui na Alemanha. Sinto falta de voces todo santo dia. Me sinto muito honrado e feliz quando lembro de toda a sua dedicacao, confianca, e amor para comigo. Obrigado por tudo!

I would like to thank Jaki's relatives for accepting me right away as a member of their family. I have had a lot of fun talking to Cathy, Doug, Mollie, Amanda, and Mike. David and Liane have helped us a lot with everything, which I will be always thankful for.

Minha ida para a Alemanha tem sido fundamental para meu engrandecimento como ser humano. Eu pensei que chegaria aqui para aprender somente os conceitos mais fundamentais da fisica. Entretanto, Deus trabalha das mais misteriosas formas ... Conhecer a Jaki, que se tornou minha esposa, aqui na Alemanha foi sem duvida o maior presente que jah ganhei na vida. Eu precisei viajar para um outro continente para entender o que eh o verdadeiro amor. Nao ha palavras o bastante para descrever o quanto ela representa para mim. Fonte inesgotavel de amor, carinho e compreensao. Esta tese nao poderia ter sido realizada sem voce minha querida sapitas.